Control of time-dependent dynamics of quantum systems: exact and approximate techniques

Boyan Tonev Torosov

Supervisor: Assoc. Prof. D.Sc. Nikolay V. Vitanov

Thesis presented for the degree of
Doctor of Philosophy

Group of Quantum Optics and Quantum Information
Theoretical Physics Division
Faculty of Physics
SOFIA UNIVERSITY "ST. KLIMENT OHRIDSKI"
Sofia

January 2010

The thesis contains 112 pages, 39 figures and 114 references. It is based upon 6 publications in peer-reviewed international journals as follows.

4 in Physical Review A

1 in Journal of Physics A

1 in Optics Communications

TO MY PARENTS

Abstract

It is well known, that the structure of atoms and molecules undergoes a transformation when exposed to interaction with radiation. Different types of radiation cause different types of evolution. The branch of physics, which deals with interaction between matter and coherent field is called coherent control. By using coherent radiation, one has a great level of control of the evolution of the quantum system. Coherent control allows preparation of atoms and molecules in specified quantum states, as well as different schemes for navigation in Hilbert state. This is a requirement in many areas of contemporary physics, for instance laser-controlled chemical reaction, isotope separation, atom optics. Recently, with the growing interest in quantum information science, coherent control is used as a tool for initialization, processing and read-out of the information, measured in qubits.

This thesis studies some of the basic principles underlying the evolution of simple quantum systems, interacting with coherent field. Techniques for navigation in Hilbert space are also described, as well as some applications in quantum computing, allowing preparation of specific gates and quantum algorithms.

Copyright

The work in this thesis is based on research carried out at the Group of Quantum Optics and Quantum information, Theoretical Physics Division, Faculty of Physics at SOFIA UNIVERSITY "ST. KLIMENT OHRIDSKI". The author of this thesis has not submitted any part of it elsewhere for any other degree or qualification.

Acknowledgements

I want to express my gratitude to the many people who have assisted me. First of all, I would like to thank Nikolay Vitanov, who was my Ph.D supervisor, for his constant support and guidance throughout the past four years. It was Nikolay who introduced me to the field of atomic physics and quantum optics. From the very beginning, he was patiently explaining many things to me and I am grateful for the encouragement, sound advice, good teaching and friendly company he has given me.

I appreciate the many useful discussions with all members and guests of the Group of Quantum Optics and Quantum information, Theoretical Physics Division, Faculty of Physics, SOFIA UNIVERSITY "ST. KLIMENT OHRIDSKI". Especially I would like to acknowledge the permission to use the LaTeX template of Andon Rangelov.

I want to thank the Department of Physics at University of Turku and also the School of Physics and Astronomy at University of Leeds for the hospitality during my visits there. This thesis probably would never be written without the supports by the European Commission projects EMALI and FASTQUAST, the Bulgarian National Science Fund grants VU-F-205/06, VU-I-301/07, D002-90/08, IRC-CoSiM, as well as Sofia University Grant No. 020/2009.

Away from the university, I would like to thank my family for their support during the years of my study and education and for all the encouragement they have always given me. Last but not least, I would like to thank all my friends for supporting me whenever I need a support and for their friendship.

Contents

Chapter 1

Introduction

The present chapter introduces the basic theory of light- atom interaction for two-state atom (e.g two-state system), as governed by the time dependent Scrödinger equation.

1.1 The Schrödinger equation

The coherently driven two-state quantum system is a fundamental object in quantum physics. In many experiments a two-state transition suffices to describe the essential changes in the internal state of a quantum system subjected to a generally time-dependent external field. Moreover, when multiple states are involved, the quantum dynamics can usually be understood only by reduction to an effective two-state dynamics.

The time evolution of a coherently driven two-state quantum system is described by the Schrödinger equation

$$i\hbar\frac{d}{dt}\mathbf{c}(t) = \mathbf{H}(t)\mathbf{c}(t), \tag{1.1}$$

where $\mathbf{c}(t) = [c_1(t), c_2(t)]^T$ is the column-vector with the probability amplitudes of the two states ψ_1 and ψ_2, while $\mathbf{H}(t)$ is the Hamiltonian of the atom-radiation system. The diagonal elements of $\mathbf{H}(t)$ are the unperturbed energies of the two states E_1 and E_2, and the off-diagonal elements contain the laser-atom dipole interaction energy. Because the populations $P_n(t) = |c_n(t)|^2$ depend only on the magnitudes of the probability amplitudes, there is some leeway in choosing the phases of these. It proves particularly convenient to incorporate the state energies as phases. Then the off-diagonal element of the Hamiltonian matrix, which is proportional to the sinusoidally oscillating laser electric feld, is multiplied by a phase factor oscillating at the Bohr transition frequency $\omega_0 = (E_2 - E_1)/\hbar$. Because the laser frequency ω is equal or very close to the transition frequency ω_0, the off-diagonal Hamiltonian element can be represented as a sum of two terms: one term oscillating rapidly at nearly twice the transition frequency $(\omega_0 + \omega)$, and

another term oscillating slowly at frequency $\Delta = \omega_0 - \omega$, the atom-laser detuning. Neglecting the rapidly oscillating term is known as the *rotating-wave approximation* (RWA) [1]. Under this approximation, the Schrödinger equation reads

$$i\frac{d}{dt}c_1(t) = \frac{1}{2}\Omega(t)e^{-iD(t)}c_2(t), \tag{1.2a}$$

$$i\frac{d}{dt}c_2(t) = \frac{1}{2}\Omega^*(t)e^{iD(t)}c_1(t), \tag{1.2b}$$

where $D = \int_0^t \Delta(t')dt'$. The coupling $\Omega(t) = -\mathbf{d}\cdot\mathbf{E}(t)/\hbar$ is the so called Rabi frequency, where $\mathbf{d}$ is the transition dipole moment and $\mathbf{E}(t)$ is the laser electric-field envelope.

Another useful representation of the Schrödinger equation, which we shall use throughout the thesis, is obtained from Eqs. (1.2) after a simple phase transformation

$$\mathbf{c}(t) \rightarrow \begin{bmatrix} e^{-iD(t)/2} & 0 \\ 0 & e^{iD(t)/2} \end{bmatrix} \mathbf{c}(t). \tag{1.3}$$

In this new picture, the Schrödinger equation reads

$$i\frac{d}{dt}\mathbf{c}(t) = \tfrac{1}{2}\begin{bmatrix} -\Delta(t) & \Omega(t) \\ \Omega(t) & \Delta(t) \end{bmatrix} \mathbf{c}(t). \tag{1.4}$$

The evolution of the probability amplitudes is usually described by the *evolution matrix* $\mathbf{U}$, also called *propagator* of the system, defined as

$$\mathbf{c}(t_f) = \mathbf{U}(t_f, t_i)\mathbf{c}(t_i). \tag{1.5}$$

It is a unitary matrix, which allows us to calculate the amplitudes at a time t_f, if we know them in the initial moment t_i.

The coherent two-state dynamics is extensively studied, particularly in relation to coherent atomic excitation [1], nuclear magnetic resonance [2], and most recently, as a qubit for quantum information processing [3, 4]. On exact resonance, when the frequency of the driving field is equal to the Bohr transition frequency, the Schrödinger equation is solved exactly, for any time dependence of the coupling $\Omega(t)$ (the Rabi frequency), and the transition probability P depends on the pulse area $A = \int_{-\infty}^{\infty}\Omega(t)dt$ only, $P = \sin^2(A/2)$. Of particular use are the π pulses ($A = \pi$ or odd-multiple of π), which produce complete population inversion (CPI) between the two states, 2π pulses ($A = 2\pi$ or even-multiple of π), which produce complete population return (CPR), and half-π pulses ($A = \pi/2$ or half-integer-multiple of π) that create an equal coherent superposition of the two states.

There are several exactly soluble *non-resonant* two-state models, including the Rabi [5], Landau-Zener [6], Rosen-Zener [7], Allen-Eberly [8, 9], Bambini-Berman [10], Demkov-Kunike

[11], Demkov [12], Nikitin [13], and Carroll-Hioe [14] models. Methods for approximate solutions are also available, such as the perturbation theory and the adiabatic approximation. Adiabatic evolution is of particular interest, because, when accompanied with an energy level crossing, it leads to CPI — usually referred to as rapid adiabatic passage [8, 15]. Noncrossing energies produce no excitation in the end of adiabatic evolution, i.e., CPR.

Analytical solutions — exact or approximate — allow one to design simple recipes for control of the transition probability, and more generally, of the entire two-state propagator. The traditional control parameters are the pulse area, the static detuning and the frequency chirp.

1.2 Exactly soluble models

In this section we will briefly review some of the most popular exactly soluble two-state quantum models, which we shall use throughout the thesis.

1.2.1 Rabi model

One of the simplest exactly soluble models is the Rabi model [5]. In this model, it is assumed that the Rabi frequency and the detuning are both constant in time:

$$\Omega(t) = \Omega_0, \quad \Delta(t) = \Delta_0. \tag{1.6}$$

The solution of the Schrödinger equation (1.4) for this model is straightforward and the elements of the propagator read:

$$\mathbf{U}(t,0) = \begin{bmatrix} a & -b^* \\ b & a^* \end{bmatrix}, \tag{1.7}$$

where

$$a = \cos\left(\frac{\sqrt{\Omega_0^2+\Delta_0^2}}{2}t\right) + i\frac{\Delta_0}{\sqrt{\Omega_0^2+\Delta_0^2}}\sin\left(\frac{\sqrt{\Omega_0^2+\Delta_0^2}}{2}t\right), \tag{1.8}$$

$$b = -i\frac{\Omega_0}{\sqrt{\Omega_0^2+\Delta_0^2}}\sin\left(\frac{\sqrt{\Omega_0^2+\Delta_0^2}}{2}t\right). \tag{1.9}$$

1.2.2 Landau-Zener model

In the Landau-Zener model [6] the coupling and the detuning are given by

$$\Omega(t) = \Omega_0, \quad \Delta(t) = A^2 t, \tag{1.10}$$

where Ω_0 and A (not to be confused with the pulse area) are positive constants. In the case when the coupling has a finite duration the solution is given in terms of Weber's parabolic cylinder functions, and it is discussed in Chapter 5. However, in the case in which the duration lasts for infinite time, the solution is simple and the propagator is easily parameterized:

$$\mathbf{U}(\infty,-\infty)=\begin{bmatrix}\sqrt{P} & \sqrt{1-P}e^{i\phi}\\ -\sqrt{1-P}e^{-i\phi} & \sqrt{P}\end{bmatrix}, \tag{1.11}$$

where

$$P=e^{-\pi\Lambda/2}, \tag{1.12}$$

$$\phi=\tfrac{1}{2}\tau^2+\tfrac{1}{4}\Lambda\ln\tau^2-\tfrac{3}{4}\pi+\arg\Gamma(1-\tfrac{1}{4}i\Lambda), \tag{1.13}$$

$$\Lambda=\frac{\Omega_0^2}{A^2},\quad \tau=\tau_f=-\tau_i,\quad \tau_i=At_i,\quad \tau_f=At_f. \tag{1.14}$$

1.2.3 Demkov-Kunike model

The Demkov-Kunike model [11] assumes a hyperbolic-secant pulsed interaction and detuning, which has a static component and a hyperbolic-tangent chirp:

$$\Omega(t)=\Omega_0\operatorname{sech}(t/T),\quad \Delta(t)=\Delta_0+B\tanh(t/T), \tag{1.15}$$

where Ω_0, Δ_0, B and T are assumed positive without loss of generality. In this case, it is more convenient to work in the interaction representation (1.2). We make a simple variable transformation $z(t)=[1+\tanh(t/T)]/2$ and introduce the dimensionless parameters

$$\alpha=\frac{\Omega_0 T}{2},\quad \beta=\frac{BT}{2},\quad \delta=\frac{\Delta_0 T}{2}. \tag{1.16}$$

The solution for the propagator is expressed in terms of the Gauss hypergeometric function $F(\lambda,\mu;\nu;z)$:

$$U_{11}(z,0)=U_{22}(z,0)^*=F(\lambda,\mu;\nu;z), \tag{1.17a}$$

$$U_{21}(z,0)=-U_{12}(z,0)^*=-i\frac{\alpha}{\nu}2^{-2i\beta}z^{\nu}(1-z)^{1-\nu-2i\beta}F(1+\lambda,1+\mu;1+\nu;z), \tag{1.17b}$$

where

$$\lambda=\sqrt{\alpha^2-\beta^2}-i\beta, \tag{1.18a}$$

$$\mu=-\sqrt{\alpha^2-\beta^2}-i\beta, \tag{1.18b}$$

$$\nu=\frac{1}{2}+i\left(\delta-\beta\right). \tag{1.18c}$$

In the case of interaction which lasts from $t\to-\infty$ to $t\to\infty$ the hypergeometric functions reduce to simpler Gamma functions. The Demkov-Kunike model, as well as its special cases, the Allen-Eberly, Rosen-Zener and Bambini-Berman models, will be examined in more details in Chapter 4.

1.2.4 Carroll-Hioe model

Another exactly soluble model, which we consider in this thesis, is the Carroll-Hioe model [14]. The coupling and detuning in this model are

$$\Omega(t) = \Omega_0 \operatorname{sech}(t/T), \quad \Delta(t) = B \tanh(t/T) + S_0 \operatorname{sech}(t/T). \tag{1.19}$$

The exact solution for this model is derived in Appendix A.4 in the general case to take into account losses of population out of the system.

1.3 Structure of the thesis

The present thesis studies different aspects of the light-matter interaction and considers specific applications. The thesis is organized as follows.

In Chapter 2 we analyze the effects of laser-induced Stark shift and irreversible population loss on the technique of chirped-frequency adiabatic passage, and the ensuing symmetries and asymmetries in the ionization and fluorescence signals. We find that the properties of the detection signal depend critically on the fashion in which it is collected: for example, the post-pulse populations of the ground and excited states, and the ionization signal collected during the excitation, possess different symmetry properties with respect to the frequency chirp rate and the static frequency detuning. We illustrate these features with two exactly soluble analytic models, which describe simultaneous excitation and ionization of a two-state quantum system, as it typically occurs in atomic excitation with femtosecond laser pulses. We find that the ionization signal may exhibit unexpected oscillations and derive the conditions for maximizing their contrast.

Chapter 3 analyzes the accuracy of the adiabatic-elimination approximation for calculating the acquired phases, caused by far-off-resonant pulsed laser fields. In this chapter we derive the conditions for the applicability of this approximation to the calculation of the phases. We account for various sources of imperfections, ranging from higher terms in the adiabatic-elimination expansion and irreversible population loss to couplings to additional states. We find that, as far as the phase shifts are concerned, the adiabatic elimination is accurate only for a very large detuning. We show that the adiabatic approximation is a far more accurate method for evaluating the phase shifts, with a vast domain of validity; the accuracy is further enhanced by superadiabatic corrections, which reduce the error well below 10^{-4}. Moreover, owing to the effect of adiabatic population return, the adiabatic and superadiabatic approximations allow one to calculate the phase shifts even for a moderately large detuning, and even when the peak Rabi frequency is larger than the detuning; in these regimes the adiabatic elimination is

completely inapplicable. We also derive several exact expressions for the phases using exactly soluble two-state and three-state analytical models.

In Chapter 4 we present an analytically exactly soluble two-state model, in which a hyperbolic-secant-shaped pulsed interaction has a phase jump of ϕ at the time of its maximum. The detuning has a constant part and a hyperbolic-tangent chirp term. For $\phi = 0$, this model reduces to the Demkov-Kunike model, which in turn contains as particular cases three other well-known models: the Rosen-Zener, Allen-Eberly and Bambini-Berman models. A nonzero ϕ induces dramatic changes in the transition probability, ranging from complete population inversion to complete population return. The analytic results are particularly instructive in the adiabatic limit and demonstrate that complete population inversion can always occur for a suitable choice of ϕ. The jump phase ϕ can therefore be used as a control parameter for the two-state transition probability.

Chapter 5 presents a class of exact analytic solutions of the time-dependent Schrödinger equation for a two-state quantum system coherently driven by a nonresonant external field. The coupling is a linear function of time with a finite duration and the detuning is constant. Four special models are considered in detail, namely the shark, double-shark, tent and zigzag models. The exact solution is derived by rotation of the Landau-Zener propagator at an angle of $\pi/4$ and is expressed in terms of Weber's parabolic cylinder function. Approximations for the transition probabilities are derived for all four models by using the asymptotics of the Weber function; these approximations demonstrate various effects of physical interest for each model.

Chapter 6 introduces a technique which allows one to connect *any* two arbitrary (pure or mixed) superposition states of an N-state quantum system. The proposed solution to this inverse quantum mechanical problem is analytical, exact and very compact. The technique uses standard and generalized quantum Householder reflections (QHR), which require external pulses of precise areas and frequencies. We show that any two pure states can be linked by two standard QHRs, or by only one generalized QHR. The transfer between any two mixed states with the same dynamic invariants (e.g., the same eigenvalues of the density matrix ρ) requires in general N QHRs. Moreover, we propose recipes for synthesis of arbitrary preselected mixed states, starting in a single basis state and using a combination of QHRs and incoherent processes (pure dephasing or spontaneous emission).

In Chapter 7, we propose a technique for design of quantum Fourier transforms, and ensuing quantum algorithms, in a single interaction step by engineered Hamiltonians of circulant symmetry. The method uses adiabatic evolution and is robust against fluctuations of the interaction parameters as long as the Hamiltonian retains a circulant symmetry.

Chapter 2

Symmetries and asymmetries in coherent atomic excitation by chirped laser pulses

Coherent excitation of a two-state atom by a laser pulse is usually associated with symmetric excitation profiles [1], i.e. the excitation probability is a symmetric (even) function of the detuning Δ and the chirp rate C. When multiple states are involved, there is always a multitude of (often interfering) excitation pathways, and a change of sign in the detuning or the chirp of the excitation pulse (or pulses) makes the system follow a different path in Hilbert space, and arrive at a different outcome. A two-state system, however, is too simple in this respect for it has only one transition path $\psi_1 \leftrightarrow \psi_2$, from which the symmetry of the excitation probability $P_{1\to 2}$ with respect to Δ and C usually, but not always, follows. Symmetries of this sort can be broken, for example, by the presence of dynamic Stark shifts and population losses (e.g., ionization) induced by the excitation pulse.

In this chapter we examine in some detail the sources of asymmetries in the two-state excitation profiles. We find that the properties of the detected signal depend significantly on its nature: for example, the post-pulse populations of the ground and excited states (probed, e.g., by subsequent laser-induced fluorescence or ionization) and the ionization signal accumulated during the excitation display different symmetry properties with respect to the frequency chirp and the detuning. To this end, we use two analytically exactly soluble models, which extend the analytic models of Demkov-Kunike [11] and Carroll-Hioe [14] to complex detuning, which is needed to model simultaneous excitation and population loss. These models allow us to describe the effects of laser-induced Stark shift and irreversible population loss (spontaneous emission, ionization, etc.) upon chirped adiabatic passage techniques; these effects become

significant in strong-field atomic excitation by ultrashort (picosecond and femtosecond) laser pulses [16–19].

The chapter is organized as follows. We introduce the model physical system in Sec. 2.1. The two-state symmetries and asymmetries are described in Sec. 2.2. The analytic models are presented and discussed in Sec. 2.3. The conclusions are summarized in Sec. 2.4.

2.1 Model physical system

2.1.1 Two-state system

Our model system comprises two states, ground ψ_1 and excited ψ_2, the transition between which is driven by an external coherent field. The evolution of this system is described by the Schrödinger equation [1]. The Hamiltonian in the rotating-wave approximation reads

$$\mathbf{H}(t) = \hbar \begin{bmatrix} 0 & \frac{1}{2}\Omega(t) \\ \frac{1}{2}\Omega(t) & \Delta(t) - \frac{1}{2}i\Gamma(t) \end{bmatrix}, \tag{2.1}$$

where $\Gamma(t)$ describes irreversible loss of population. The detuning $\Delta(t)$ is real and may have an arbitrary time dependence, which may occur through temporal variation of either the laser frequency $\omega(t)$ (by frequency chirping) or the atomic transition frequency $\omega_0(t)$ (by using controlled Stark or Zeeman shifts induced by time-varying electric or magnetic fields). The Rabi frequency $\Omega(t)$ quantifies the field-induced coupling between the two states. For single-photon electric-dipole excitation, we have $\Omega(t) = -\mathbf{d} \cdot \mathbf{E}(t)/\hbar$. For two-photon excitation, the Rabi frequency is proportional to $\mathbf{E}^2(t)$. This follows from the fact that such processes correspond to second-order terms in perturbation theory [1]. The Rabi frequency $\Omega(t)$ is assumed real, positive and pulse-shaped. The irreversible-loss rate $\Gamma(t)$ is real and positive and may be constant or pulse-shaped. The latter situation, of pulse-shaped $\Gamma(t)$ occurs, for instance, when the driving pulse, while acting upon the transition $\psi_1 \leftrightarrow \psi_2$, simultaneously ionizes the population of the excited state ψ_2; this typically occurs in excitation by femtosecond laser pulses.

We shall be concerned with excitation of a two-state atom by a single intense laser pulse, which may have the following simultaneous actions: (i) excite the transition $\psi_1 \leftrightarrow \psi_2$; (ii) ionize the population from state ψ_2 with a rate $\Gamma(t)$; (iii) induce dynamic Stark shifts caused by the presence of the other, far off-resonance states in the atom. Let the time dependence of the laser electric field be described by the function $f(t)$; hence the laser intensity is $I(t) = I_0 f(t)^2$. Then the Rabi frequency $\Omega(t)$ will be proportional to either $f(t)$ or $f(t)^2$, whereas the dynamic Stark shift $S(t)$ and the ionization rate $\Gamma(t)$ (for one-photon ionization) are both proportional

to $f(t)^2$,

$$\Omega(t) = \begin{cases} \Omega_0 f(t) \propto \sqrt{I(t)} & \text{(one-photon transition)}, \\ \Omega_0 f(t)^2 \propto I(t) & \text{(two-photon transition)}, \end{cases} \tag{2.2a}$$

$$S(t) = S_0 f(t)^2 \propto I(t), \tag{2.2b}$$

$$\Gamma(t) = \Gamma_0 f(t)^2 \propto I(t). \tag{2.2c}$$

Since the analytical models that we consider comprise symmetric pulse shapes, unless specified otherwise, we shall assume that the pulse shape $f(t)$ is a symmetric (even) function of time,

$$f(-t) = f(t). \tag{2.3}$$

However, general results for asymmetric shapes are also derived. The detuning may have a static component Δ_0 and a chirped (time-dependent) part $B(t)$, which may be linear,

$$B(t) = Ct, \tag{2.4}$$

or nonlinear, e.g. $B(t) = B\tanh(t/T)$.

The dynamic Stark shift is included in the detuning, i.e. we have

$$\Delta(t) = \Delta_0 + S(t) + B(t). \tag{2.5}$$

We shall therefore assume that the detuning contains two parts: a symmetric one (even function of time) $\Delta_\mathrm{e} = \Delta_0 + S(t)$ and an antisymmetric one (odd function of time) $\Delta_\mathrm{o} = B(t)$.

The system is supposed to be initially in state ψ_1 [$c_1(t_i) = 1$, $c_2(t_i) = 0$] and we are interested in the occupation probabilities after the interaction, $P_{1\to1} = |c_1(t_f)|^2$ and $P_{1\to2} = |c_2(t_f)|^2$, and the accumulated population loss (ionization) $P_\mathrm{ion} = 1 - P_{1\to1} - P_{1\to2}$.

2.1.2 Detection signals

In a two-state system, the detection signal may be measured by at least three different scenarios.

- Measurement of the *post-pulse population* of the excited state ψ_2 (the transition probability $P_{1\to2}$) via fluorescence from this state or probe-pulse ionization, Fig. 2.1(a).

- Measurement of the *post-pulse population* of the initial state ψ_1 (the survival probability $P_{1\to1}$) by using a probe laser pulse to an auxiliary excited state and the ensuing fluorescence or ionization from this state, Fig. 2.1(b).

- Measurement of the ionization signal P_ion from the excited state ψ_2, caused by the excitation pulse itself, and therefore collected *during* the excitation, Fig. 2.1(c).

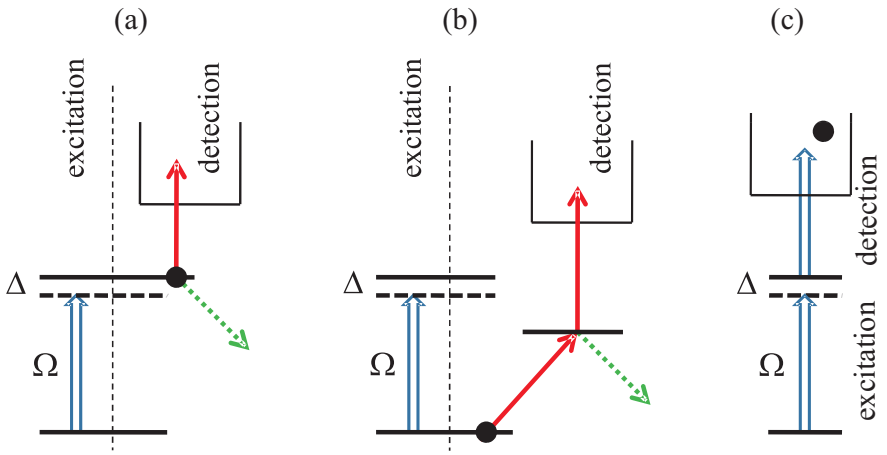

Figure 2.1: Different approaches to measure the detection signal in a two-state system, as explained in Sec. 2.1.2: (a) post-pulse population of the excited state ψ_2 probed by a subsequent fluorescence or laser-induced ionization; (b) post-pulse population of the initial state ψ_1 probed by a subsequent laser-induced fluorescence or ionization; (c) ionization signal P_{ion} from the excited state ψ_2, caused by the excitation pulse itself.

In this chapter we show that the three signals $P_{1\to1}$, $P_{1\to2}$ and P_{ion} may contain different information, for example, they may have different symmetry properties. It is therefore very important in an experiment, even for such a simple two-state system, to pay attention to *how* the signal has been collected.

2.2 Asymmetries in two-state excitation

The time-dependent two-state quantum system possesses various symmetries. We shall now describe some cases when asymmetries emerge, and then analyze what can be accomplished by means of chirped pulses.

In the numerical simulations below we use symmetric $f_s(t)$ and asymmetric $f_a(t)$ pulse shapes,

$$f_s(t) = e^{-t^2/T^2}, \tag{2.6a}$$

$$f_a(t) = e^{-t^2/T^2}\left[1 + \tanh\left(t/T\right)\right]/2, \tag{2.6b}$$

The Rabi frequency and the Stark shift are taken as

$$\Omega(t) = \Omega_0 f_{s,a}(t), \tag{2.6c}$$

$$S(t) = s\Omega(t) = S_0 f_{s,a}(t), \tag{2.6d}$$

with $S_0 = s\Omega_0$.

2.2.1 Sign inversion symmetries in a two-state system

Sign inversion of the detuning and the Rabi frequency

In the lossless case ($\Gamma = 0$), the sign flip in the detuning $\Delta(t) \rightarrow -\Delta(t)$ is equivalent to a complex conjugation of both $c_1(t)$ and $c_2(t)$, and a change of sign in the amplitude $c_1(t)$. Neither of these operations change the transition probability, which is therefore invariant to the sign flip of the detuning. The presence of losses ($\Gamma > 0$) does not change these arguments because the above operations do not change the sign of the Γ-term.

The sign flip of the Rabi frequency $\Omega(t) \rightarrow -\Omega(t)$ is equivalent to the sign flip $c_2(t) \rightarrow -c_2(t)$, and hence this operation does not alter the probabilities either. Again, this conclusion does not depend on the presence of losses.

Time inversion

In the lossless case ($\Gamma = 0$), the probabilities are invariant upon time inversion. This feature follows from the following arguments. The propagator $\mathbf{U}(t_f, t_i)$ from the initial time t_i to the final time t_f is defined via

$$\mathbf{c}(t_f) = \mathbf{U}(t_f, t_i)\mathbf{c}(t_i). \tag{2.7}$$

Time inversion means to propagate from t_f to t_i, which occurs through the inverse of the propagator,

$$\mathbf{c}(t_i) = \mathbf{U}^{-1}(t_f, t_i)\mathbf{c}(t_f) = \mathbf{U}^{\dagger}(t_f, t_i)\mathbf{c}(t_f), \tag{2.8}$$

because for coherent evolution the Hamiltonian is hermitian and the propagator is unitary, $\mathbf{U}^{-1}(t_f, t_i) = \mathbf{U}^{\dagger}(t_f, t_i)$. In the interaction representation the propagator belongs to the SU(2) group and can be parameterized by the Cayley-Klein parameters [20] a and b as

$$\mathbf{U}(t_f, t_i) = \begin{bmatrix} a & -b^* \\ b & a^* \end{bmatrix}. \tag{2.9}$$

Therefore, the transition probability from t_i to t_f is $P^{if}_{1\rightarrow 2} = |b|^2$, and the transition probability from t_f to t_i is $P^{fi}_{1\rightarrow 2} = |-b|^2 = P^{if}_{1\rightarrow 2}$; hence the forward and backward transition probabilities are equal.

This property holds only when: (i) there are only two states [only then the off-diagonal Cayley-Klein parameters are equal in absolute value, Eq. (2.9)]; (ii) there are no incoherent processes [only then Eq. (2.8) holds]. When there are incoherent processes, or/and more than two states, the forward and backward transition probabilities generally differ. For example, in stimulated Raman adiabatic passage (STIRAP) [21], the forward (with counterintuitive pulse order) and backward (with intuitive order) processes lead to substantially different results.

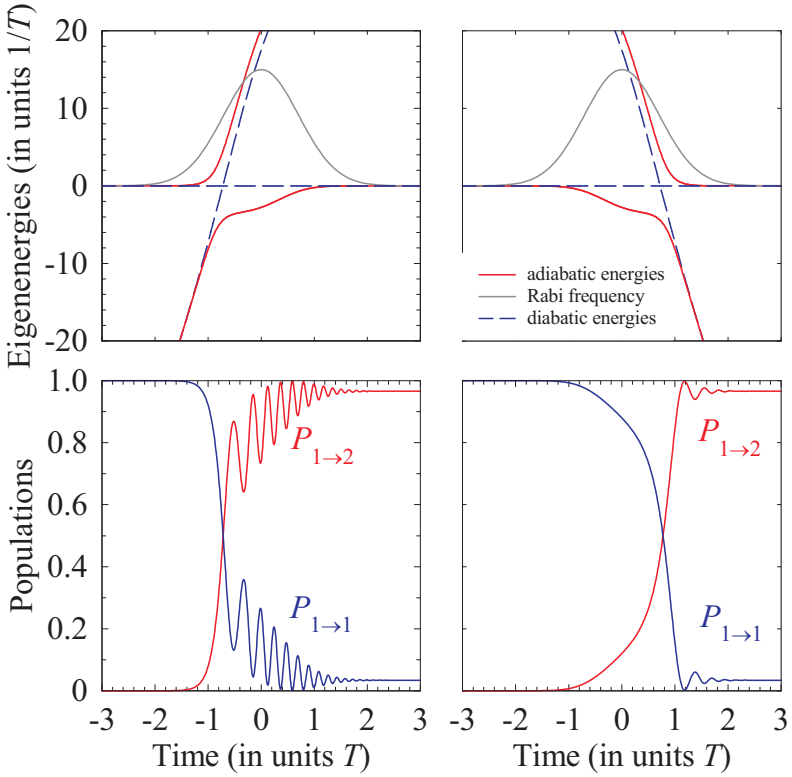

Figure 2.2: The Rabi frequency and the energies in a two-state system (upper plots) and the populations (bottom plots) for a symmetric Gaussian pulse (2.6a) with a peak Rabi frequency $\Omega_0 = 15/T$, for a linear chirp (2.4), with static detuning $\Delta_0 = 10/T$, relative Stark shift $s = 0.5$, and no population loss ($\Gamma = 0$). Left frames: up-chirp, $C = 20/T^2$, right frames: down-chirp, $C = -20/T^2$.

2.2.2 Chirped-pulse excitation

Chirped laser pulses introduce further symmetries and asymmetries in two-state excitation.

Lossless case ($\Gamma = 0$)

Symmetric pulse shape. In the lossless case ($\Gamma = 0$), when all terms but the chirp are even functions of time and the chirp is an odd function of time, Eqs. (2.2), (2.3) and (2.6), the sign flip of the chirp is equivalent to a time inversion; then if the up-chirp corresponds to the forward process, the down-chirp corresponds to the backward process. An example is shown in Fig. 2.2 where the Rabi frequency and the energies (diabatic and adiabatic) are plotted together with the time evolution of the populations in the absence of losses ($\Gamma = 0$). The pulsed field creates an avoided crossing of the adiabatic (dressed) energies. The sign of the chirp (up-chirp or down-chirp) determines when the crossing occurs: at early (for up-chirp) or late (for down-chirp) times. The final transition probability is the same for up and down chirps

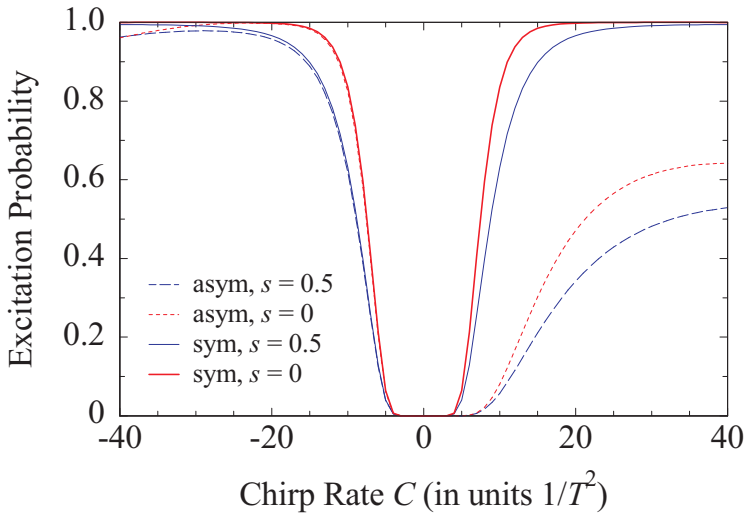

Figure 2.3: Excitation probability vs the chirp rate C in the absence of losses ($\Gamma = 0$). The four curves represent combinations of presence ($s = 0.5$) or absence ($s = 0$) of Stark shift, and symmetric (sym) or asymmetric (asym) pulse shapes. The peak Rabi frequency is $\Omega_0 = 15/T$ and the static detuning is $\Delta_0 = 10/T$.

because of the symmetries discussed above. However, the population histories are different and this makes a difference when a population loss mechanism is present, such as ionization induced by the excitation pulse. Then an *early* crossing will expose *more* population to ionization and therefore will produce a *larger* ionization signal. The presence or absence of ac Stark shift does not alter qualitatively the picture in this case.

By combining arguments from the above discussion it is readily seen that the populations are invariant to the sign change of the symmetric part $\Delta_e(t)$ of the detuning, e.g., the static part Δ_0 for zero Stark shift. Indeed, the sign change $\Delta_e(t) \to -\Delta_e(t)$ is equivalent to the combination of the two sign changes $\Delta_o(t) \to -\Delta_o(t)$ and $\Delta(t) \to -\Delta(t)$, which, as we showed above, do not change the post-pulse populations. The implication is that the excitation line profile $P_{1\to 2}(\Delta_0)$ is a symmetric function (in the absence of Stark shift), even in the presence of a frequency chirp.

Asymmetric pulse shape. If the pulse shape is asymmetric in time, the sign flip of the chirp is *not* equivalent to time inversion and the transition probabilities for up-chirp and down-chirp may differ. This is easily understood from another viewpoint, when the chirp is sufficiently large to create an energy level crossing (at time t_c): for an asymmetric pulse, an up-chirp can create a level crossing at different value of the Rabi frequency than does a down-chirp; hence the transition probabilities, which depend primarily on the ratio $\Omega(t_c)^2/|C|$, will differ in general [6, 22].

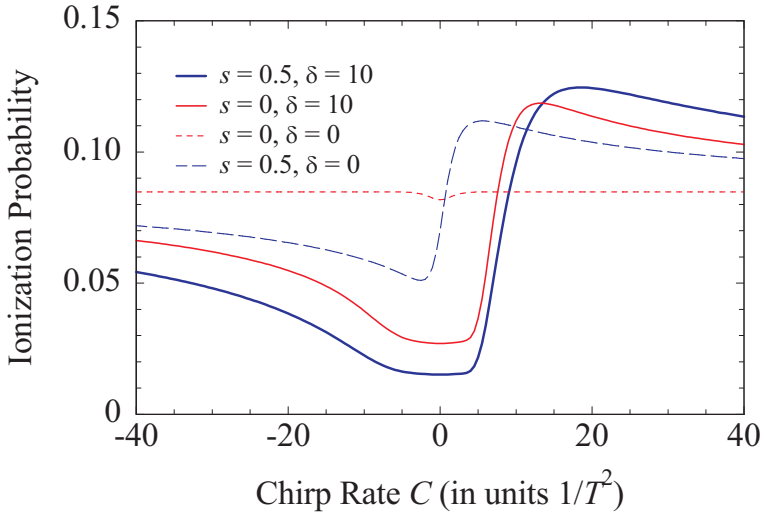

Figure 2.4: Ionization probability vs the chirp rate C in the presence of ionization losses ($\Gamma_0 = 0.1/T$). The four curves represent combinations of presence or absence of Stark shift and static detuning, for symmetric pulse shapes. The peak Rabi frequency is $\Omega_0 = 15/T$.

Figure 2.3 illustrates these properties for symmetric and asymmetric pulse shapes, in the presence and absence of ac Stark shift, and for linear chirp. The figure shows that the chirp asymmetry occurs only for asymmetric pulse shape (2.6b). The presence of ac Stark shift (whenever present it is assumed quite strong, $S_0 = 0.5\Omega_0$) has only a marginal effect. The very small value of the excitation probability around zero chirp is due to the large static detuning Δ_0.

Lossy case ($\Gamma > 0$)

The presence of ionization loss breaks the symmetry of the Hamiltonian (2.1). Then even if the pulse shape $f(t)$ is symmetric the ionization probability $P_{\rm ion}$ exhibits asymmetry with respect to the sign of the chirp C. This is demonstrated in Fig. 2.4. The only case when $P_{\rm ion}$ is symmetric vs C is when the static detuning and the ac Stark shift both vanish, $\Delta_0 = 0$ and $S_0 = 0$; then the change of sign of the chirp is equivalent to sign inversion of the detuning, with no effect on the probabilities. Similar asymmetry as in $P_{\rm ion}$ emerges in the excitation probability $P_{1\to 2}$.

It is far less evident that the *survival* probability $P_{1\to 1}$ *retains* its symmetry versus the chirp, even though $P_{\rm ion}$ and $P_{1\to 2}$ are asymmetric. It is shown in Appendix A.3 that if the Rabi frequency $\Omega(t)$ and the loss rate $\Gamma(t)$ are even functions of time, while the detuning is a sum of an even part $\Delta_{\rm e}$ (the static component and the Stark shift) and an odd part $\Delta_{\rm o}$ (the chirp component), then changing the sign of the odd (or the even) part leaves the final survival probability unchanged, although the evolution can be different. The implication is that the survival probability $P_{1\to 1}$ is an even function of the chirp rate C (regardless of the Stark shift).

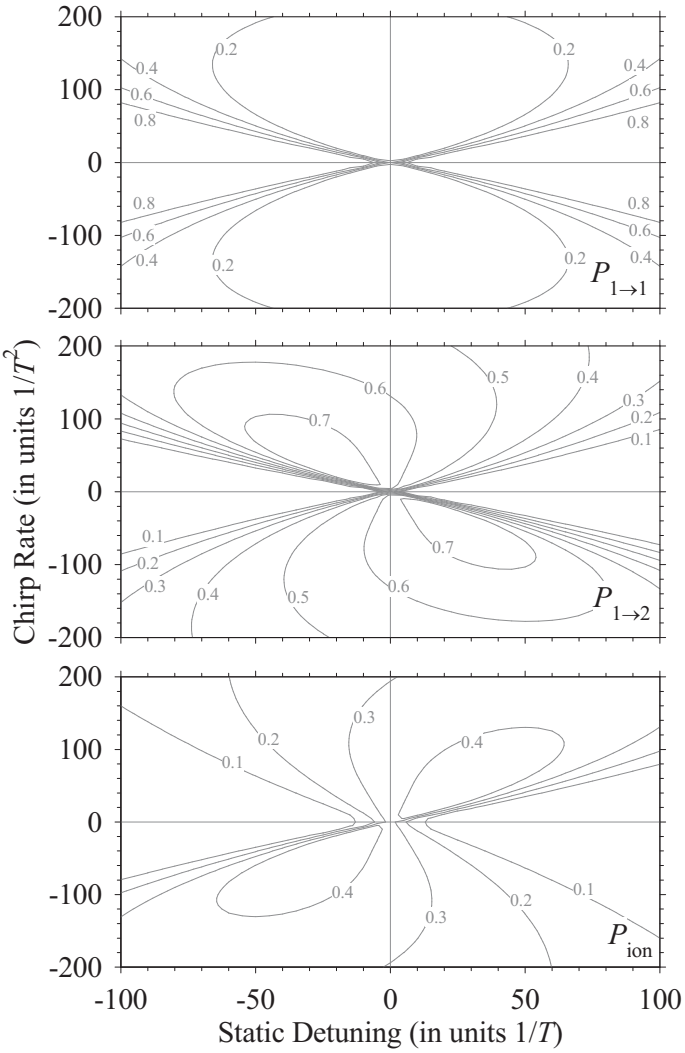

Figure 2.5: Probabilities $P_{1\to1}$ and $P_{1\to2}$ and the ionization probability $P_{\rm ion}$ vs the static detuning Δ_0 and the chirp rate C in the presence of ionization losses ($\Gamma_0 = 0.5/T$) and in the absence of Stark shift, $s = 0$. The pulse shape is Gaussian, Eq. (2.6a), with a peak Rabi frequency $\Omega_0 = 15/T$.

The survival probability $P_{1\to1}$ is an even function of the static detuning Δ_0 only in the absence of Stark shift ($s = 0$), because the symmetric part of the detuning $\Delta_{\rm e}$ is a sum of the static detuning and the Stark shift. With nonzero Stark shift, the symmetry is lost and $P_{1\to1}$ is asymmetric vs Δ_0.

These features are illustrated in Fig. 2.5, which shows a contour plot of the probabilities $P_{1\to1}$ and $P_{1\to2}$ and the ionization probability $P_{\rm ion}$ vs the static detuning Δ_0 and the chirp rate C. The transition probability $P_{1\to2}$ and the ionization probability $P_{\rm ion}$ are highly asymmetric vs both Δ_0 and C. Because the pulse shape is symmetric, this asymmetry is caused by the presence of ionization losses. However, the ground-state probability $P_{1\to1}$ (i.e. the survival probability) is symmetric vs the chirp C, in complete agreement with the property proved in

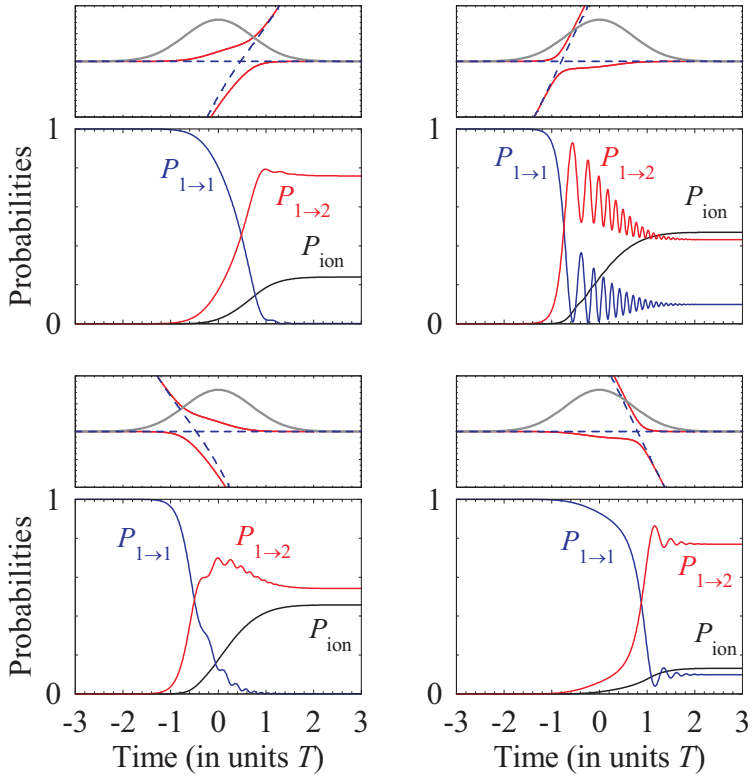

Figure 2.6: Time evolution of the probabilities $P_{1\to1}$ and $P_{1\to2}$ and the ionization probability $P_{\rm ion}$ in the presence of ionization losses ($\Gamma_0 = 0.5/T$) and ac Stark shift, $s = 0.5$. The pulse shape is a Gaussian, with a peak Rabi frequency $\Omega_0 = 15/T$. The four frames correspond to four combinations of positive and negative Δ_0 and C: (i) upper left: $\Delta_0 = -20/T$, $C = 30/T^2$; (ii) upper right: $\Delta_0 = 20/T$, $C = 30/T^2$; (iii) lower left: $\Delta_0 = -20/T$, $C = -30/T^2$; (iv) lower right: $\Delta_0 = 20/T$, $C = -30/T^2$. On the top of each frame with the probabilities, the corresponding energy diagram is displayed. Thin solid curves show the adiabatic (dressed) energies, the dashed curves show the diabatic energies, and the thick curves the laser pulse envelope.

Appendix A.3. Because of the absence of Stark shift, $P_{1\to1}$ is also symmetric vs Δ_0.

The fact that asymmetry exists follows from the broken symmetries of the Hamiltonian in the presence of losses, as explained above. The details of this asymmetry, e.g. which chirp favours ionization, can be understood by looking at the time evolution of the probabilities and the respective energy diagram. Figure 2.6 presents a typical example of time evolution for four different combinations of detunings and chirps. As discussed above, an early crossing induces a larger ionization signal. An early crossing occurs when both the static detuning Δ_0 and the chirp rate C have the same sign, positive (top right frame) or negative (bottom left frame); as expected, the ionization signal in these cases is larger.

2.3 Analytic models

Now we shall present two exactly soluble analytic models, which will allow us to illustrate explicitly the features discussed above.

2.3.1 Generalized Demkov-Kunike model

The generalized Demkov-Kunike (DK) model is defined by

$$\Omega(t) = \Omega_0 \operatorname{sech}(t/T), \quad \Delta(t) = \Delta_0 + B\tanh(t/T), \tag{2.10}$$

where Ω_0, Δ_0 and B are real parameters and the loss rate of the excited state is $\Gamma(t) = \Gamma_0 = \text{const} \geqq 0$. Because of the constant population loss this model is suitable to describe excitation in the presence of fluorescence from the excited state to other states outside the system, or in the presence of ionization from the excited state induced by another, cw laser, coupling this state to the continuum. In the original DK model, there is no population loss, $\Gamma_0 = 0$ [11]. By following the derivation in [23] we can solve the generalized DK model for $\Gamma_0 \geqq 0$. The exact survival probability (the ground-state population) at $t \to \infty$ is [23]

$$P_{1\to 1} = \left| \frac{\Gamma[\frac{1}{2}(1+\frac{1}{2}\gamma + i(\delta-\beta))]\Gamma[\frac{1}{2}(1+\frac{1}{2}\gamma + i(\delta+\beta))]}{\Gamma[\frac{1}{2}(1+\frac{1}{2}\gamma + \varkappa + i\delta)]\Gamma[\frac{1}{2}(1+\frac{1}{2}\gamma - \varkappa + i\delta)]} \right|^2 \tag{2.11}$$

with $\alpha = \Omega_0 T$, $\beta = BT$, $\gamma = \Gamma_0 T$, $\delta = \Delta_0 T$ and $\varkappa = \sqrt{\alpha^2 - \beta^2}$. In the absence of decay, when $\gamma = 0$, this probability coincides with the original DK probability [11]:

$$P_{1\to 1} = \frac{\cosh(\pi\delta) + \cos(\pi\varkappa)}{\cosh(\pi\delta) + \cosh(\pi\beta)}. \tag{2.12}$$

The transition probability $P_{1\to 2}$ vanishes as $t \to \infty$ because of the constant loss, $P_{1\to 2} \to 0$. The ionization is

$$P_{\text{ion}} = 1 - P_{1\to 1}. \tag{2.13}$$

Equations (2.11) and (2.13) show that the survival probability $P_{1\to 1}$ and the ionization P_{ion} are symmetric versus the signs of Δ_0 and B, as expected from the general theory in Sec. 2.2. This property is illustrated in Fig. 2.7, where the survival and ionization probabilities are plotted versus the static detuning Δ_0 and the chirp rate B.

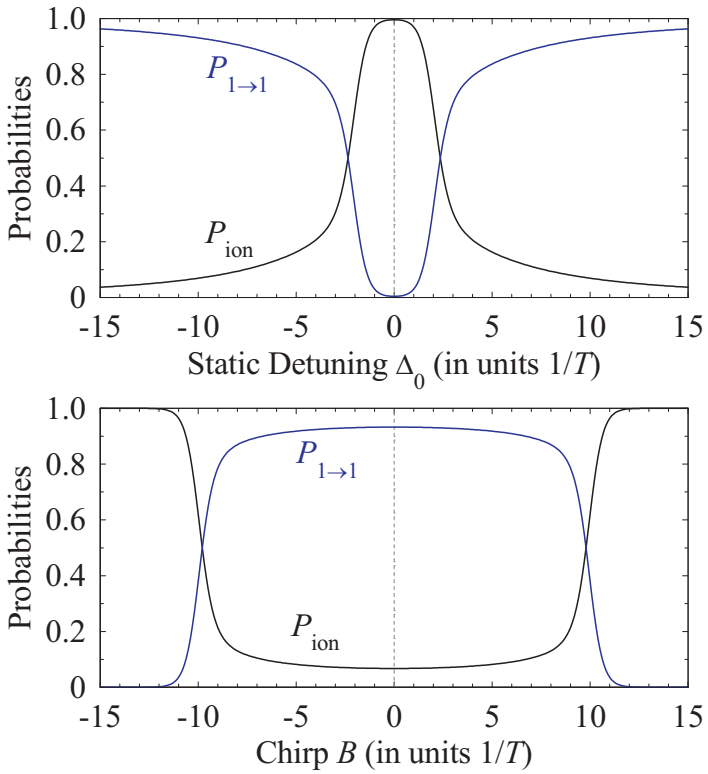

Figure 2.7: Survival probability $P_{1\to1}$ and ionization P_{ion} for the Demkov-Kunike model vs. the static detuning δ (for $\alpha = 10, \beta = 2, \gamma = 0.2$) (top) and the chirp β (for $\alpha = 10, \delta = 10, \gamma = 0.2$) (bottom).

2.3.2 Generalized Carroll-Hioe model

The model

Another exactly soluble analytic model is defined by

$$\Omega(t) = \Omega_0 \,\mathrm{sech}\,(t/T), \tag{2.14a}$$

$$\Delta(t) = B \tanh(t/T) + S_0 \,\mathrm{sech}\,(t/T). \tag{2.14b}$$

When Ω_0, B, and S_0 are real the solution has been derived by Carroll and Hioe (CH) [14]. Here we extend this model to nonzero loss rate,

$$\Gamma(t) = \Gamma_0 \,\mathrm{sech}\,(t/T); \tag{2.15}$$

the exact solution is derived in Appendix A.4. This model allows us to describe two-photon excitation with a tanh chirp, in the presence of ac Stark shift and single-photon ionization. Because the Rabi frequency, the Stark shift and the population loss rate are all proportional to the same function $\mathrm{sech}\,(t)$, this model is particularly suitable for two-photon excitation with simultaneous single-photon ionization; then the CH model imposes a hyperbolic-secant temporal dependence on the intensity of the laser pulse.

Transition probabilities: exact

The transition probabilities are derived in Appendix A.4 and read

$$P_{1\to1} = e^{-\pi\gamma}\left|\frac{e^{\pi\beta/2}\cos 2\pi q - e^{-\pi\beta/2}\cos 2\pi r}{\sinh\pi\beta}\right|^2, \tag{2.16a}$$

$$\begin{aligned} P_{1\to2} = e^{-\pi\gamma}&\left(\frac{\pi^2\alpha\beta}{2\sinh\pi\beta}\right)^2 \\ &\times\left|\Gamma(1-i\beta/2+r+q)\Gamma(1-i\beta/2+r-q)\right|^{-2} \\ &\times\left|\Gamma(1-i\beta/2-r+q)\Gamma(1-i\beta/2-r-q)\right|^{-2}, \end{aligned} \tag{2.16b}$$

$$\begin{aligned} P_{2\to1} = e^{-\pi\gamma}&\left(\frac{\pi^2\alpha\beta}{2\sinh\pi\beta}\right)^2 \\ &\times\left|\Gamma(1+i\beta/2+r+q)\Gamma(1+i\beta/2+r-q)\right|^{-2} \\ &\times\left|\Gamma(1+i\beta/2-r+q)\Gamma(1+i\beta/2-r-q)\right|^{-2}, \end{aligned} \tag{2.17a}$$

$$P_{2\to2} = e^{-\pi\gamma}\left|\frac{e^{-\pi\beta/2}\cos 2\pi q - e^{\pi\beta/2}\cos 2\pi r}{\sinh\pi\beta}\right|^2, \tag{2.17b}$$

where

$$r = \tfrac{1}{4}\sqrt{\alpha^2+(\sigma+i\beta-i\gamma)^2}, \tag{2.18a}$$

$$q = \tfrac{1}{4}\sqrt{\alpha^2+(\sigma-i\beta-i\gamma)^2}, \tag{2.18b}$$

with $\alpha = \Omega_0 T$, $\beta = BT$, $\gamma = \Gamma_0 T$, and $\sigma = S_0 T$. It is easy to verify that for $\gamma = 0$ we have $P_{1\to1} = P_{2\to2}$ and $P_{1\to2} = P_{2\to1}$ because $r = q^*$. For $\gamma \neq 0$ these equalities do not hold.

For a system initially in state 1, the ionization signal is

$$P_{\rm ion} = 1 - P_{1\to1} - P_{1\to2}. \tag{2.19}$$

Obviously, the survival probabilities $P_{1\to1}$ and $P_{2\to2}$, Eqs. (2.16a) and (2.17b), are even functions of B and S_0, as it follows also from the general theory. The transition probabilities $P_{1\to2}$ and $P_{2\to1}$, however, are not invariant upon the sign flip $B \to -B$ or $S_0 \to -S_0$. We illustrate this property in Fig. 2.8, where the populations and the ionization are plotted vs the chirp rate B. The survival probability $P_{1\to1}$ is an even function of B, whereas the transition probability $P_{1\to2}$ and the ionization $P_{\rm ion}$ are asymmetric vs B.

In the absence of Stark shift and losses, $S_0 = \Gamma_0 = 0$, the Carroll-Hioe model reduces to the *Allen-Eberly model*, the transition probability for which reads [8, 9]

$$P^{\rm AE}_{1\to2} = P^{\rm AE}_{2\to1} = 1 - \frac{\cos^2(\pi\varkappa/2)}{\cosh^2(\pi\beta/2)}, \tag{2.20}$$

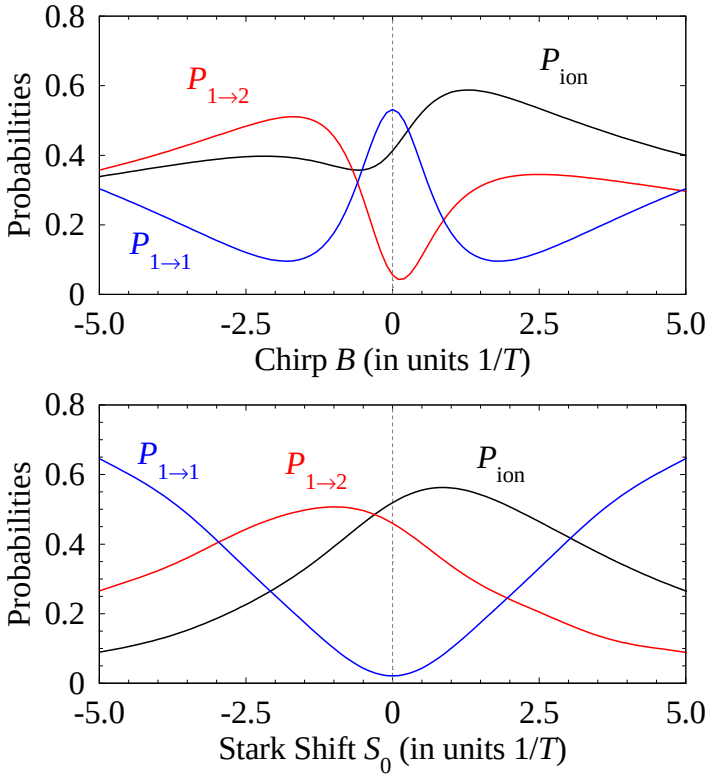

Figure 2.8: Probabilities $P_{1\to1}$, $P_{1\to2}$ and the ionization $P_{\rm ion}$ for the Carroll-Hioe model as a function of the chirp rate β (for $\alpha = 2$, $\sigma = 1$, $\gamma = 0.5$) (top) and the Stark shift σ (for $\alpha = 2$, $\beta = 2$, $\gamma = 0.5$) (bottom).

where $\varkappa = \sqrt{\alpha^2 - \beta^2}$. For a sufficiently large chirp rate B and peak Rabi frequency Ω_0, this transition probability approaches unity,

$$P_{1\to2}^{\rm AE} \to 1 \qquad (\Omega_0 \gtrsim B \gtrsim 1/T); \tag{2.21}$$

this is an example of chirped-pulse adiabatic passage [15].

Transition probabilities: asymptotics

The extension of the Carroll-Hioe model to complex parameters presented above allows us to study quantitatively how adiabatic passage is affected by the presence of Stark shift and irreversible ionization losses.

We are interested primarily in the regime of *small* values of σ and γ, $|\sigma - i\gamma| \ll 1$. We use the expansions

$$r \sim \frac{\varkappa}{4} + \frac{\beta(\gamma + i\sigma)}{4\varkappa} + \mathcal{O}(|\sigma - i\gamma|^2), \tag{2.22a}$$

$$q \sim \frac{\varkappa}{4} - \frac{\beta(\gamma + i\sigma)}{4\varkappa} + \mathcal{O}(|\sigma - i\gamma|^2). \tag{2.22b}$$

and expand the sine and cosine in Eq. (2.16a) to find the following asymptotics of the survival probability

$$P_{1\to 1} \sim P_{1\to 1}^{\mathrm{AE}} e^{-\pi\gamma} \left[1 + \pi\gamma \frac{\beta}{\varkappa} \frac{\tan(\pi\varkappa/2)}{\tanh(\pi\beta/2)} + \mathcal{O}(\sigma^2, \gamma^2)\right]. \tag{2.23}$$

For the transition probability we find from Eq. (2.16b) the asymptotics

$$P_{1\to 2} \sim P_{1\to 2}^{\mathrm{AE}} \mathrm{e}^{-\pi\gamma} \left[1 + \mathcal{O}(\sigma^2, \gamma^2)\right]. \tag{2.24}$$

Equations (2.23) and (2.24) show that the Stark shift affects the probabilities only in second order $\mathcal{O}(\sigma^2)$. If $\varkappa = 0$ (i.e. for $\alpha = \beta$), it can be shown that Eqs. (2.23) and (2.24) hold up to first order $\mathcal{O}(\sigma, \gamma)$.

Using Eqs. (2.23) and (2.24) we obtain the asymptotics of the ionization signal,

$$P_{\mathrm{ion}} \sim 1 - e^{-\pi\gamma} - e^{-\pi\gamma}\pi\gamma \frac{\beta}{\varkappa} \frac{\sin(\pi\varkappa)}{\sinh(\pi\beta)} + \mathcal{O}(\sigma^2, \gamma^2). \tag{2.25}$$

This formula reveals a curious feature of the ionization signal: it exhibits damped oscillations versus the peak Rabi frequency (through $\varkappa$). This feature is indeed intriguing because the unstructured ionization continuum is usually seen as an incoherent medium, void of interference patterns and oscillations. Here we find that the oscillation frequency depends only on $\varkappa = \sqrt{\alpha^2 - \beta^2} \equiv T\sqrt{\Omega_0^2 - B^2}$, i.e. on the peak Rabi frequency Ω_0 and the chirp rate B, but not on the Stark shift S_0 and the decay rate Γ_0. The amplitude of the oscillations depends on all these parameters but S_0; most notably, it vanishes rapidly with the decay rate Γ_0 and the chirp rate B, but only slowly with Ω_0, as a sinc function.

These features are illustrated in Fig. 2.9, where the ionization signal is plotted versus the peak Rabi frequency for different sets of parameters. When the loss rate Γ_0 is increased the ionization oscillates around an increased asymptotic value, $1 - e^{-\pi\gamma}$, and the oscillation amplitude varies as $\gamma e^{-\pi\gamma}$ (the maximum amplitude is for $\gamma = 1/\pi$), but the phase of the ionization oscillations is almost unaffected. Finally, as follows from Eq. (2.25), the oscillation amplitude decreases with the chirp rate B, and it is maximal at zero chirp.

2.4 Conclusions

In this chapter we have presented a detailed study of the effects of Stark shift and irreversible population loss (ionization) upon chirped adiabatic passage in a two-state quantum system. We have shown that in the presence of population loss channel, various symmetries that exist in the lossless case are broken, whereas others remain intact. We have shown that three conventional detection signals — the post-excitation populations of states 1 and 2 and the

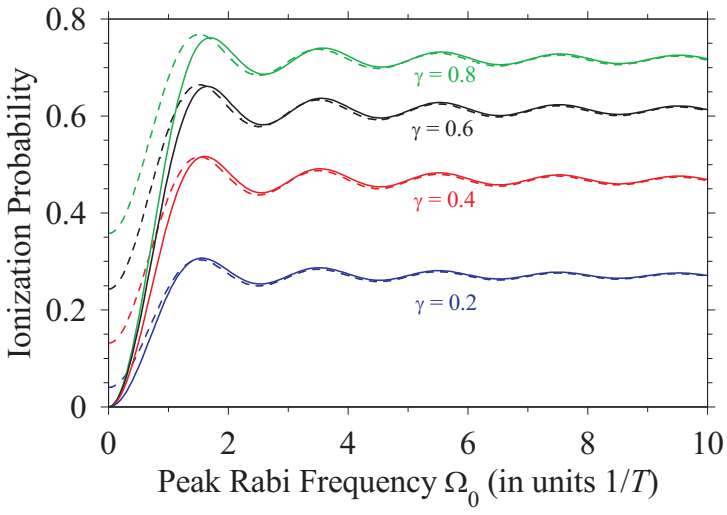

Figure 2.9: Ionization in the Carroll-Hioe model as a function of the peak Rabi frequency Ω_0 for different values of the ionization rate $\gamma = \Gamma_0 T$. The chirp rate is $BT = 0.5$ and the Stark shift is $S_0 = 0.1\Omega_0$. The solid curves show the exact values, calculated numerically, and the dashed curves present the asymptotics (2.25).

ionization signal collected during the excitation — exhibit different symmetries. In particular, the post-excitation population of the initial state (the survival probability) retains its symmetry with respect to sign flip of the even part (typically the static detuning) or the odd part (typically the chirp) of the detuning. The post-excitation population of the other state and the ionization signal, though, do not have this symmetry, and are therefore asymmetric with respect to the chirp and the static detuning.

These features can be observed in a single-photon transition between two states, in which the upper state is ionized by the excitation pulse. A three-state ladder system, with a far-off-resonance intermediate state (which can be eliminated adiabatically), provides another convenient playground for testing these symmetries; For example, the ladder 3s-3p-4s in sodium atom appears particularly suitable [16].

We have made use of two exactly soluble analytic models, which are extensions of the models of Demkov-Kunike and Carroll-Hioe to complex parameters. Both models assume a hyperbolic-secant time dependence of the Rabi frequency. The Demkov-Kunike detuning is a sum of a constant term, the real part of which describes a static detuning and the imaginary part a constant probability loss, and a hyperbolic-tangent chirp. The Carroll-Hioe detuning is a sum of a hyperbolic-secant term, the real part of which describes a Stark shift and the imaginary part an ionization (both caused by the excitation pulse), and a hyperbolic-tangent chirp. This model therefore can be used to describe a two-photon excitation accompanied by simultaneous single-photon ionization.

The analytic solutions make it possible, besides illustrating explicitly the symmetries in the signals, to derive the corrections to the adiabatic passage solution introduced by the Stark shift and the population loss. We have found an interesting oscillatory behavior in the ionization signal. The phase of these oscillations depends primarily on the Rabi frequency, and to a lesser extend on the chirp, but not on the loss rate or the Stark shift. We have used the generalized Carroll-Hioe solution to establish the optimal conditions for experimental observation.

Chapter 3

Phase shifts in nonresonant coherent excitation

Far-off-resonant laser pulses are a popular tool for inducing controllable phase shifts in atomic states. These phase shifts — usually referred to as dynamic Stark shifts — are frequently used in the construction of dynamic phase gates, which are a basic tool in quantum information processing [3, 4]. In many algorithms (e.g. Grover's quantum search [24]) one has to prepare such phase shifts very accurately [25]. Insofar as quantum algorithms involve a great number of phase gates, the accuracy of the latter is of crucial importance for high-fidelity quantum information processing.

There are three major types of phase gates: dynamic [25], geometric [26] and using relative laser phases [27]. While the latter two types have certain advantages in terms of robustness against parameter fluctuations, these come at the cost of more demanding implementations. The dynamic phase gate benefits from the simplicity of implementation (because, unlike the other phase gates, it requires just a single off-resonant pulsed field), which determines its widespread use.

We emphasize that such phase shifts also emerge in various more traditional dynamical problems involving complicated linkage patterns. The quantum dynamics of these multistate systems can often be understood only by reduction to simpler two- or three-state systems by using *adiabatic elimination* of all far-off-resonant (virtual) states. For instance, it is mandatory to account for such dynamic Stark shifts in excitation of multiphoton transitions by femtosecond laser pulses [17, 28].

As far as a phase shift of π is concerned the simplest approach is to use a resonant 2π pulse. A variable phase shift ϕ, however, requires a field with a suitable detuning and intensity; such a variable phase shift is required, for example, in deterministic quantum search [29].

The dynamic Stark shift, and the ensuing phase shift, are usually calculated by eliminating adiabatically the off-resonant state(s). In this chapter we show that, unless applied very carefully, the adiabatic elimination (AE) approximation can lead to significant errors in the value of the phase. We analyze various sources of errors, ranging from higher terms in the AE expansion to population decay and shifts from additional states [30], and show that the standard AE approximation is accurate only for *very* large detuning Δ (Sec. 3.2). We then present a method for the evaluation of the phase based on the adiabatic approximation (Sec. 3.3). This approximation provides a simple formula for the gate phase, which contains the AE phase as a limiting case for $|\Delta| \to \infty$, but it is also valid for moderately large detunings ($|\Delta|T \gtrsim 1$, with T being the pulse width). Then we include superadiabatic corrections (Sec. 3.3.3), dissipation (Sec. 3.3.4), effects of additional states (Sec. 3.4), and several exact solutions (Sec. 3.5).

3.1 Background

We consider a two-state quantum system (a qubit) interacting with a coherent field (Fig. 3.1, left) and we wish to estimate the accumulated phase during this interaction. The phase gate is defined as

$$\mathbf{F} = \begin{bmatrix} e^{i\phi} & 0 \\ 0 & e^{-i\phi} \end{bmatrix}, \tag{3.1}$$

where $\mathbf{F} = \mathbf{U}(t_\mathrm{f})$ is the desired form of the propagator $\mathbf{U}(t)$ at the final time t_f. The propagator $\mathbf{U}(t)$ satisfies the Schrödinger equation [1],

$$i\hbar\partial_t \mathbf{U}(t) = \mathbf{H}(t)\mathbf{U}(t), \tag{3.2}$$

with the initial condition $\mathbf{U}(t_\mathrm{i}) = \mathbf{I}$ at time t_i. This propagator allows us to calculate the phases of the two states, accumulated during the interaction, for arbitrary initial conditions. The Hamiltonian in the interaction representation and the rotating-wave approximation reads

$$\mathbf{H}(t) = \frac{\hbar}{2} \begin{bmatrix} 0 & \Omega(t)e^{-iD(t)} \\ \Omega(t)e^{iD(t)} & 0 \end{bmatrix}, \tag{3.3}$$

For simplicity, we assume hereafter that the detuning is constant, $\Delta = \mathrm{const}$; the results can be readily extended to time-dependent $\Delta(t)$.

In terms of the two probability amplitudes of the qubit states $c_1(t)$ and $c_2(t)$, the Schrödinger equation reads

$$i\hbar\partial_t \mathbf{c}(t) = \mathbf{H}(t)\mathbf{c}(t), \tag{3.4}$$

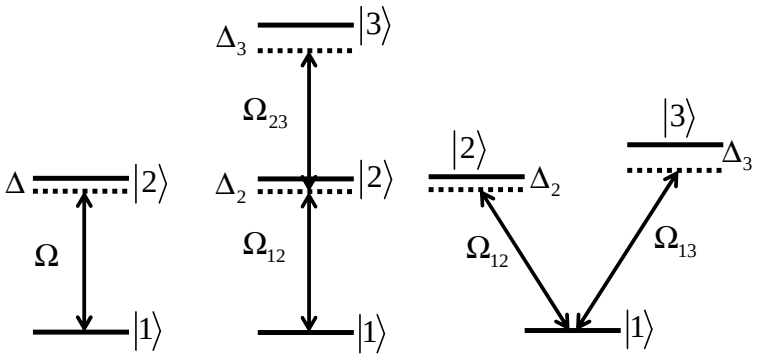

Figure 3.1: Linkage diagram for a two-state system (left), a three-state system in a ladder configuration (middle), and a three-state system in a V configuration (right).

with $\mathbf{c}(t) = [c_1(t), c_2(t)]^T$. For initial conditions $c_1(t_\mathrm{i}) = 1$ and $c_2(t_\mathrm{i}) = 0$, the action of the phase gate $\mathbf{F}$ reads

$$\mathbf{F}c_1(t_\mathrm{i}) = e^{i\phi}c_1(t_\mathrm{i}), \qquad \mathbf{F}c_2(t_\mathrm{i}) = 0. \tag{3.5}$$

For initial conditions $c_1(t_\mathrm{i}) = 0$ and $c_2(t_\mathrm{i}) = 1$, we have

$$\mathbf{F}c_1(t_\mathrm{i}) = 0, \qquad \mathbf{F}c_2(t_\mathrm{i}) = e^{-i\phi}c_2(t_\mathrm{i}). \tag{3.6}$$

Solving the Schrödinger equation (3.4) for the initial conditions $c_1(t_\mathrm{i}) = 1,\ c_2(t_\mathrm{i}) = 0$ is sufficient for the calculation of the gate phase: if the Hamiltonian (3.3) produces the phase change (3.5), it will produce the phase gate (3.1).

3.2 Adiabatic-elimination approximation

3.2.1 Steady-state solution

We begin with the traditional adiabatic elimination. To this end, it is suitable, with the phase transformation $c_1(t) = b_1(t)$, $c_2(t) = b_2(t)e^{-iD(t)}$, to write the Schrödinger equation (3.4) in the energy picture,

$$i\partial_t b_1(t) = \tfrac{1}{2}\Omega(t)b_2(t), \tag{3.7a}$$

$$i\partial_t b_2(t) = \tfrac{1}{2}\Omega(t)b_1(t) + \Delta b_2(t), \tag{3.7b}$$

with the initial conditions $b_1(t_\mathrm{i}) = 1$ and $b_2(t_\mathrm{i}) = 0$. The AE approximation is applicable when the field is tuned far off resonance ($|\Delta| \gg \Omega$), which implies a small transition probability. Then we set $\dot{b}_2(t) = 0$, find $b_2(t)$ from Eq. (3.7b), and substitute it in Eq. (3.7a). The result is a solution of the form (3.5), with a zero transition probability and a phase factor

$$\phi = \int_{t_\mathrm{i}}^{t_\mathrm{f}} \frac{\Omega(t)^2}{4\Delta}\,\mathrm{d}t. \tag{3.8}$$

In fact, this is the *steady-state solution*, that is just the first term in an asymptotic expansion over Δ. Unfortunately, this expression has only a small region of validity $|\Delta| \gg \Omega$ and does not give us a rigorous error estimation.

3.2.2 Adiabatic elimination: higher terms

In order to find the next terms in the asymptotic expansion over Δ it is more convenient to start from the original interaction representation, Eqs. (3.3) and (3.4),

$$i\partial_t c_1(t) = \tfrac{1}{2}\Omega(t)e^{-iD(t)}c_2(t), \tag{3.9a}$$

$$i\partial_t c_2(t) = \tfrac{1}{2}\Omega(t)e^{iD(t)}c_1(t). \tag{3.9b}$$

A formal integration gives

$$c_2(t) = -\frac{i}{2}\int_{-\infty}^{t} \Omega(t')e^{i\Delta t'}c_1(t')\,\mathrm{d}t'. \tag{3.10}$$

Now we integrate by parts,

$$\begin{aligned} c_2(t) &= -\int_{-\infty}^{t} \frac{\Omega(t')}{2\Delta}c_1(t')\,\mathrm{d}e^{i\Delta t'} \\ &= -\frac{\Omega(t)}{2\Delta}c_1(t)e^{i\Delta t} + \int_{-\infty}^{t} \frac{e^{i\Delta t'}}{2\Delta}\partial_{t'}\left[\Omega(t')c_1(t')\right]\,\mathrm{d}t' \\ &= -\frac{\Omega(t)}{2\Delta}c_1(t)e^{i\Delta t} + \frac{1}{2i\Delta^2}\partial_t\left[\Omega(t)c_1(t)\right]e^{i\Delta t} \\ &\quad -\frac{1}{2i\Delta^2}\int_{-\infty}^{t} e^{i\Delta t'}\partial_{t't'}\left[\Omega(t')c_1(t')\right]\,\mathrm{d}t'. \end{aligned} \tag{3.11}$$

We substitute this expression in Eq. (3.9a) and obtain

$$c_1(t) = e^{-\gamma(t)}e^{i\phi(t)}, \tag{3.12}$$

where $\gamma \approx 0$ for a large detuning. Indeed, for smooth pulse shapes, the transition probability ($1-e^{-2\gamma}$ here) vanishes exponentially with Δ. For example, for a Gaussian pulse, the transition probability vanishes as $\sim \operatorname{sech}^2[\pi\Delta T/2\ln(\Omega_0 T)]$ [31], whereas for a hyperbolic-secant pulse it vanishes as $\sim \operatorname{sech}^2(\pi\Delta T/2)$ [7].

The phase in Eq. (3.12) reads

$$\phi_{\mathrm{ae}} = \int_{t_\mathrm{i}}^{t_\mathrm{f}} \left[\frac{\Omega(t)^2}{4\Delta} - \frac{\Omega(t)^4 + 4\Omega(t)\ddot{\Omega}(t)}{16\Delta^3} + \mathcal{O}\left(\frac{\Omega^6}{\Delta^5}\right)\right]\,\mathrm{d}t. \tag{3.13}$$

The calculation of the higher terms is increasingly complicated and barely useful. We will refer to this phase as AE2, in order to distinguish it from the AE phase (3.8). This expression shows that the AE approximation is good only for a very large detuning and a smooth pulse (because

of the presence of $\ddot{\Omega}(t)$). The reason is that in an expansion for a phase it is not sufficient to retain the leading term and demand the next term to be much smaller than it; one must also demand *all* neglected terms to be *much smaller than unity*. Obviously, terms of the order of unity or larger cannot be discarded in the estimate of the phase because the latter is defined modulo 2π; hence the leading term alone may provide a value that is not even close to the exact value. We emphasize, however, that if the *transition probability* is concerned, then the leading term in the AE approximation, which is of order $\mathcal{O}(\Omega_0^2/\Delta^2)$, provides an adequate estimate.

We are now in a position to estimate the necessary values of the interaction parameters. Let us express the time-dependent Rabi frequency of the pulse as $\Omega(t) = \Omega_0 f(t/T)$, where Ω_0 is its peak value, T is the characteristic pulse width, and $f(t/T)$ describes the pulse shape. The AE approximation demands $|\Delta| \gg \Omega_0$. The value of the phase is in general of order $\mathcal{O}(1)$; this implies $\Omega_0^2 T \sim |\Delta|$. Hence we must have $(\Omega_0 T)^2 \sim |\Delta| T \gg \Omega_0 T$, which in turn implies

$$|\Delta| \gg \Omega_0 \gg 1/T, \tag{3.14}$$

i.e. the detuning Δ and the peak Rabi frequency Ω_0 must be large compared to the Fourier bandwidth of the pulse $1/T$.

3.2.3 Examples

Gaussian pulse. For a *Gaussian* pulse,

$$\Omega(t) = \Omega_0 e^{-t^2/T^2}, \tag{3.15}$$

where T and Ω_0 are positive constants, the Schrödinger equation cannot be solved exactly and only some approximations are known [31]. The AE approximation (3.13) gives

$$\phi_{\mathrm{ae}}^{\mathrm{G}} \sim \frac{\Omega_0^2 T\sqrt{\pi}}{4\sqrt{2}\Delta} - \frac{\Omega_0^2\sqrt{\pi}(\Omega_0^2 T^2 - 4\sqrt{2})}{32\Delta^3 T} + \mathcal{O}(\Omega_0^6/\Delta^5). \tag{3.16}$$

Due to condition (3.14), the "roughness" term $-4\sqrt{2}$ in the second term, which derives from the $\ddot{\Omega}(t)$-term in Eq. (3.13), is small compared to the term $\Omega_0^2 T^2$.

A meaningful phase gate requires that $\phi \sim \pi$, which implies that we must have $\Omega_0^2 T \sim 4\sqrt{2\pi}\,|\Delta|$. Then the second term in Eq. (3.16) is $\sim \pi^{3/2}/(\Delta T)$, which provides an estimate of the error in the phase. For an error $\lesssim 10^{-4}$, we must have $|\Delta| T \gtrsim 5 \times 10^4$. This is indeed a very large value, particularly in many-particle systems where a variety of modes exists, and such a detuning may violate the condition of single-mode coupling.

Figure 3.2 shows the phase shift after an interaction with an off-resonant Gaussian pulse. The AE phase (3.16) approaches the exact phase only when the detuning Δ exceeds the peak

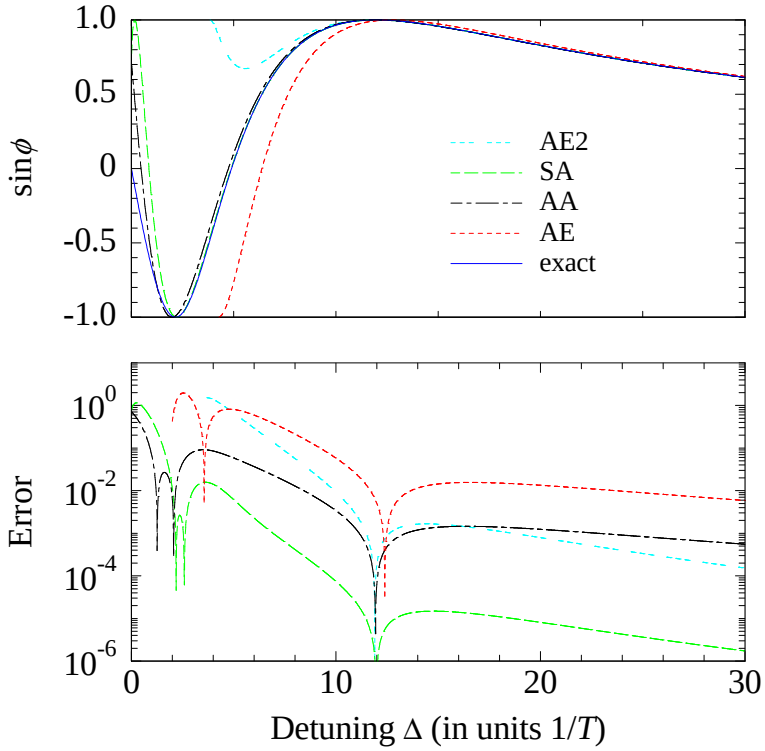

Figure 3.2: Phase shift vs the detuning Δ for a Gaussian pulse shape with a peak Rabi frequency $\Omega_0 = 8/T$. The exact phase, calculated numerically by solving the Schrödinger equation, is compared with the AE and AE2 approximations, the adiabatic (AA) and superadiabatic (SA) phases. Top: the phase shift; bottom: the absolute error of the respective approximation.

Rabi frequency Ω_0 The error of the first (steady-state) term in the AE phase barely drops to 1% in the shown range. The second term in the AE expansion (3.16) is seen to improve the accuracy as $|\Delta|$ increases. The other, more accurate phases shown in the same figure are derived in the following section.

Figure 3.3 shows the same phases versus the peak Rabi frequency Ω_0. Similar conclusions can be drawn, as for Fig. 3.2: the AE approximation gives reasonable results only when the detuning Δ greatly exceeds the peak Rabi frequency Ω_0. The other two phases, to be discussed below, clearly provide much better fits to the exact phase for the entire ranges in Figs. 3.2-3.3.

Hyperbolic secant pulse. The sech pulse,

$$\Omega(t) = \Omega_0 \,\mathrm{sech}(t/T), \tag{3.17}$$

describes the pulse shape in the famous exactly-soluble Rosen-Zener model [7]; we shall return to it in Sec. 3.5. The AE approximation (3.13) gives for it

$$\phi_{\rm ae}^{\rm sech} \sim \frac{\Omega_0^2 T}{2\Delta} - \frac{\Omega_0^2(\Omega_0^2 T^2 - 2)}{12\Delta^3 T} + \mathcal{O}(\Omega_0^6/\Delta^5). \tag{3.18}$$

This approximation is compared in Fig. 3.4 with the exact values. Similar conclusions as for

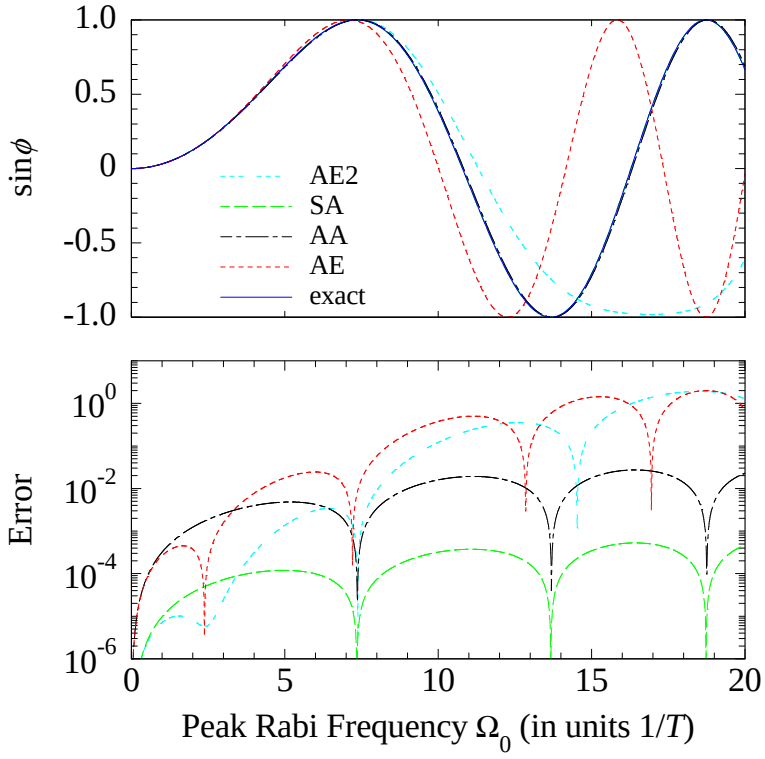

Figure 3.3: Phase shift vs the peak Rabi frequency Ω_0 for a Gaussian pulse shape and a detuning $\Delta = 10/T$. The exact phase, calculated numerically by solving the Schrödinger equation, is compared with the AE and AE2 approximations, the adiabatic (AA) and superadiabatic (SA) phases. Top: the phase shift; bottom: the absolute error of the respective approximation.

the Gaussian pulse in Figs. 3.2 and 3.3 apply: the AE approximation provides a reasonable estimate for the phase shift only when the detuning Δ greatly exceeds the peak Rabi frequency Ω_0. Keeping more terms in the expansion (3.18) improves the accuracy to some extent for large detunings, but this neither extends the range of validity of this approximation nor reaches the accuracy of the adiabatic and superadiabatic approximations, to which we turn our attention now.

3.3 Adiabatic approximation

We shall now demonstrate that the adiabatic approximation is a very accurate tool for calculation of the phase shift, with a vast domain of validity.

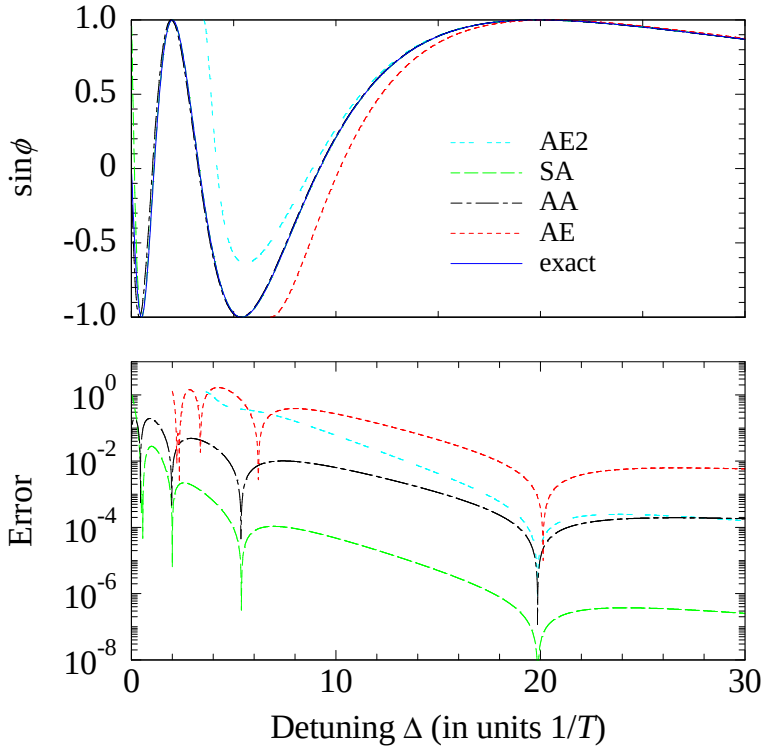

Figure 3.4: The same as Fig. 3.2 but for a hyperbolic-secant pulse shape.

3.3.1 Two-state adiabatic solution

The adiabatic states $\varphi_+(t)$ and $\varphi_-(t)$ are the eigenstates of the time-dependent Hamiltonian in the Schrödinger representation (3.7), with eigenvalues

$$\lambda_\pm(t) = \tfrac{1}{2}[\Delta \pm \lambda(t)]. \tag{3.19}$$

with $\lambda(t) = \sqrt{\Omega(t)^2 + \Delta^2}$. The amplitudes in the adiabatic basis $\mathbf{a}(t) = [a_+(t), a_-(t)]^T$ are connected with the diabatic ones $\mathbf{b}(t)$ via the rotation matrix

$$\mathbf{R}(\theta) = \begin{bmatrix} \cos\theta & \sin\theta \\ -\sin\theta & \cos\theta \end{bmatrix}, \tag{3.20}$$

as $\mathbf{b}(t) = \mathbf{R}(\theta(t))\mathbf{a}(t)$, where $\theta = \frac{1}{2}\arctan(\Omega/\Delta)$. The Schrödinger equation in the adiabatic basis reads

$$i\hbar\partial_t \mathbf{a}(t) = \mathbf{H}_a(t)\mathbf{a}(t), \tag{3.21}$$

where

$$\mathbf{H}_a(t) = \hbar \begin{bmatrix} \lambda_-(t) & -i\dot{\theta}(t) \\ i\dot{\theta}(t) & \lambda_+(t) \end{bmatrix}. \tag{3.22}$$

If $|\dot{\theta}(t)| \ll \lambda_+(t) - \lambda_-(t) = \lambda(t)$, then the evolution is adiabatic and the propagator in the adiabatic basis reads

$$\mathbf{U}_a = \begin{bmatrix} e^{-i\Lambda_-} & 0 \\ 0 & e^{-i\Lambda_+} \end{bmatrix}, \tag{3.23}$$

where $\Lambda_\pm = \int_{t_\mathrm{i}}^{t_\mathrm{f}} \lambda_\pm(t)\,\mathrm{d}t$. We find readily that the propagator $\mathbf{U}$ in the original basis (3.2) is the phase gate (3.1), $\mathbf{U} = \mathbf{F}$, with the phase $\phi = -\Lambda_-$, or explicitly,

$$\phi_\mathrm{a} = \tfrac{1}{2}\int_{t_\mathrm{i}}^{t_\mathrm{f}} [\sqrt{\Omega(t)^2 + \Delta^2} - \Delta]\,\mathrm{d}t. \tag{3.24}$$

This phase reduces to the AE approximation (3.8) for large detuning, $|\Delta| \gg \Omega_0$. However, Eq. (3.24) is valid also for $|\Delta| < \Omega_0$, provided the adiabatic approximation holds.

Figures 3.2-3.4 show that the adiabatic phase (3.24) provides a considerable improvement of accuracy over the AE phase for all detunings $|\Delta| \gtrsim 1/T$. Unless a very high accuracy is required (error $< 10^{-4}$) the adiabatic phase must suffice in applications. The key to the understanding of the reason for its accuracy is hidden in the adiabatic condition.

3.3.2 Adiabatic condition

For adiabatic evolution, the nonadiabatic coupling $|\dot{\theta}(t)|$ must be small compared to the splitting $\lambda(t)$, in order to suppress transitions between the adiabatic states. For a constant detuning, the adiabatic condition reads

$$|\dot{\Omega}(t)\Delta| \ll 2[\Omega(t)^2 + \Delta^2]^{3/2}. \tag{3.25}$$

For Gaussian [31] and sech [7] pulse shapes this condition reduces to

$$\text{Gaussian:} \qquad |\Delta| \gg \Delta_0 = \frac{2}{3\sqrt{3}\,T}\sqrt{\ln(\Omega_0 T)}, \tag{3.26a}$$

$$\text{sech :} \qquad |\Delta| \gg \Delta_0 = \frac{1}{3\sqrt{6}\,T}. \tag{3.26b}$$

Adiabatic evolution is achieved for a sufficiently large detuning. The sech pulse is obviously more adiabatic for it requires a lower detuning. The Gaussian pulse is less adiabatic; moreover, unlike the sech pulse it exhibits a logarithmic power broadening.

The important message for the present context is that the adiabatic approximation requires a *much lower* value of the detuning than the AE approximation. Conditions (3.26) are only indicative: a more thourough analysis shows that the nonadiabatic deviation vanishes exponentially with the detuning [7,31,32]. Consequently, the necessary detuning increases logarithmically with the required accuracy. The implication is that the adiabatic phase gate can operate also at intermediate detunings, moreover, regardless of the value of Ω_0, because the

adiabatic condition does not depend (or depends very weakly) on Ω_0. Thus the condition for the adiabatic phase gate is

$$|\Delta|T \gg 1; \tag{3.27}$$

then the effect of *coherent population return* [33–35] — the adiabatic return of the population to the initial state in the absence of a level crossing — ensures a negligibly small transition probability in the end of the interaction.

We point out, however, that the perturbative estimate for the *transient* excitation is still

$$P_e \sim \frac{\Omega(t)^2}{2[\Omega(t)^2+\Delta^2]}; \tag{3.28}$$

hence there may be a significant transient excitation unless $|\Delta| \gg \Omega_0$. The adiabatic phase gate, therefore, can be used for $\Omega_0 > |\Delta|$ only if the relaxation times of the two qubit states are large compared to the pulse duration — a condition that must be fulfilled for any practical qubit for all types of operations.

3.3.3 Superadiabatic phase

If the evolution is not perfectly adiabatic, we can diagonalize the adiabatic Hamiltonian (3.22) by the transformation $\mathbf{a}(t) = \mathbf{R}(\chi(t))\mathbf{s}(t)$, where $\chi(t) = \frac{1}{2}\arctan[\dot\theta(t)/\lambda(t)]$ and the vector $\mathbf{s}(t)$ contains the amplitudes in the *superadiabatic* basis; they satisfy the equation

$$i\hbar\partial_t\mathbf{s}(t) = \mathbf{H}_\mathrm{s}(t)\mathbf{s}(t), \tag{3.29}$$

where

$$\mathbf{H}_\mathrm{s}(t) = \hbar\begin{bmatrix} \mu_-(t) & -i\dot\chi(t) \\ i\dot\chi(t) & \mu_+(t) \end{bmatrix} \tag{3.30}$$

and $\mu_\pm = (\Delta \pm \sqrt{\Omega^2+\Delta^2+4\dot\theta^2})/2$. The condition for superadiabatic evolution is $|\dot\chi(t)| \ll \mu_+(t)-\mu_-(t)$; if it holds then the propagator in the superadiabatic basis is

$$\mathbf{U}_\mathrm{s} = \begin{bmatrix} e^{-iM_-} & 0 \\ 0 & e^{-iM_+} \end{bmatrix}, \tag{3.31}$$

where $M_\pm = \int_{t_\mathrm{i}}^{t_\mathrm{f}} \mu_\pm(t)\,\mathrm{d}t$. The propagator in the original basis (3.2) is the phase gate (3.1), $\mathbf{U} = \mathbf{F}$, with the superadiabatic phase $\phi = -M_-$, or explicitly,

$$\phi_\mathrm{s} = \tfrac{1}{2}\int_{t_\mathrm{i}}^{t_\mathrm{f}} \left[\sqrt{\Omega(t)^2+\Delta^2+\frac{\dot\Omega(t)^2\Delta^2}{[\Omega(t)^2+\Delta^2]^2}} - \Delta\right] \mathrm{d}t. \tag{3.32}$$

The derivative term is the superadiabatic correction to the adiabatic phase (3.24). The condition this correction to be small is the same as the adiabatic condition (3.25).

As evident from Figs. 3.2-3.4, the superadiabatic phase (3.32) is extremely accurate for all detunings except $\Delta \to 0$, with an error comfortably below 10^{-4} (the usual fault tolerance in quantum computing). The results clearly demonstrate that the superadiabatic phase outperforms the adiabatic phase, let alone the AE phase.

Following the same diagonalization procedure, one can go to the next superadiabatic bases and achieve an even higher accuracy. However, as Figs. 3.2-3.4 suggest, this is unnecessary since the superadiabatic phase already easily satisfies the commonly accepted accuracy goal.

3.3.4 Dissipation effects

Dissipation is detrimental for quantum information processing and various proposals have been put forward to reduce its effects [3, 4]. Because it is impossible to treat here all aspects of dissipation we restrict ourselves only to the simplest case of irreversible population loss. In femtosecond physics, where the present results can be particularly useful, this is a very reasonable assumption because population loss can occur through ionization induced by the driving laser pulse, whereas the other types of dissipation (dephasing, spontaneous emission, etc.) are irrelevant due to the ultrashort time scale.

In order to account for the population loss, we write the Hamiltonian in the form

$$\mathbf{H}(t) = \frac{\hbar}{2} \begin{bmatrix} 0 & \Omega(t) \\ \Omega(t) & 2\Delta(t) - i\Gamma(t) \end{bmatrix}. \tag{3.33}$$

Next, we go to the adiabatic basis, formed of the eigenstates of the Hamiltonian without losses ($\Gamma = 0$). In this basis the Hamiltonian reads

$$\mathbf{H} = \hbar \begin{bmatrix} \lambda_- - \frac{1}{2} i\Gamma \sin^2\theta & \frac{1}{4} i\Gamma \sin 2\theta - i\dot{\theta} \\ \frac{1}{4} i\Gamma \sin 2\theta + i\dot{\theta} & \lambda_+ - \frac{1}{2} i\Gamma \cos^2\theta \end{bmatrix}, \tag{3.34}$$

where for brevity the argument t is omitted. In the adiabatic limit, we can neglect $\dot{\theta}$, as was done in Sec. 3.3.1. Next, we recognize that the first (second) adiabatic state coincides at $t \to \pm\infty$ with the first (second) diabatic state. We eliminate adiabatically the second adiabatic state and obtain the phase and the population of state 1,

$$\phi = -\int_{t_\mathrm{i}}^{t_\mathrm{f}} \left[\lambda_-(t) + \frac{\Gamma(t)^2 \sin^2 2\theta(t)}{16\lambda(t)} \right] \mathrm{d}t, \tag{3.35a}$$

$$P_1 = \left| \exp\left[-\tfrac{1}{2} \int_{t_\mathrm{i}}^{t_\mathrm{f}} \Gamma(t) \sin^2\theta(t)\, \mathrm{d}t \right] \right|^2. \tag{3.35b}$$

We note that the population is much more sensitive (exponentially) to losses than the phase, which in the lowest order is quadratic in Γ. This conclusion is demonstrated in Fig. 3.5. The

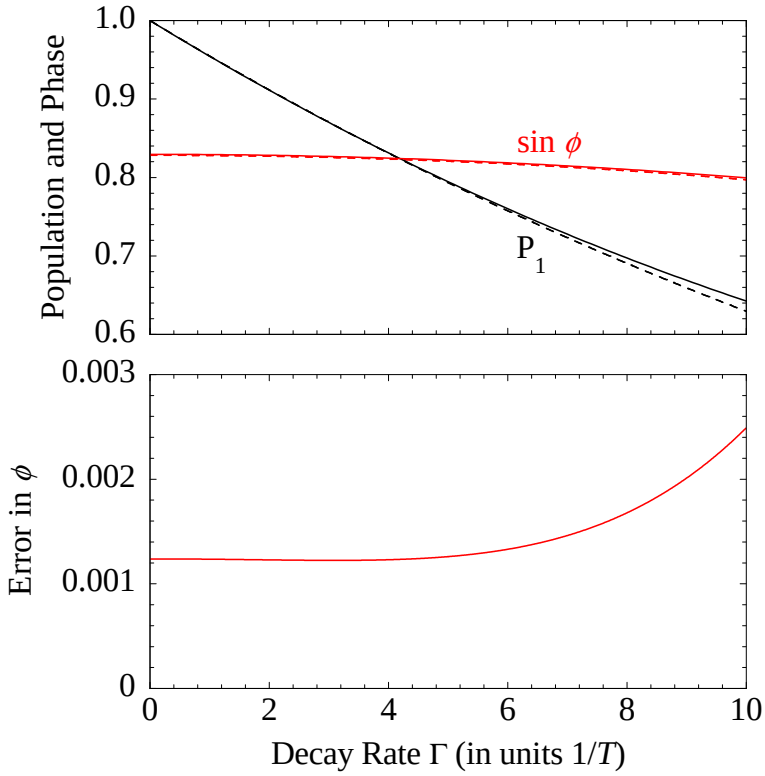

Figure 3.5: The initial-state population and phase vs the loss rate Γ for a Gaussian pulse with $\Omega_0 = 8/T$ and $\Delta = 20/T$. The solid lines represent the exact values and the dashed lines are for the approximations (3.35).

phase barely changes its value as the loss rate changes from zero to $10/T$, even as the population of the initial state decreases considerably. We note that the displayed range of loss rates is much larger than what can be tolerated in quantum computing; nevertheless the phase itself and the approximation to it are very stable against such losses.

3.4 Effects of additional states

3.4.1 Ladder configuration

Adiabatic elimination. We shall now find how the presence of an additional state affects the phase shift. For this purpose let us consider a three-state system in the ladder configuration, wherein nonzero dipole moments only link state 1 with state 2 and state 2 with state 3 (Fig. 3.1, middle), as described by the Hamiltonian

$$\mathbf{H}(t) = \frac{\hbar}{2}\begin{bmatrix} 0 & \Omega_{12}(t) & 0 \\ \Omega_{12}(t) & 2\Delta_2 & \Omega_{23}(t) \\ 0 & \Omega_{23}(t) & 2\Delta_3 \end{bmatrix}. \tag{3.36}$$

For the first-order (steady-state) AE approximation, we set $\dot{c}_2(t) = 0$ and $\dot{c}_3(t) = 0$, and find from the Schrödinger equation the accumulated phase in state 1 to be

$$\phi = \int_{t_\mathrm{i}}^{t_\mathrm{f}} \frac{\Delta_3 \Omega_{12}(t)^2}{4\Delta_2\Delta_3 - \Omega_{23}(t)^2}\,\mathrm{d}t. \tag{3.37}$$

As expected, in the limits $\Omega_{23} \to 0$ or $|\Delta_3| \to \infty$, this expression reduces to Eq. (3.8). When $4|\Delta_2\Delta_3| \gg \Omega_{23}(t)^2$ we obtain

$$\phi = \int_{t_\mathrm{i}}^{t_\mathrm{f}} \frac{\Omega_{12}(t)^2}{4\Delta_2}\,\mathrm{d}t + \int_{t_\mathrm{i}}^{t_\mathrm{f}} \frac{\Omega_{12}(t)^2\Omega_{23}(t)^2}{16\Delta_2^2\Delta_3}\,\mathrm{d}t + \ldots \tag{3.38}$$

We conclude that for $\Omega_{12} \sim \Omega_{23}$ and $\Delta_2 \sim \Delta_3$, the correction from the presence of an additional state is of the same order as the second term in the AE expansion (3.13).

Adiabatic approximation. For simplicity and without loss of generality, we will assume $\Delta_3 > \Delta_2 > 0$. In order to find the eigenvalues of the Hamiltonian (3.36), we have to solve the cubic characteristic equation

$$\varepsilon^3 + a\varepsilon^2 + b\varepsilon + c = 0, \tag{3.39}$$

where $a = -\Delta_2 - \Delta_3,\ b = \Delta_2\Delta_3 - (\Omega_{12}^2 + \Omega_{23}^2)/4,\ c = \Delta_3\Omega_{12}^2/4$. The three roots of this equation are the quasienergies of the three-state system [1],

$$\varepsilon_1 = -\frac{a}{3} - \frac{2p}{3}\cos\frac{\beta - \pi}{3}, \tag{3.40a}$$

$$\varepsilon_2 = -\frac{a}{3} - \frac{2p}{3}\cos\frac{\beta + \pi}{3}, \tag{3.40b}$$

$$\varepsilon_3 = -\frac{a}{3} + \frac{2p}{3}\cos\frac{\beta}{3}, \tag{3.40c}$$

where

$$p = \sqrt{a^2 - 3b}, \qquad \cos\beta = \frac{9ab - 2a^3 - 27c}{2p^3}. \tag{3.41}$$

The adiabatic phase is just an integral over $\varepsilon_1(t)$ [1],

$$\phi = -\int_{t_\mathrm{i}}^{t_\mathrm{f}} \varepsilon_1(t)\,\mathrm{d}t. \tag{3.42}$$

In order to exhibit the effect of the third state on the phase gate, we derive the asymptotics of the quasienergy ε_1 for large Δ_3 and substitute it in Eq. (3.42); we find

$$\phi = -\int_{t_\mathrm{i}}^{t_\mathrm{f}} \varepsilon_-(t)\,\mathrm{d}t - \int_{t_\mathrm{i}}^{t_\mathrm{f}} \frac{\varepsilon_-(t)\Omega_{23}(t)^2}{4\Delta_3(t)\sqrt{\Delta_2(t)^2 + \Omega_{12}(t)^2}}\,\mathrm{d}t, \tag{3.43}$$

where $\varepsilon_- = (\Delta_2 - \sqrt{\Delta_2^2 + \Omega_{12}^2})/2$.

[1] This is valid for the choice $\Delta_3 > \Delta_2 > 0$. For other choices the phase will be an integral over some of the other energies ε_2 or ε_3.

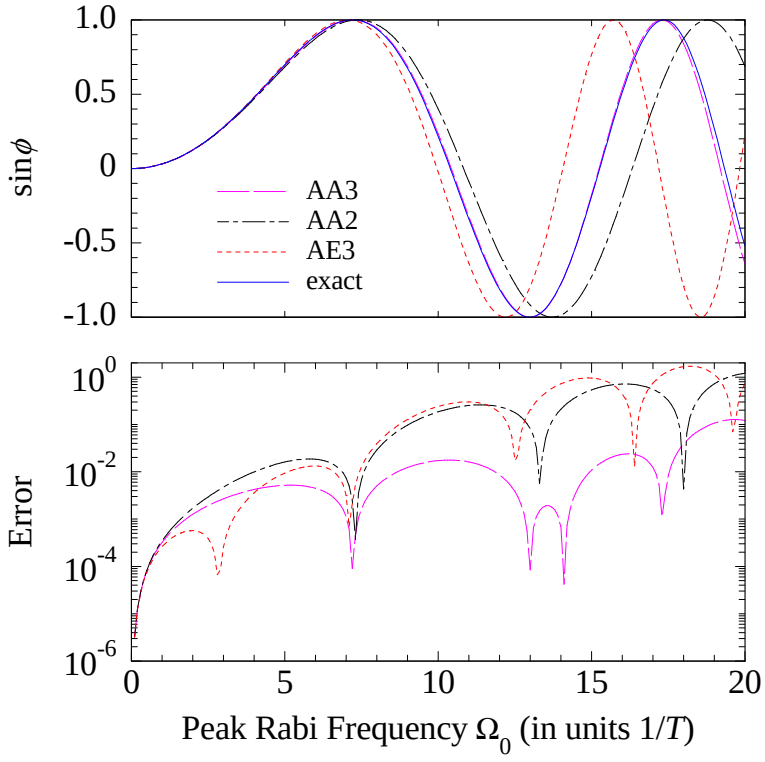

Figure 3.6: Phase shift of the lowest state in a three-state ladder with detunings $\Delta_3 = 2\Delta_2 = 20/T$ vs the peak Rabi frequency Ω_0. The Rabi frequencies for the two transitions are equal and have Gaussian shapes. The phases from the adiabatic approximation for two (AA2) and three (AA3) states, Eqs. (3.24) and (3.42), and the AE approximation for three states (3.38) are compared to the exact values. The AA3 curve is nearly indiscernible from the exact one.

Figure 3.6 compares the AE and adiabatic approximations to the exact phase shift in a ladder system. The three-state adiabatic phase (3.42) is very accurate throughout, as already anticipated, whereas the AE phase (3.38) departs from the exact one when the Rabi frequency becomes comparable and exceeds the detunings. We note that the error of the AE phase is of the same order as the error from the neglect of the additional state, Eq. (3.24).

3.4.2 V configuration

If the three-state system is in a V configuration (Fig. 3.1, right), the Hamiltonian reads

$$\mathbf{H}(t) = \frac{\hbar}{2}\begin{bmatrix} 0 & \Omega_{12}(t) & \Omega_{13}(t) \\ \Omega_{12}(t) & 2\Delta_2 & 0 \\ \Omega_{13}(t) & 0 & 2\Delta_3 \end{bmatrix}. \tag{3.44}$$

Then the AE approximation, applied in a similar fashion as for the ladder system above, gives in the first order the expression

$$\phi = \int_{t_\mathrm{i}}^{t_\mathrm{f}} \frac{\Omega_{12}(t)^2}{4\Delta_2(t)}\,\mathrm{d}t + \int_{t_\mathrm{i}}^{t_\mathrm{f}} \frac{\Omega_{13}(t)^2}{4\Delta_3(t)}\,\mathrm{d}t. \tag{3.45}$$

The contributions from each arm in the V system are independent. Higher-order terms mix the contributions from the two arms.

The adiabatic phase is calculated in a similar manner as for the ladder system, in the form of an integral over the respective eigenenergy.

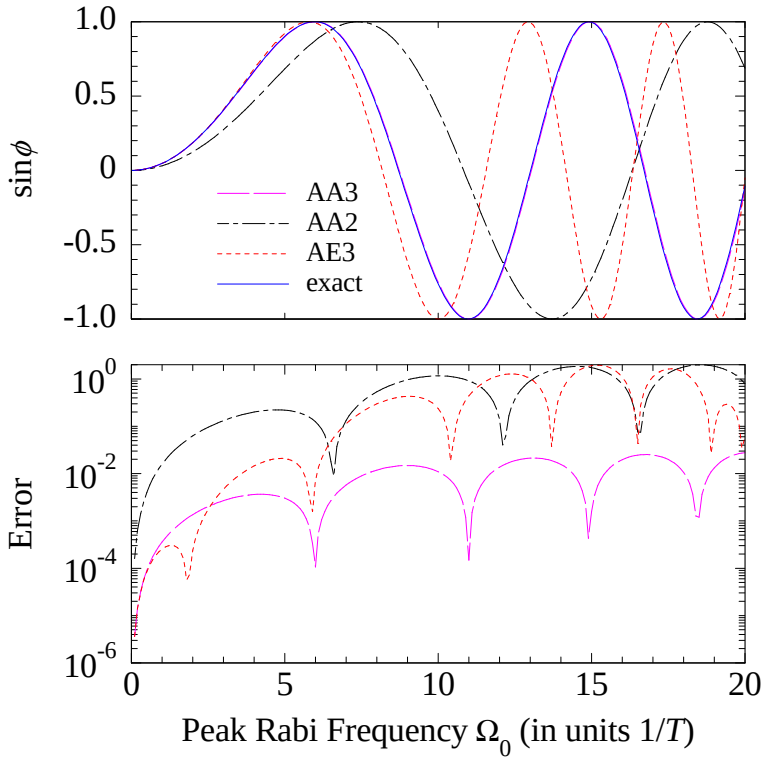

Figure 3.7: Phase shift of the lowest state in a three-state V-system with detunings $\Delta_3 = 2\Delta_2 = 20/T$ vs the peak Rabi frequency Ω_0. The Rabi frequencies for the two transitions are equal and have Gaussian shapes. The phases from the adiabatic approximation for two (AA2) and three (AA3) states, and the AE approximation for three states (3.45) are compared to the exact values. The AA3 curve is indiscernible from the exact one.

In Fig. 3.7 we compare various expressions for the dynamic phase in a three-state V system. The figure reveals that, once again, the three-state adiabatic approximation (AA3) provides a very accurate estimate. On the contrary, the error of the AE approximation is comparable to the effect of the additional third state.

To conclude this section, we point out that a third state in the considered ladder or V systems distorts the symmetry of the phase gate (3.1) because the third state is coupled differently to

the two qubit states: directly to one of them and indirectly (via a two-photon transition) to the other state. For each qubit state, the additional state will make the linkage look either as a ladder (if connected to the other qubit state) or V (if connected to the same qubit state). Consequently, the phase shifts for the two qubit states are different, as evident when one compares the expressions for the ladder and V systems above. We note that a Lambda-system, with the population initially in one of the lower states is equivalent in the present context to a ladder system (population initially in the end of the chain). The phase shifts in such a system have been studied recently [30], in a slightly different context.

In the next section we compare these approximations with the values of several exactly-soluble two-state and three-state models.

3.5 Exact solutions

We shall present the solutions of three exactly soluble models. The first one is the famous Rosen-Zener (RZ) model, which assumes a sech pulse shape (3.17) and a constant detuning, and the others extend the RZ model to systems with three states. The latter are solved by using the Majorana decomposition [36, 37] for a ladder system and the Morris-Shore transformation [38] for a V system.

3.5.1 Two states: Rosen-Zener model

The exact solution for the phase in the RZ model (3.17) is [7, 39]

$$\phi = \arg\left[\frac{\Gamma\left(\frac{1}{2}+\frac{1}{2}i\delta\right)^2}{\Gamma\left(\frac{1}{2}+\frac{1}{2}i\delta-\frac{1}{2}\alpha\right)\Gamma\left(\frac{1}{2}+\frac{1}{2}i\delta+\frac{1}{2}\alpha\right)}\right], \tag{3.46}$$

where $\alpha = \Omega_0 T$, $\delta = \Delta T$, and $\Gamma(z)$ stands for the gamma function [40]. Using the Stirling asymptotics of $\Gamma(z)$ [40], we obtain

$$\phi \sim \frac{\Omega_0^2 T}{2\Delta} - \frac{\Omega_0^2(\Omega_0^2 T^2 - 2)}{12\Delta^3 T} + \ldots \quad (|\Delta| \gg 1/T, \Omega_0). \tag{3.47}$$

This is exactly the result from the AE expansion (3.13).

The exact expression for the phase (3.46) allows us to perform a theoretically *exact* phase gate operation with a variable phase ϕ by selecting a suitable detuning Δ. By using standard properties of the gamma functions, one can show that the transition probability vanishes exactly for a pulse area $A = \pi\Omega_0 T = 2n\pi$, where n is an integer. For these values ($\alpha = 2n$), Eq. (3.46) reduces to [39]

$$\phi = n\pi + 2\arg\left[\prod_{k=1}^{n}(2k - 1 - i\Delta T)\right]. \tag{3.48}$$

For any desired phase ϕ the corresponding detuning is found by solving the latter equation for Δ. For example, a phase shift $\phi = \pi$ can be obtained by any odd value of $n = 1, 3, 5, \ldots$ and $\Delta = 0$ (a property that is well known for any pulse shape). The same phase shift can also be produced by a pulse area $A = 4\pi$ ($n = 2$) and $\Delta T = \sqrt{3}$. As further examples, phase shifts of $\phi = \pi/2$, $\pi/3$, $\pi/4$, and $\pi/6$ can be obtained for $n = 1$ by choosing, respectively, $\Delta T = 1$, $\sqrt{3}$, $1 + \sqrt{2}$, and $2 + \sqrt{3}$.

3.5.2 Three-state ladder

We consider a three-state system in a ladder configuration (Fig. 3.1, middle), described by the Hamiltonian (3.36), assuming that

$$\Omega_{12}(t) = \Omega_{23}(t) = \Omega_0 \operatorname{sech}(t), \quad \Delta_3 = 2\Delta_2 = 2\Delta. \tag{3.49}$$

This model has a simple exact solution [41]: the amplitude of state 1 is just the square of the amplitude for a two-state problem with a Rabi frequency $\Omega(t) = \Omega_{12}(t)/\sqrt{2}$. Because this is the two-state RZ model, we find the phase of state 1 to be

$$\phi = 2 \arg \left[\frac{\Gamma\left(\frac{1}{2} + \frac{1}{2} i\delta\right)^2}{\Gamma\left(\frac{1}{2} + \frac{1}{2} i\delta - \frac{1}{2\sqrt{2}}\alpha\right) \Gamma\left(\frac{1}{2} + \frac{1}{2} i\delta + \frac{1}{2\sqrt{2}}\alpha\right)} \right], \tag{3.50}$$

with $\alpha = \Omega_0 T$ and $\delta = \Delta T$. The exact expression (3.50) allows one to design an *exact* phase gate even in the presence of an additional state. For example, a gate phase $\phi = \pi$ can be obtained for $\Omega_0 T = 2n\sqrt{2}$ with any odd value of $n = 1, 3, 5, \ldots$ and $\Delta = 0$; the same phase can be produced by a pulse area $A = 4\pi\sqrt{2}$ ($n = 2$) and $\Delta T = \sqrt{3}$. A phase shift of $\phi = \pi/2$ can be obtained for $A = 2\pi\sqrt{2}$ and $\Delta T = 1$.

The asymptotics of this phase reads

$$\phi \sim \frac{\Omega_0^2 T}{2\Delta} - \frac{\Omega_0^2(\Omega_0^2 T^2 - 4)}{24\Delta^3 T} + \ldots \quad (|\Delta| \gg 1/T, \Omega_0). \tag{3.51}$$

The comparison with Eq. (3.47) shows that the effect of the third state emerges only in the second term in the expansion over Δ, a feature that appeared earlier in the AE expansion (3.38) and in the adiabatic expansion (3.43).

3.5.3 Three-state V-system

If the system is in a V configuration (Fig. 3.1, right), and if

$$\Omega_{12} = \varkappa_{12} \Omega_0 \operatorname{sech}(t/T), \tag{3.52a}$$

$$\Omega_{13} = \varkappa_{13} \Omega_0 \operatorname{sech}(t/T), \tag{3.52b}$$

$$\Delta_2 = \Delta_3 = \Delta, \tag{3.52c}$$

with $\varkappa_{12}$ and $\varkappa_{13}$ arbitrary constants, then we can use a simple change of basis, known as the Morris-Shore transformation [38]. The latter transforms the V-system into an uncoupled dark state and a two-state system, with a detuning Δ and a Rabi frequency $\varkappa\Omega(t)$, where $\varkappa = \sqrt{\varkappa_{12}^2 + \varkappa_{13}^2}$. In this manner it can readily be shown that the argument of the amplitude of state 1 is [42]

$$\phi = 2\arg\left[\frac{\Gamma\left(\frac{1}{2}+\frac{1}{2}i\delta\right)^2}{\Gamma\left(\frac{1}{2}+\frac{1}{2}i\delta-\frac{1}{2}\varkappa\alpha\right)\Gamma\left(\frac{1}{2}+\frac{1}{2}i\delta+\frac{1}{2}\varkappa\alpha\right)}\right]. \tag{3.53}$$

The asymptotics reads

$$\phi \sim \frac{\varkappa^2\Omega_0^2}{2\Delta} - \frac{\varkappa^2\Omega_0^2(\varkappa^2\Omega_0^2-2)}{12\Delta^3} + \ldots \quad (|\Delta| \gg 1/T, \Omega_0). \tag{3.54}$$

The leading term is a sum of two independent phase shifts induced by each of the two arms of the V-system, in agreement with Eq. (3.45), while the $\varkappa^4$-part in the second term represents a combined contribution of the two arms.

3.6 Conclusions

We have presented a detailed analysis of the accuracy of the adiabatic elimination approach, which allows one to eliminate weakly coupled far-off-resonant states and reduce the interaction dynamics of a quantum system to a smaller effective one. We have put a special emphasis on the acquired phase shifts in the probability amplitudes after the interaction with an off-resonant pulsed field. The results have direct implications in the construction of variable dynamic phase gates, which are of major importance in quantum information processing.

We have shown that in the traditional implementation with a far off-resonance pulsed field, the formula for the gate phase derived by the adiabatic-elimination approximation, has to be used with great care because it is just the first term of a series expansion in the inverse detuning $1/\Delta$; higher terms, unless negligible in value with respect to unity, may render the formula irrelevant. This formula requires a *very large detuning* in order to be sufficiently accurate, because including corrections from higher terms is barely useful due to their complexity and slow convergence. However, quantum information processing involves operations with entangled many-qubit systems, possessing a variety of frequency modes; there a very large detuning may violate the assumption of single-mode interactions.

We have proposed to use a much more accurate formula for the phase shift, derived within the adiabatic-following approximation. The advantage of this adiabatic phase is that the condition for adiabatic evolution is much more relaxed than the condition for adiabatic elimination. The adiabatic phase contains the AE approximation as a limiting case for $|\Delta| \to \infty$; however,

it also applies to *moderate* detunings. The adiabatic phase applies also to the case when the peak Rabi frequency Ω_0 exceeds the detuning Δ; in this case the phase gate operates due to the effect of adiabatic population return. A superadiabatic correction is demonstrated to further improve the accuracy, to errors comfortably below the fault-tolerance limit of 10^{-4} in quantum computing. We have also derived the corrections to the gate phase from additional states coupled to the two qubit states.

In addition, we have derived several *exact* expressions for the gate phase in several exactly soluble analytical two-state and three-state models, assuming a hyperbolic-secant pulse shape. The exact analytical formulae allow us to design highly accurate phase gates, however, at the expense ot the requirement for a special pulse shape. We have also used the exact expressions to test the accuracy of the derived AE and adiabatic approximations.

The results in this chapter have potential applications not only in the calculation of dynamical Stark phase shifts in simple phase gates but also in complicated multistate linkage patterns, which can be factorized to simpler systems by utilizing the intrinsic symmetries, e.g. by the Morris-Shore transformation [38, 43].

Chapter 4

Coherent control of a quantum transition by a phase jump

In this chapter we show that the transition probability in a two-state quantum system can be controlled efficiently by a new control parameter: a *phase jump* of the field amplitude, i.e. in the Rabi frequency. To this end, we present an exact analytical solution of a model with a Rabi frequency of hyperbolic-secant shape and a phase jump of ϕ at the time of its maximum. The detuning is a sum of a constant (static) detuning Δ_0 and a hyperbolic-tangent chirp term. For $\phi = 0$ this model reduces to the Demkov-Kunike (DK) model [11], with its three well-known special cases: the Rosen-Zener (RZ) [7], Allen-Eberly (AE) [8,9], and Bambini-Berman (BB) [10] models. For nonzero ϕ, however, a variety of unexpected features occur. For example, in the adiabatic limit, the transition probability for $\phi = 0$ is 0 for the RZ model, 1 for the AE model, and 0.5 for the BB model. For $\phi = \pm\pi$, however, it is 1 for the RZ model, 0 for the AE model, and again 0.5 for the BB model; for $\phi = \pm\pi/2$ the transition probability for the BB model oscillates between 0 and 1, as for resonant excitation.

The CPI limit has been discussed for the RZ model for $\phi = \pi$ [44]. This CPI has been found to be robust against variations in the experimental parameters, a feature reminiscent of adiabatic passage. The phase-jump CPI mechanism, however, is not adiabatic passage, but it is induced by a δ-function-shaped interaction (nonadiabatic coupling) in the adiabatic basis. Here we generalize this result for arbitrary ϕ, and moreover, we solve the more general phase-step DK model.

This chapter is organized as follows. We derive the exact analytical solution for the phase-jump DK model in Sec. 4.1. We then discuss the three important special cases of the RZ, AE and BB models in Sec. 4.2. We derive the adiabatic solution in Sec. 4.3, which provides a particularly clear picture of the dependence on ϕ. We discuss experimental feasibility in Sec.

4.4 and present a summary in Sec. 4.5.

4.1 Demkov-Kunike model with a phase jump

We shall derive the solution of the Schrödinger equation in the interaction representation,

$$i\frac{d}{dt}c_1(t) = \frac{1}{2}\Omega(t)e^{-iD(t)}c_2(t), \tag{4.1a}$$

$$i\frac{d}{dt}c_2(t) = \frac{1}{2}\Omega^*(t)e^{iD(t)}c_1(t), \tag{4.1b}$$

for a model, in which the coupling and the detuning are given by

$$\Omega(t) = \begin{cases} \Omega_0\mathrm{sech}(t/T) & (t<0) \\ e^{i\phi}\Omega_0\mathrm{sech}(t/T) & (t \geqq 0) \end{cases}, \tag{4.2a}$$

$$\Delta(t) = \Delta_0 + B\tanh(t/T). \tag{4.2b}$$

Without loss of generality the constant real frequencies Ω_0, Δ_0 and B and the pulse width T will be assumed positive. We shall use the characteristic pulse duration T as the unit of time and $1/T$ as the frequency unit. The phase-jump model (4.2) resembles the DK model [11], where the coupling $\Omega(t)$ is a bell-shaped sech function at all times, without the phase jump at $t = 0$. We shall therefore follow the derivation of [11] up to time $t = 0$, where the phase jump will be dealt with.

The first step is to decouple Eqs. (4.1); we find

$$\ddot{c}_1 - \left(\frac{\dot{\Omega}}{\Omega} - i\Delta\right)\dot{c}_1 + \tfrac{1}{4}|\Omega|^2 c_1 = 0, \tag{4.3}$$

with the overdot hereafter denoting a time derivative. The next step is to change the independent variable from t to $z(t) = [1 + \tanh(t/T)]/2$; then $z(-\infty) = 0$, $z(0) = \frac{1}{2}$, and $z(+\infty) = 1$, and Eq. (4.3) transforms into

$$z(1-z)\frac{d^2C_1}{dz^2} + \left[\frac{1}{2} + i\,(\delta - \beta) - (1 - 2i\beta)z\right]\frac{dC_1}{dz} + \alpha^2 C_1 = 0, \tag{4.4}$$

where $C_n(z) = c_n(t(z))$ and

$$\alpha = \frac{\Omega_0 T}{2}, \quad \beta = \frac{BT}{2}, \quad \delta = \frac{\Delta_0 T}{2}. \tag{4.5}$$

Equation (4.4) has the same form as the Gauss hypergeometric equation and its solution can be expressed in terms of the Gauss hypergeometric function $F(\lambda, \mu; \nu; z)$ [40] as

$$C_1(z) = A_1 F(\lambda, \mu; \nu; z) + A_2 z^{1-\nu} F(\lambda + 1 - \nu, \mu + 1 - \nu; 2 - \nu; z), \tag{4.6}$$

where A_1 and A_2 are integration constants and

$$\lambda = \sqrt{\alpha^2 - \beta^2} - i\beta, \tag{4.7a}$$

$$\mu = -\sqrt{\alpha^2 - \beta^2} - i\beta, \tag{4.7b}$$

$$\nu = \frac{1}{2} + i\,(\delta - \beta)\,. \tag{4.7c}$$

By using Eqs. (4.1a), (A.1.2a), (A.1.2b), and the relation $e^{iD} = 2^{-2i\beta} z^{\nu-\frac{1}{2}}\,(1-z)^{\frac{1}{2}-\nu-2i\beta}$ one obtains

$$\begin{aligned} C_2(z) &= i2^{-2i\beta}(1-z)^{1-\nu-2i\beta} \\ &\quad \times \Big[-A_1\frac{\alpha}{\nu} z^{\nu} F(\lambda+1, \mu+1; \nu+1; z) \\ &\quad + A_2 \frac{1-\nu}{\alpha} F(\lambda+1-\nu, \mu+1-\nu; 1-\nu; z)\Big]\,. \end{aligned} \tag{4.8}$$

The constants A_1 and A_2 are determined from the initial conditions $C_1(0)$ and $C_2(0)$,

$$A_1 = C_1(0), \qquad A_2 = \frac{-i\alpha 2^{2i\beta}}{1-\nu} C_2(0). \tag{4.9}$$

The complete solution is expressed by the propagator $\mathbf{U}(z,0)$, which is defined by $\mathbf{C}(z) = \mathbf{U}(z,0)\mathbf{C}(0)$, with $\mathbf{C}(z) = [C_1(z), C_2(z)]^T$. The propagator from $t \to -\infty$ ($z = 0$) to time $t = 0$ ($z = \frac{1}{2}$) reads

$$\mathbf{U}(\tfrac{1}{2}, 0) = \begin{bmatrix} a & -b^* \\ b & a^* \end{bmatrix}, \tag{4.10}$$

where the Cayley-Klein parameters are

$$a = F(\lambda, \mu; \nu; \tfrac{1}{2}), \tag{4.11a}$$

$$b = -i\frac{\alpha}{2\nu} F(1+\lambda, 1+\mu; 1+\nu; \tfrac{1}{2}). \tag{4.11b}$$

For $t \geqq 0$, a similar derivation as for $t < 0$ delivers the propagator from $t = 0$ ($z = \frac{1}{2}$) to $t \to \infty$ ($z = 1$),

$$\mathbf{U}(1, \tfrac{1}{2}) = \begin{bmatrix} c^* & -d^* e^{i\phi} \\ d e^{-i\phi} & c \end{bmatrix}, \tag{4.12}$$

with

$$c = F(\lambda, \mu; 1+\lambda+\mu-\nu; \tfrac{1}{2}), \tag{4.13a}$$

$$d = -\frac{i\alpha F(1+\lambda, 1+\mu; 2+\lambda+\mu-\nu; \frac{1}{2})}{2\,(1+\lambda+\mu-\nu)}. \tag{4.13b}$$

The full propagator is $\mathbf{U}(1,0) = \mathbf{U}(1, \frac{1}{2})\mathbf{U}(\frac{1}{2}, 0)$, or explicitly

$$\mathbf{U}(1,0) = \begin{bmatrix} ac^* - bd^* e^{i\phi} & -b^* c^* - a^* d^* e^{i\phi} \\ bc + ade^{-i\phi} & a^* c - b^* d e^{-i\phi} \end{bmatrix}. \tag{4.14}$$

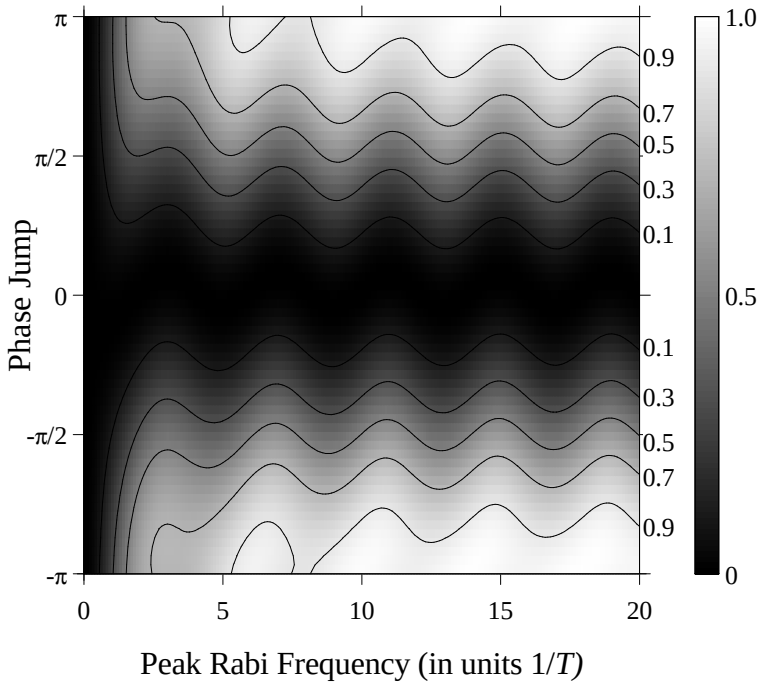

Figure 4.1: Contour plot of the transition probability P^{ϕ}_{RZ} for the RZ model, Eq. (4.19), vs the peak Rabi frequency Ω_0 and the phase jump ϕ for $B = 0$ and $\Delta_0 = 2/T$.

The transition probability therefore reads

$$P^{\phi}_{DK} = |U_{12}|^2 = |ad|^2 + |bc|^2 + 2\mathrm{Re}(a^* b c d^* e^{i\phi}). \tag{4.15}$$

For $\phi = 0$ (DK model) the transition probability (4.15) can be expressed in terms of elementary functions [11]

$$P_{DK} = \frac{\cosh(2\pi\beta) - \cos(2\pi\sqrt{\alpha^2 - \beta^2})}{\cosh(2\pi\delta) + \cosh(2\pi\beta)}. \tag{4.16}$$

For $\phi \neq 0$, the transition probability is expressed by the hypergeometric functions of Eqs. (4.11) and (4.13).

4.2 Special cases

We are going to examine three important special cases of our model, namely when $B = 0$, $\Delta_0 = 0$ and $\Delta_0 = B$, which in the absence of a phase jump ($\phi = 0$) represent the RZ [7], AE [8] and BB [10] models, respectively.

4.2.1 Rosen-Zener model ($B = 0$)

In the RZ model ($B = 0$) Eqs. (4.7) reduce to $\lambda = -\mu = \alpha$, $\nu = \frac{1}{2} + i\delta$. Then, using Eqs. (A.1.2g) and (A.1.2h), Eqs. (4.11) reduce to

$$a = c^* = \pi^{1/2} 2^{-\nu} \Gamma(\nu) \left(\xi + \eta\right), \tag{4.17a}$$

$$b = -d^* = -i\pi^{1/2} 2^{-\nu} \Gamma(\nu) \left(\xi - \eta\right), \tag{4.17b}$$

with

$$\xi = \left[\Gamma\left(\tfrac{1}{4} + \tfrac{1}{2}\alpha + \tfrac{1}{2}i\delta\right) \Gamma\left(\tfrac{3}{4} - \tfrac{1}{2}\alpha + \tfrac{1}{2}i\delta\right)\right]^{-1}, \tag{4.18a}$$

$$\eta = \left[\Gamma\left(\tfrac{3}{4} + \tfrac{1}{2}\alpha + \tfrac{1}{2}i\delta\right) \Gamma\left(\tfrac{1}{4} - \tfrac{1}{2}\alpha + \tfrac{1}{2}i\delta\right)\right]^{-1}. \tag{4.18b}$$

The transition probability reads

$$P_{RZ}^{\phi} = \left\{ \left[\cos\pi\alpha \sin\chi - \sin\pi\alpha \tanh\pi\delta \cos\chi\right] \sin\frac{\phi}{2} + \sin\pi\alpha \,\mathrm{sech}\pi\delta \cos\frac{\phi}{2} \right\}^2, \tag{4.19}$$

where

$$\chi = 2 \arg\left[\Gamma\left(\tfrac{1}{4} - \tfrac{1}{2}\alpha - \tfrac{1}{2}i\delta\right) \Gamma\left(\tfrac{1}{4} + \tfrac{1}{2}\alpha + \tfrac{1}{2}i\delta\right)\right]. \tag{4.20}$$

For $\phi = 0$ Eq. (4.19) reduces to the RZ formula [7]

$$P_{RZ} = \frac{\sin^2\pi\alpha}{\cosh^2\pi\delta}. \tag{4.21}$$

When $\phi = \pm\pi$, Eq. (4.19) coincides with the transition probability in the step-sech model [44].

When $|\alpha + i\delta|$ and δ are large we use Eqs. (A.1.3) and (A.1.4b) to obtain

$$\chi \sim \frac{\pi}{2} + \pi\alpha - \arctan\frac{\delta}{\alpha} - 2e^{-\pi\delta}\cos 2\pi\alpha + \ O(e^{-2\pi\delta}, |\alpha + i\delta|^{-2}), \tag{4.22}$$

and hence

$$P_{RZ}^{\phi} \sim \left[\frac{\alpha}{\sqrt{\alpha^2 + \delta^2}} \left(1 - \frac{2\delta}{\alpha} e^{-\pi\delta}\cos\pi\alpha\right) \sin\frac{\phi}{2} + 2e^{-\pi\delta}\sin\pi\alpha\cos\frac{\phi}{2}\right]^2. \tag{4.23}$$

The transition probability (4.23) can be represented as a sum of two terms, smooth $\overline{P}$ and oscillatory $\widetilde{P}$ (vs α),

$$P_{RZ}^{\phi} = \overline{P} + \widetilde{P}, \tag{4.24a}$$

$$\overline{P} = \frac{\alpha^2}{\alpha^2 + \delta^2} \sin^2\frac{\phi}{2}, \tag{4.24b}$$

$$\widetilde{P} = -\frac{4\alpha\delta}{\alpha^2 + \delta^2} e^{-\pi\delta}\cos\pi\alpha \sin^2\frac{\phi}{2} + \frac{2\alpha}{\sqrt{\alpha^2 + \delta^2}} e^{-\pi\delta}\sin\pi\alpha\sin\phi. \tag{4.24c}$$

In the limit of large coupling ($\alpha \gg \delta$) and sufficiently large detuning ($\delta \gtrsim 1$) one finds $\overline{P} \to \sin^2(\phi/2)$, $\widetilde{P} \to 0$, and hence the transition probability depends only on the parameter ϕ.

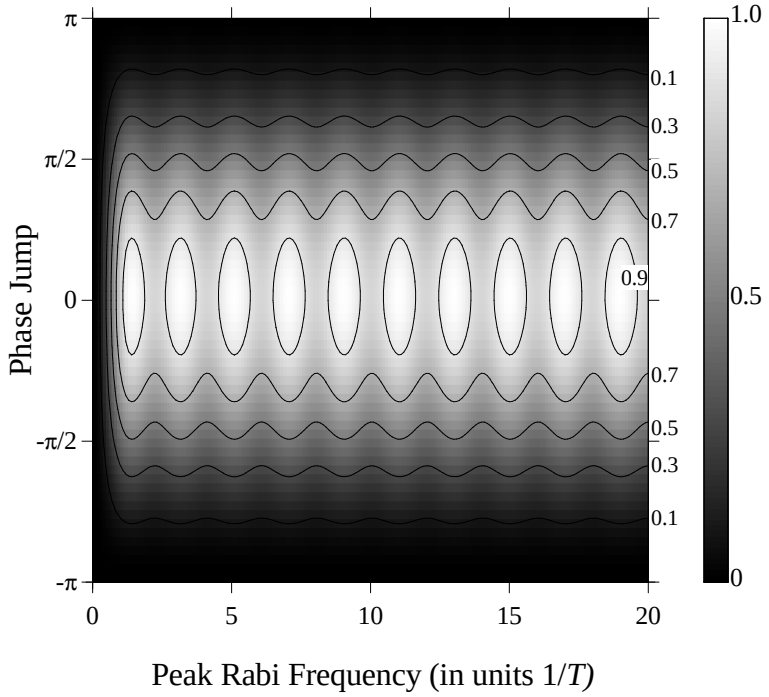

Figure 4.2: Contour plot of the transition probability P_{AE}^{ϕ} for the AE model vs the peak Rabi frequency Ω_0 and the phase jump ϕ for $\Delta_0 = 0$ and $B = 1/T$.

The plot in Fig. 4.1 shows the exact transition probability (4.19) as a function of the peak Rabi frequency Ω_0 and the phase jump ϕ. This plot is reminiscent of the "fitness landscape" plots in optimal control theory [45]. For zero phase jump the transition probability is given by the RZ formula (4.21) and it is small because of the relatively large detuning ($\Delta_0 T = 2$). As the phase ϕ increases the probability landscape is dominated by oscillations, as evident from the exact solution (4.19) and the approximation (4.24).

When $\phi = \pm\pi$ the probability tends to unity for large Ω_0, which leads to complete population inversion [44] as is easily seen from Eqs. (4.24).

4.2.2 Allen-Eberly model ($\Delta_0 = 0$)

For the AE model ($\Delta_0 = 0$), we have $\nu = \frac{1}{2} - i\beta$. Then, using Eq. (A.1.2f), Eqs. (4.11) and (4.13) reduce to

$$a = c = \frac{\sqrt{\pi}\Gamma(\nu)}{\Gamma(\frac{\lambda+1}{2})\Gamma(\frac{\mu+1}{2})}, \tag{4.25a}$$

$$b = d = \frac{2i}{\alpha}\frac{\sqrt{\pi}\Gamma(\nu)}{\Gamma(\frac{\lambda}{2})\Gamma(\frac{\mu}{2})}. \tag{4.25b}$$

The transition probability (4.15) reads

$$P_{AE}^{\phi} = \left(1 - \frac{\cos^2 \pi\sqrt{\alpha^2 - \beta^2}}{\cosh^2 \pi\beta}\right)\cos^2\frac{\phi}{2}. \tag{4.26}$$

For $\phi = 0$, Eq. (4.26) reduces to the AE formula [8]

$$P_{AE} = 1 - \frac{\cos^2 \pi\sqrt{\alpha^2 - \beta^2}}{\cosh^2 \pi\beta}. \tag{4.27}$$

Equation (4.26) shows that the phase ϕ factorizes in the probability. The conditions for complete population inversion are $\phi = 0$ and $\sqrt{\alpha^2 - \beta^2} = n + \frac{1}{2}$, where n is an integer. Moreover, for adiabatic evolution ($\alpha > \beta \gg 1$) and $\phi = 0$, the transition probability tends to unity. A contour plot of the probability (4.26) is presented in Fig. 4.2. For zero jump phase ($\phi = 0$) the transition probability is given by the AE formula (4.27) and exhibits small-amplitude oscillations that regularly touch unity. As the phase ϕ departs from zero, the oscillations in the probability "landscape" gradually decrease.

As the figure demonstrates, and as it is also evident from Eq. (4.26), the transition probability vanishes identically when $\phi = \pm\pi$. The physical reason is that the Hamiltonian is then an antisymmetric function of time, which leads to complete population return (symmetry-forbidden transition) [46].

4.2.3 Bambini-Berman model ($\Delta_0 = B$)

For the BB model ($\Delta_0 = B$), the transition probability (4.15), which is plotted in Fig. 4.3, cannot be expressed by means of simple functions. The probability landscape is dominated by large-amplitude oscillations, ranging from zero to unity, both versus Ω_0 and ϕ. We see areas of complete population inversion for $\phi \approx \pm\pi/2$ and for specific values of Ω_0. We shall explain this unexpected feature in the next section using the adiabatic solution for the DK model.

4.3 Adiabatic solution

We shall now derive the adiabatic solution for the phase-jump DK model (4.2). To this end, it is convenient to write Eqs. (4.1) in the matrix form

$$i\hbar\frac{d}{dt}\mathbf{c}(t) = \mathbf{H}(t)\mathbf{c}(t), \tag{4.28}$$

where $\mathbf{c}(t) = [c_1(t), c_2(t)]^T$ and the Hamiltonian, after a (population-preserving) phase transformation, has the form

$$\mathbf{H} = \frac{\hbar}{2}\begin{bmatrix} -\Delta & \Omega \\ \Omega^* & \Delta \end{bmatrix}, \tag{4.29}$$

The adiabatic states φ_+ and φ_- are defined as eigenstates of the Hamiltonian, $\mathbf{H}(t)\varphi_\pm(t) = \hbar\epsilon_\pm(t)\varphi_\pm(t)$, and the eigenvalues are $\hbar\epsilon_\pm(t)$, with

$$\epsilon_\pm(t) = \pm\frac{1}{2}\sqrt{|\Omega(t)|^2 + \Delta^2(t)}. \tag{4.30}$$

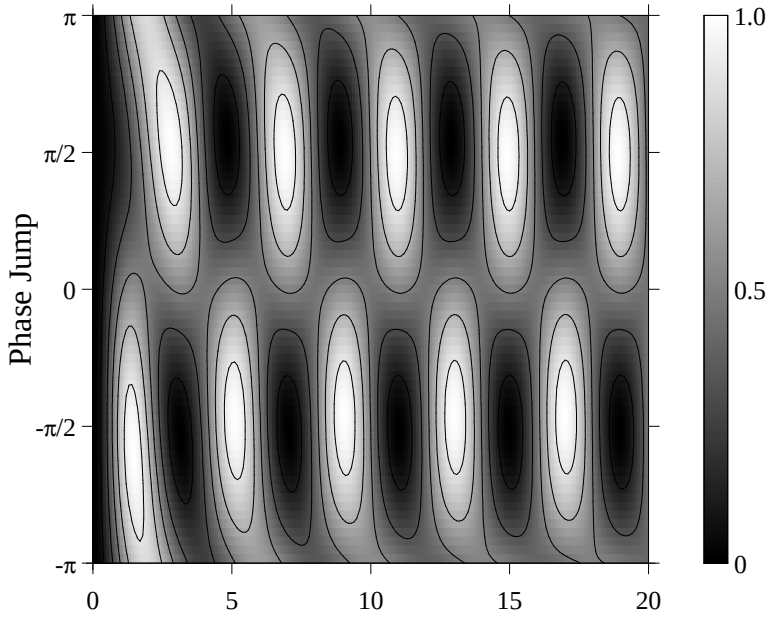

Figure 4.3: Contour plot of the transition probability P_{BB}^{ϕ} for the BB model vs the peak Rabi frequency Ω_0 and the phase jump ϕ for $B = \Delta_0 = 1/T$.

The amplitudes of the adiabatic states $\mathbf{a}(t) = [a_+(t), a_-(t)]^T$ are connected with the diabatic (original) ones $\mathbf{c}(t)$ via the rotating matrix

$$\mathbf{R}(\theta) = \begin{bmatrix} \cos\theta & \sin\theta \\ -\sin\theta & \cos\theta \end{bmatrix} \tag{4.31}$$

as $\mathbf{c}(t) = \mathbf{R}(\theta(t))\mathbf{a}(t)$, where $\theta = \frac{1}{2}\arctan(\Omega/\Delta)$. The Schrödinger equation in the adiabatic basis reads

$$i\hbar\frac{d}{dt}\mathbf{a}(t) = \mathbf{H}_a(t)\mathbf{a}(t), \tag{4.32}$$

where

$$\mathbf{H}_a = \hbar \begin{bmatrix} \epsilon_- & -i\dot{\theta} \\ i\dot{\theta} & \epsilon_+ \end{bmatrix}. \tag{4.33}$$

If $|\dot{\theta}| \ll |\epsilon_\pm| \equiv \epsilon$, then the evolution is adiabatic and the solution for the propagator in the adiabatic basis from an initial time $t = t_i$ to a final time $t = t_f$ reads

$$\mathbf{U}_a(t_f, t_i) = \begin{bmatrix} e^{i\zeta} & 0 \\ 0 & e^{-i\zeta} \end{bmatrix}, \tag{4.34}$$

where $\zeta = \int_{t_i}^{t_f} \epsilon(t)dt$. The full propagator in the original basis for the model (4.2) reads

$$\mathbf{U}(t_f, t_i) = \mathbf{\Phi}^*\mathbf{R}(\theta(t_f))\mathbf{U}_a(t_f, 0)\mathbf{R}(-\theta(0))\mathbf{\Phi}\mathbf{R}(\theta(0))\mathbf{U}_a(0, t_i)\mathbf{R}(-\theta(t_i)), \tag{4.35}$$

with

$$\mathbf{\Phi} = \begin{bmatrix} 1 & 0 \\ 0 & e^{i\phi} \end{bmatrix}. \tag{4.36}$$

Rosen-Zener model ($B = 0$). In this case $\theta(-\infty) = \theta(\infty) = 0$ and $\theta(0) = \frac{1}{2}\arctan(\alpha/\delta)$. The transition probability, obtained as $|U_{12}|^2$ from Eq. (4.35), reads

$$P^a_{RZ} = \frac{\alpha^2}{\alpha^2 + \delta^2} \sin^2 \frac{\phi}{2}, \tag{4.37}$$

which is equal to the probability (4.23) when $\delta \gtrsim 1$ (which is the adiabatic condition for the RZ model).

Allen-Eberly model ($\Delta_0 = 0$). For this model we have $\theta(-\infty) = \pi/2$, $\theta(0) = \pi/4$ and $\theta(\infty) = 0$. Hence we obtain from Eq. (4.35)

$$P^a_{AE} = \cos^2 \frac{\phi}{2}, \tag{4.38}$$

which coincides with the probability (4.26) when $\alpha > \beta \gg 1$ (which is the adiabatic condition for the AE model).

Bambini-Berman model ($B = \Delta_0$). In this case, $\theta(-\infty) = \pi/4$, $\theta(0) = \frac{1}{2}\arctan(\alpha/\beta)$ and $\theta(\infty) = 0$. We obtain from Eq. (4.35)

$$P^a_{BB} = \frac{1}{2} + \frac{1}{2} \sin 2\zeta_0 \sin 2\theta(0) \sin\phi - \frac{1}{2} \cos 2\zeta_0 \sin 4\theta(0) \sin^2 \frac{\phi}{2}, \tag{4.39}$$

where $\zeta_0 = \int_{-\infty}^{0} \frac{1}{2}\sqrt{\Omega^2(t) + \Delta^2(t)}dt$. For $\alpha \gg \beta$, $\theta(0) \approx \pi/4 - \beta/2\alpha$ and Eq. (4.39) reduces to

$$P^a_{BB} \approx \frac{1}{2} + \frac{1}{2} \sin 2\zeta_0 \sin\phi - \frac{\beta}{\alpha} \cos 2\zeta_0 \sin^2 \frac{\phi}{2}. \tag{4.40}$$

Now, when $\phi = \pm\pi/2$ the probability oscillates between zero and unity. From Eq. (4.40) we also see that there is an asymmetry in the maxima and minima for $\phi = \pi/2$ and $\phi = -\pi/2$, as seen in Fig. 4.3.

In Fig. 4.4 we compare the adiabatic solution (4.39) with the exact solution (4.15) for the transition probability vs the peak Rabi frequency Ω_0. We see that the adiabatic solution is indiscernible from the exact solution except for small values of Ω_0. For $\phi = 0$ the adiabatic solution gives a constant transition probability of $\frac{1}{2}$. For $\phi = \pm\frac{\pi}{2}$ it oscillates between zero and unity and finally, for $\phi = \pi$ the transition probability tends to $\frac{1}{2}$ in an oscillatory fashion. The difference between the manner the asymptotic value of $\frac{1}{2}$ is reached for $\phi = 0$ and $\phi = \pi$, which is observed if Fig. 4.4, is easily revealed upon a closer inspection of the adiabatic solution (4.39). Indeed, for $\phi = 0$ only the first term of $\frac{1}{2}$ survives, whereas for $\phi = \pi$ also the last term with $\sin^2(\phi/2)$ is present and it generates oscillations in the transition probability.

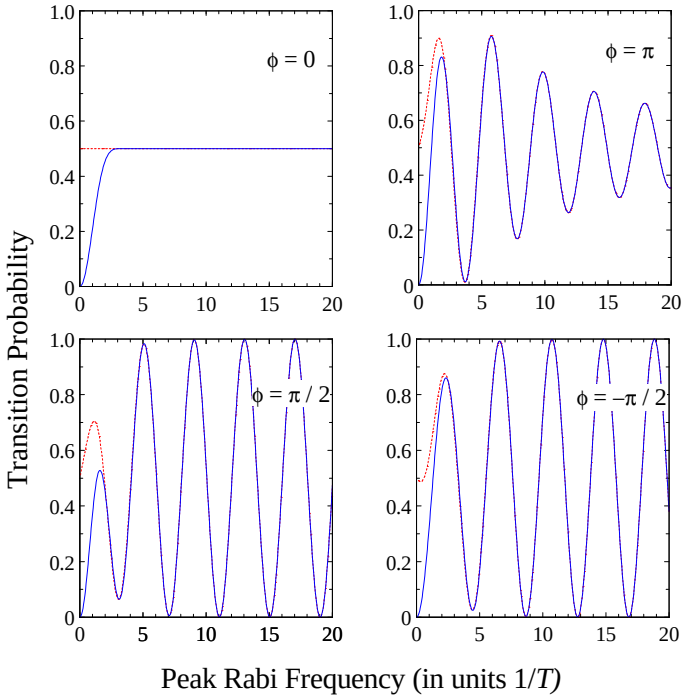

Figure 4.4: Comparison between the exact solution (solid curve) and the adiabatic solution (4.39) (dashed curve) for the Bambini-Berman model (with $B = \Delta_0 = 3/T$) as a function of the peak Rabi frequency Ω_0 for $\phi = 0$, $\phi = \pm\pi/2$ and $\phi = \pi$.

4.4 Experimental implementation

The phase step in the time dependence of the Rabi frequency (4.2a) can be realized by modern femtosecond pulse-shaping technology [17, 28, 47]. The Fourier transform of the pulse (4.2a) is (up to a global phase factor $e^{i\phi/2}$)

$$\widetilde{\Omega}(\omega) = \sqrt{\frac{\pi}{2}}\frac{\cos(\phi/2)}{\cosh(\pi\omega/2)} + \frac{\sin(\phi/2)}{\sqrt{2\pi}}\mathrm{Im}\left[\psi\left(\frac{3+i\omega}{4}\right) - \psi\left(\frac{1+i\omega}{4}\right)\right], \tag{4.41}$$

where $\psi(z)$ is the psi (polygamma) function [48]. This Fourier transform is shown in Fig. 4.5 for phase jumps of $\phi = 0, \pi/2$ and π. The phase jump in the temporal domain makes the Fourier spectrum asymmetric. It is important that this spectrum is modulated by a (rapidly vanishing) pulse-shaped (sech) function of ω, which confines the Fourier spectrum within a limited frequency range. Such a spectrum can therefore be easily produced by modern pulse shapers.

4.5 Conclusions

In this chapter, we have presented an analytically exactly soluble two-state model, in which the time-dependent interaction has a hyperbolic-secant pulse shape, with a phase jump of ϕ at

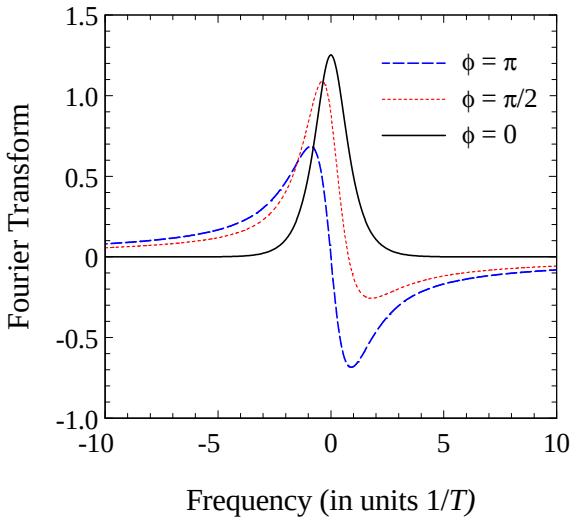

Figure 4.5: Fourier transform of the sech pulse for a jump phase of 0, $\pi/2$ and π.

the time of its maximum. The detuning has a constant part and a hyperbolic-tangent chirp term. For $\phi = 0$, this model reduces to the Demkov-Kunike model, which in turn contains as particular cases three other well-known models: the RZ, AE and BB models. A nonzero ϕ induces dramatic changes in the transition probability, from complete population inversion to complete population return. The analytic results are particularly transparent in the adiabatic limit, which demonstrate that complete population inversion can always occur for a suitable choice of ϕ: for $\phi = \pm\pi$ in the RZ model, for $\phi = 0$ in the AE model, and for $\phi = \pm\pi/2$ in the BB model. The phase ϕ can therefore be used as a control parameter for the two-state transition probability. Moreover, ϕ can serve as a control parameter also when the jump occurs at any other instant of time. However, the present choice of jump at $t = 0$ is the simplest and most natural choice.

The phase effects reported here are not limited to the sech pulse shape or the tanh frequency chirp, as it is evident from the adiabatic solution. For instance, these effects can be demonstrated by Gaussian pulses.

In conclusion, the exact solution derived in this chapter, supported by the adiabatic solution applicable to more general time dependences, clearly demonstrates that a single phase jump in the driving field can be used as an efficient control tool for quantum state engineering. In a future publication we shall describe how phase jumps can be used to steer population transfer in multistate systems.

Chapter 5

Exactly soluble two-state quantum models with linear couplings

Among the exactly soluble models, the Landau-Zener (LZ) model is undoubtedly the most popular one, for it provides a very simple expression for the transition probability across a level crossing. This simplicity is somewhat surprising because the straightforward derivation uses Weber's parabolic cylinder functions, which in the end reduce to a simple exponent. (The LZ phases, though, are more complicated and involve Gamma functions.) One of the unresolved mysteries of the LZ model is that despite its very simple time dependences – linearly changing energies and a constant interaction of infinite duration – it often provides much more accurate results than expected when applied to real physical systems with sophisticated time dependences. Another puzzle is that, when applied to the LZ model, various approximations, such as the Dykhne-Davis-Pechukas approximation [32] and the quasistationary adiabatic-elimination approximation [23], produce the exact result.

In this chapter we use the LZ solution in a different manner: to derive a new class of exact analytical solutions to the two-state problem when the coupling is a linear function of time and the detuning is constant. Because the coupling and the detuning in our model exchange their time dependences in comparison to the LZ model, the Hamiltonians, and the respective propagators, in our model and the LZ model are connected by a basis rotation at an angle $\pi/4$. We use this rotation to derive the propagator and the transition probability for our model in terms of sums of products of Weber functions. We apply this solution to four special cases of physical interest: shark, double-shark, tent and zigzag pulses, each of which exhibits distinctive physical features. In order to reveal these features, we apply two types of asymptotics of the Weber function and derive simpler expressions in terms of elementary functions.

This chapter is organized as follows. We derive the exact analytical solution of the Schrödinger

equation for our general model in Sec. 5.1. In Secs. 5.2-5.5 we present the shark, double-shark, tent and zigzag models. In Sec. 5.6 we derive the respective adiabatic solutions. The conclusions are summarized in Sec. 5.7.

5.1 Exact solution

The time evolution of a coherently driven two-state quantum system is described by two coupled ordinary differential equations for the probability amplitudes $C_1(t)$ and $C_2(t)$ of states ψ_1 and ψ_2,

$$i\hbar\frac{d}{dt}\mathbf{C}(t) = \mathbf{H}(t)\mathbf{C}(t). \tag{5.1}$$

where $\mathbf{C}(t) = [C_1(t), C_2(t)]^T$ is a column vector with the probability amplitudes and

$$\mathbf{H}(t) = \frac{\hbar}{2}\begin{bmatrix} -\Delta(t) & \Omega(t) \\ \Omega(t) & \Delta(t) \end{bmatrix}. \tag{5.2}$$

We shall derive the solution of Eqs. (5.1) for a model, in which the coupling and the detuning are given by

$$\Omega(t) = \begin{cases} \beta^2 t & \text{for } t_i \le t \le t_f, \\ 0 & \text{elsewhere,} \end{cases} \tag{5.3a}$$

$$\Delta(t) = \Delta_0, \tag{5.3b}$$

where β and Δ_0 are assumed positive without loss of generality (our main concern will be the transition probability, which does not depend on the signs of β and Δ_0). The turn-on time t_i and the turn-off time t_f can be positive, negative or zero. The model (5.3) resembles the exactly soluble LZ model [6], where the detuning is a linear function of time and the coupling is constant; here their time dependences are interchanged. The two models are related to each other by a basis rotation at an angle $\pi/4$,

$$\widetilde{\mathbf{C}}(t) = \mathbf{R}(\pi/4)\mathbf{C}(t), \tag{5.4}$$

where $\widetilde{\mathbf{C}}(t) = [\widetilde{C}_1(t), \widetilde{C}_2(t)]^T$ are the probability amplitudes in the LZ model and $\mathbf{R}$ is the rotation matrix

$$\mathbf{R}(\theta) = \begin{bmatrix} \cos\theta & \sin\theta \\ -\sin\theta & \cos\theta \end{bmatrix}. \tag{5.5}$$

The LZ Hamiltonian reads $\widetilde{\mathbf{H}}(t) = \mathbf{R}(\pi/4)\mathbf{H}(t)\mathbf{R}(-\pi/4)$, or

$$\widetilde{\mathbf{H}}(t) = \frac{\hbar}{2}\begin{bmatrix} \beta^2 t & \Delta_0 \\ \Delta_0 & -\beta^2 t \end{bmatrix}. \tag{5.6}$$

The elements of the ensuing LZ propagator $\widetilde{\mathbf{U}}$ read [49]

$$\widetilde{U}_{11}(t_f,t_i) = \frac{\Gamma(1+i\delta^2)}{\sqrt{2\pi}}\left[D_{-i\delta^2}(\alpha_f e^{i\pi/4})D_{-1-i\delta^2}(\alpha_i e^{-3i\pi/4})\right.$$
$$\left. + D_{-i\delta^2}(\alpha_f e^{-3i\pi/4})D_{-1-i\delta^2}(\alpha_i e^{i\pi/4})\right], \tag{5.7a}$$
$$\widetilde{U}_{12}(t_f,t_i) = \frac{\Gamma(1+i\delta^2)}{\delta\sqrt{2\pi}}e^{-i\pi/4}\left[D_{-i\delta^2}(\alpha_f e^{i\pi/4})D_{-i\delta^2}(\alpha_i e^{-3i\pi/4})\right.$$
$$\left. - D_{-i\delta^2}(\alpha_f e^{-3i\pi/4})D_{-i\delta^2}(\alpha_i e^{i\pi/4})\right], \tag{5.7b}$$
$$\widetilde{U}_{21}(t_f,t_i) = -\widetilde{U}^*_{12}(t_f,t_i), \tag{5.7c}$$
$$\widetilde{U}_{22}(t_f,t_i) = \widetilde{U}^*_{11}(t_f,t_i), \tag{5.7d}$$

where $D_\nu(z)$ is Weber's parabolic cylinder function [40] and we have introduced the dimensionless parameters

$$\alpha_i = \beta t_i, \quad \alpha_f = \beta t_f, \quad \delta = \frac{\Delta_0}{2\beta}. \tag{5.8}$$

The parameters α_i and α_f are related to the temporal pulse areas $A_i = \alpha_i^2/2$ and $A_f = \alpha_f^2/2$, respectively, from time $t = 0$ to time t_i or t_f.

The propagator of our system $\mathbf{U}$, defined by the relation $\mathbf{C}(t_f) = \mathbf{U}(t_f,t_i)\mathbf{C}(t_i)$, is connected to the LZ propagator $\widetilde{\mathbf{U}}$ as $\mathbf{U}(t_f,t_i) = \mathbf{R}(-\pi/4)\widetilde{\mathbf{U}}(t_f,t_i)\mathbf{R}(\pi/4)$; explicitly

$$\mathbf{U}(t_f,t_i) = \begin{bmatrix} \mathrm{Re}\widetilde{U}_{11} - i\mathrm{Im}\widetilde{U}_{12} & \mathrm{Re}\widetilde{U}_{12} + i\mathrm{Im}\widetilde{U}_{11} \\ -\mathrm{Re}\widetilde{U}_{12} + i\mathrm{Im}\widetilde{U}_{11} & \mathrm{Re}\widetilde{U}_{11} + i\mathrm{Im}\widetilde{U}_{12} \end{bmatrix}. \tag{5.9}$$

Therefore the transition probability is

$$P = |U_{21}|^2 = (\mathrm{Re}\widetilde{U}_{12})^2 + (\mathrm{Im}\widetilde{U}_{11})^2. \tag{5.10}$$

Two asymptotic behaviors are of particular interest: (i) the large area and small detuning ($\alpha \gg \delta, 1$) asymptotics (to be referred to as *asymptotics I*), and (ii) the large area and large detuning ($\alpha, \delta \gg 1$) asymptotics (to be referred to as *asymptotics II*), with $\alpha = |\alpha_i|$ or α_f. The (perturbation theory) limit of small areas ($\alpha \ll 1$) is not interesting for it produces a very small transition probability; interesting features appear for sufficiently strong fields. According to Eqs. (5.7), asymptotics I requires the conventional large-argument asymptotics of the Weber function [40]. Asymptotics II requires the lesser known large-argument-and-large-order asymptotics of the Weber function, which has been derived by Olver in the general case [50]; the explicit expressions [49] for the particular Weber functions involved in the LZ model are supplied in the Appendix.

In the next sections we will consider four exactly soluble models of physical interest, which are special cases, or variations, of the above model. The detuning is constant in all cases and the Rabi frequencies of these models are shown in Fig. 5.1.

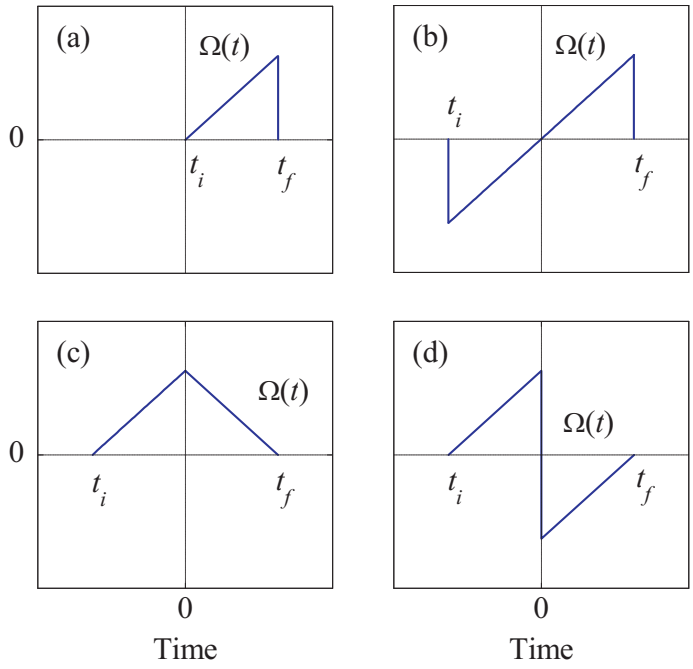

Figure 5.1: Time dependences of the Rabi frequencies of the models considered in this chapter. (a) shark pulse; (b) double-shark pulse; (c) tent pulse; (d) zigzag pulse.

5.2 Shark pulse

We begin with a model in which the interaction begins at time $t_i = 0$ and ends at time $t_f = \tau > 0$, thereby forming a triangular "shark fin" pattern, as illustrated in Fig. 5.1(a). By using Eq. (A.2.6) the LZ propagator elements (5.7) become $\widetilde{U}_{11}(\tau, 0) = a$ and $\widetilde{U}_{12}(\tau, 0) = b$, with

$$a = \frac{2^{i\delta^2/2}}{2\sqrt{\pi}}\Gamma(\tfrac{1}{2} + \tfrac{1}{2}i\delta^2)\Big[(1 + e^{-\pi\delta^2})D_{-i\delta^2}(\alpha e^{i\pi/4}) - \frac{i\sqrt{2\pi}}{\Gamma(i\delta^2)}e^{-\pi\delta^2/2}D_{-1+i\delta^2}(\alpha e^{-i\pi/4})\Big], \tag{5.11a}$$

$$b = \frac{2^{i\delta^2/2}}{\delta\sqrt{2\pi}}\Gamma(1 + \tfrac{1}{2}i\delta^2)e^{-i\pi/4}\Big[(1 - e^{-\pi\delta^2})D_{-i\delta^2}(\alpha e^{i\pi/4}) + \frac{i\sqrt{2\pi}}{\Gamma(i\delta^2)}e^{-\pi\delta^2/2}D_{-1+i\delta^2}(\alpha e^{-i\pi/4})\Big], \tag{5.11b}$$

with $\alpha = \beta\tau$. The shark propagator reads $\mathbf{U}(\tau, 0) = \mathcal{U}$, with

$$\mathcal{U} = \begin{bmatrix} \mathrm{Re}a - i\mathrm{Im}b & \mathrm{Re}b + i\mathrm{Im}a \\ -\mathrm{Re}b + i\mathrm{Im}a & \mathrm{Re}a + i\mathrm{Im}b \end{bmatrix}. \tag{5.12}$$

We shall use this propagator $\mathcal{U}$ to express the propagators for the other three models in the next sections. The exact transition probability for the shark model is

$$P = (\mathrm{Im}a)^2 + (\mathrm{Re}b)^2. \tag{5.13}$$

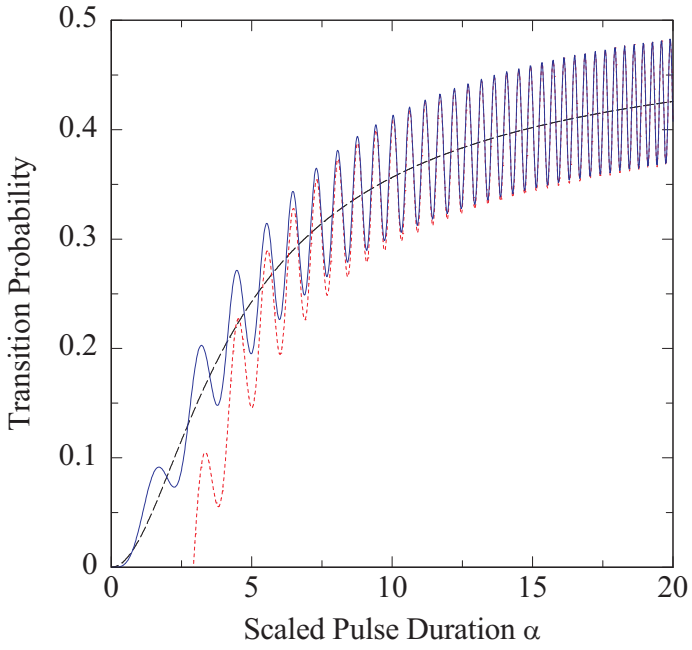

Figure 5.2: The transition probability for a *shark pulse* vs the dimensionless parameter α for $\delta = 1.5$. The solid curve shows the exact values (5.13), the short-line dashed curve shows asymptotics I (5.14) and the long-line dashed curve is asymptotics II (5.16).

Asymptotics I for the transition probability is derived by using Eq. (A.2.7),

$$\begin{aligned} P \;\sim\; & \tfrac{1}{2}(1-e^{-\pi\delta^2})\cos^2\phi_1 + \tfrac{1}{2}(1+e^{-\pi\delta^2})\sin^2\phi_2 \\ & -\frac{\delta}{\alpha}\sqrt{1-e^{-2\pi\delta^2}}\;\cos\left(\phi_1-\phi_2\right) \quad (\alpha \gg 1, \delta), \end{aligned} \tag{5.14}$$

where

$$\phi_1 = \arg\Gamma(1-\tfrac{1}{2}i\delta^2) + \frac{\alpha^2}{4} + \frac{\delta^2}{2}\ln\frac{\alpha^2}{2} + \frac{\pi}{4}, \tag{5.15a}$$

$$\phi_2 = \arg\Gamma(\tfrac{1}{2}-\tfrac{1}{2}i\delta^2) + \frac{\alpha^2}{4} + \frac{\delta^2}{2}\ln\frac{\alpha^2}{2}. \tag{5.15b}$$

We conclude that for large α the transition probability oscillates vs α with an amplitude depending on δ: for small δ ($\delta \lesssim 1$) the oscillation amplitude is large, while for large δ it decreases rapidly. These oscillations can be seen in Fig. 5.2 where the transition probability is plotted as a function of α. The asymptotics (5.14) is seen to match the exact values increasingly well as α increases.

Asymptotics II for P is derived by using Eqs. (A.2.9),

$$P \sim \tfrac{1}{2} - \frac{\delta}{\sqrt{\alpha^2+4\delta^2}} \quad (\alpha, \delta \gg 1). \tag{5.16}$$

This expression, and the comparison with Eq. (5.14), demonstrate that the increasing δ damps the oscillations. In the limit $\alpha \gg \delta \gg 1$, we find $P \sim \frac{1}{2} - \delta/\alpha$, that is the probability tends

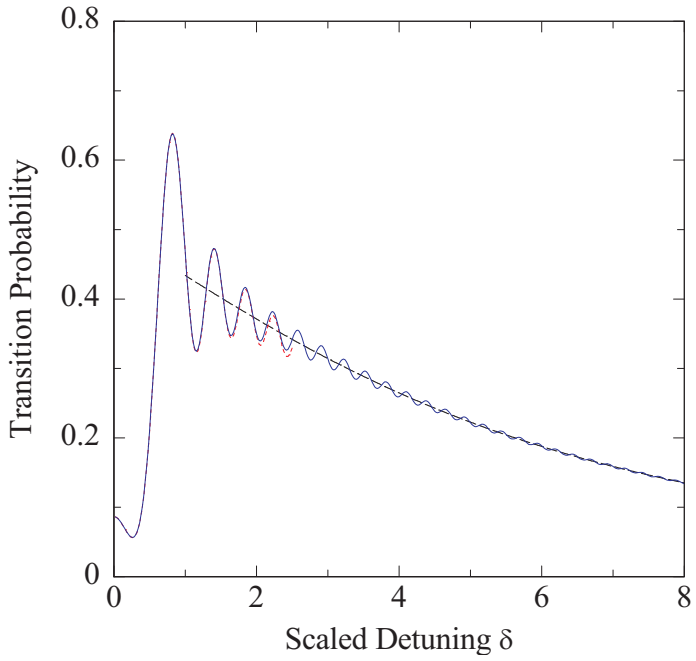

Figure 5.3: The transition probability for a *shark pulse* vs the dimensionless parameter δ for $\alpha = 15$. The solid curve shows the exact values (5.13), the short-line dashed curve is asymptotics I (5.14) and the long-line dashed curve is asymptotics II (5.16).

to $\frac{1}{2}$, a characteristic feature for asymmetric pulses in the adiabatic limit [51]. The same result can be obtained from Eq. (5.14) if we demand $\delta \gg 1$ and use the Stirling asymptotics for the Gamma functions [40] in the phases ϕ_1 and ϕ_2 to find

$$\phi_1 - \phi_2 \sim \frac{1}{4\delta^2} \quad (\delta \gg 1). \tag{5.17}$$

On the contrary, in the limit $\delta \gg \alpha \gg 1$, we find $P \sim \alpha^2/16\delta^2$; hence the probability vanishes as δ^{-2} as δ increases. This latter feature is characteristic for models (e.g., the Rabi model) in which the coupling has sudden changes (discontinuities), such as the sudden termination of the shark pulse at $t_f = \tau$. This feature is illustrated in Fig. 5.3 where the transition probability is plotted as a function of δ. The small-δ asymptotics (5.14) is seen to provide a good fit to the exact values in its domain of validity. The large-δ asymptotics (5.16) describes very accurately the average value of P in both Figs. 5.2 and 5.3.

5.3 Double-shark pulse

We now turn to the double-shark pulse, for which $t_i = -\tau$ and $t_f = \tau$, as displayed in Fig. 5.1(b). To find the propagator for this model we separate the interaction into two parts: from $t_i = -\tau$ to $t = 0$, and from $t = 0$ to $t_f = \tau$. The propagator $\mathbf{U}(\tau, 0)$ in the interval $[0, \tau]$ is the same as the one (5.12) for the shark pulse in the preceding section, $\mathbf{U}(\tau, 0) = \mathcal{U}$. From

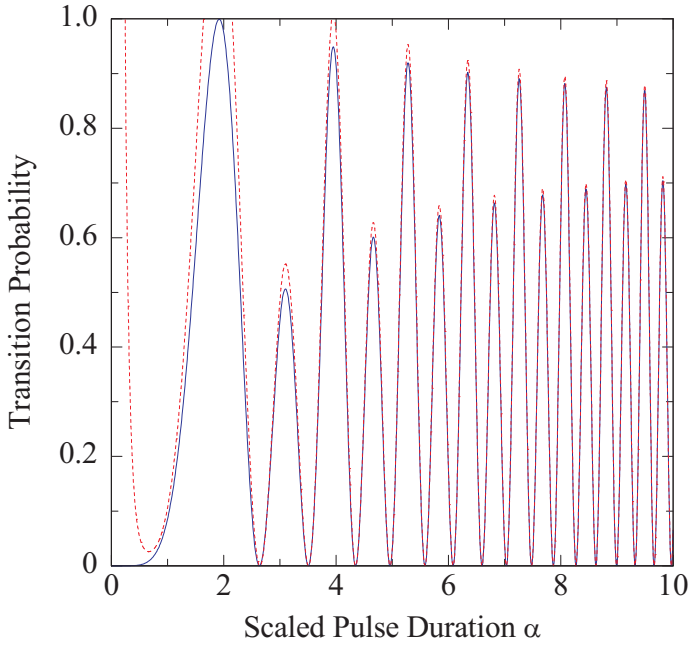

Figure 5.4: The transition probability for a *double-shark pulse* vs the dimensionless parameter α for $\delta = 0.5$. The solid curve shows the exact values (5.19) and the dashed curve is asymptotics I (5.20).

the symmetry of the Schrödinger equation it can easily be shown that the propagator for the interval $[-\tau, 0]$ is expressed with the help of the Pauli matrix σ_3 as $\mathbf{U}(0,-\tau) = \sigma_3 \mathcal{U}^T \sigma_3$. The full propagator reads $\mathbf{U}(\tau,-\tau) = \mathbf{U}(\tau,0)\mathbf{U}(0,-\tau) = \mathcal{U}\,\sigma_3 \mathcal{U}^T \sigma_3$, or explicitly,

$$\mathbf{U}(\tau,-\tau) = \begin{bmatrix} (\mathrm{Re}a - i\mathrm{Im}b)^2 - (\mathrm{Re}b + i\mathrm{Im}a)^2 & 2(\mathrm{Re}a\mathrm{Re}b - \mathrm{Im}a\mathrm{Im}b) \\ -2(\mathrm{Re}a\mathrm{Re}b - \mathrm{Im}a\mathrm{Im}b) & (\mathrm{Re}a + i\mathrm{Im}b)^2 - (\mathrm{Re}b - i\mathrm{Im}a)^2 \end{bmatrix}. \tag{5.18}$$

The exact transition probability is therefore

$$P = 4(\mathrm{Re}a\mathrm{Re}b - \mathrm{Im}a\mathrm{Im}b)^2. \tag{5.19}$$

We point out that the transition probability for this pulse can be derived directly from the general formulae (5.7) and (5.10) because the double-shark model is a special case of the general model (5.3) for $t_i = -\tau$ and $t_f = \tau$. However, the approach we use is more instructive and applicable to the other models that follow.

Asymptotics I for P is derived by using Eq. (A.2.7),

$$P \sim \left[\sqrt{1 - e^{-2\pi\delta^2}}\cos(\phi_1 + \phi_2) - \frac{2\delta e^{-\pi\delta^2}}{\alpha}\right]^2 \quad (\alpha \gg 1, \delta). \tag{5.20}$$

This asymptotics is shown in Fig. 5.4 versus α and compared with the exact solution (5.19). The oscillations in Eq. (5.20) have an amplitude which tends to a constant value when α increases; this value is determined by δ.

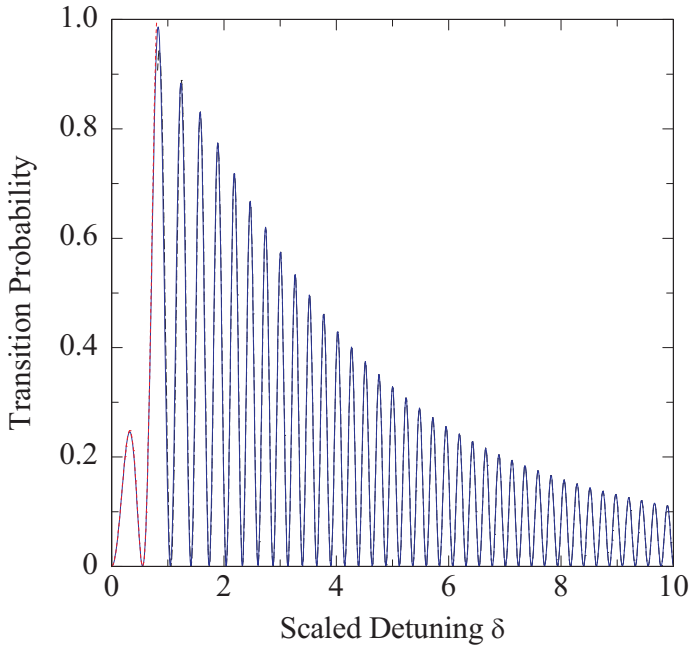

Figure 5.5: The transition probability for a *double-shark pulse* vs the dimensionless parameter δ for $\alpha = 7$. The solid curve shows the exact values (5.19), the short-line dashed curve is asymptotics I (5.20) and the long-line dashed curve is asymptotics II (5.21) (barely discernible).

Asymptotics II is obtained by using Eqs. (A.2.9),

$$P \sim \frac{\alpha^2}{\alpha^2+4\delta^2}\cos^2\left(\frac{\alpha}{2}\sqrt{\alpha^2+4\delta^2}+2\delta^2\ln\frac{\alpha+\sqrt{\alpha^2+4\delta^2}}{2\delta}\right) \quad (\alpha,\delta\gg 1); \tag{5.21}$$

hence the oscillations survive even for large δ. The oscillation amplitude is damped vs δ in a Lorentzian manner. On the contrary, it approaches unity as α increases; the same result follows from Eq. (5.20) in the limit $\alpha \gg \delta \gg 1$.

The transition probability P is plotted in Fig. 5.5 as a function of δ. An excellent agreement is observed between the asymptotics (5.20) and (5.21) and the exact values.

The oscillations that dominate both Figs. 5.4 and 5.5 originate from the presence of two clearly separated parts of the interaction: one for $t < 0$ and another for $t > 0$, which is reminiscent of Ramsey-type interference. This feature is the physical reason for the presence of considerably more oscillations for the double-shark pulse compared to the shark pulse.

The double-shark pulse is remarkable in another aspect: it has a zero pulse area. Such pulses produce no excitation on resonance ($\delta = 0$). However, they can produce considerable excitation off resonance; this problem has been studied in detail elsewhere [44, 52]. Indeed, as visible in both Figs. 5.4 and 5.5, for suitable values of the detuning and the coupling, the transition probability may even reach unity.

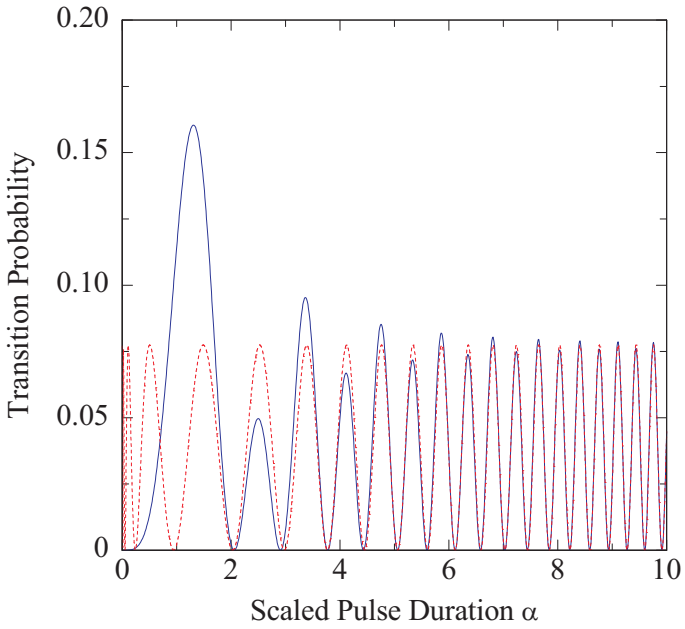

Figure 5.6: The transition probability for a *tent pulse* vs the dimensionless parameter α for $\delta = 1$. The solid curve depicts the exact values (5.23) and the dashed curve is asymptotics I (5.24).

5.4 Tent pulse

The tent model is not a special case of the model (5.3), but has a linear coupling with a positive slope from $t_i = -\tau$ to $t = 0$ and a negative slope (with the same absolute value) from $t = 0$ to $t_f = \tau$, as shown in Fig. 5.1(c). As in Sec. 5.3, we exploit the symmetry of the Schrödinger equation to find $\mathbf{U}(0, -\tau) = \mathcal{U}$ and $\mathbf{U}(\tau, 0) = \mathcal{U}^T$. The full propagator is $\mathbf{U}(\tau, -\tau) = \mathcal{U}^T\mathcal{U}$, or explicitly,

$$\mathbf{U}(\tau,-\tau) = \begin{bmatrix} (\mathrm{Re}a - i\mathrm{Im}b)^2 + (\mathrm{Re}b - i\mathrm{Im}a)^2 & 2i(\mathrm{Re}a\mathrm{Im}a - \mathrm{Re}b\mathrm{Im}b) \\ 2i(\mathrm{Re}a\mathrm{Im}a - \mathrm{Re}b\mathrm{Im}b) & (\mathrm{Re}a + i\mathrm{Im}b)^2 + (\mathrm{Re}b + i\mathrm{Im}a)^2 \end{bmatrix}. \tag{5.22}$$

The exact transition probability reads

$$P = 4(\mathrm{Re}a\mathrm{Im}a - \mathrm{Re}b\mathrm{Im}b)^2. \tag{5.23}$$

Asymptotics I for P is derived by using Eq. (A.2.7),

$$P \sim \tfrac{1}{4}\left[(1 - e^{-\pi\delta^2})\sin 2\phi_1 - (1 + e^{-\pi\delta^2})\sin 2\phi_2\right]^2 \quad (\alpha \gg 1, \delta). \tag{5.24}$$

The amplitude of the oscillations in Eq. (5.24) is constant vs α, as indeed seen in Fig. 5.6 for large α. A good agreement is observed between the exact probability (5.23) and its asymptotics (5.24).

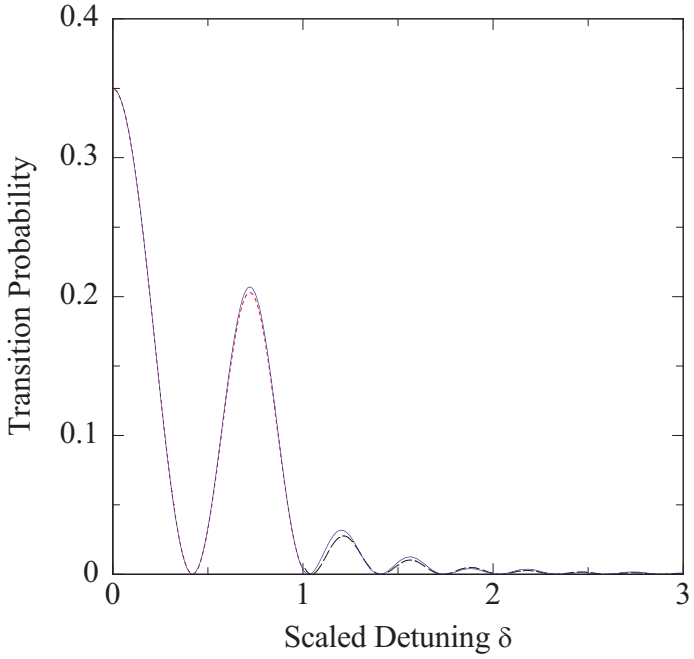

Figure 5.7: The transition probability for a *tent pulse* vs the dimensionless parameter δ for $\alpha = 7$. The solid curve shows the exact values (5.23), the short-line dashed curve is asymptotics I (5.24) and the long-line dashed curve is asymptotics II (5.25).

Asymptotics II is obtained by using Eqs. (A.2.9); it reads

$$P \sim \frac{1}{16\delta^4} \cos^2 \left(\frac{\alpha}{2} \sqrt{\alpha^2 + 4\delta^2} + 2\delta^2 \ln \frac{\alpha + \sqrt{\alpha^2 + 4\delta^2}}{2\delta} \right) \quad (\alpha, \delta \gg 1). \tag{5.25}$$

The transition probability P decreases vs δ as δ^{-4}, i.e. faster than for the shark and double-shark pulses, where $P \sim \delta^{-2}$. The reason is the absence of a discontinuity in the Hamiltonian for the tent pulse; however, there is a discontinuity in the adiabatic basis, which results in the polynomial δ^{-4}-dependence. The rapid decrease of these oscillations vs δ is indeed observed in Fig. 5.7. A very good agreement between the exact probability (5.23) and the asymptotics is found once again.

5.5 Zigzag pulse

The zigzag pulse, seen in Fig. 5.1(d), has a linearly increasing coupling from $t_i = -\tau$ to $t = 0$, with a sudden sign jump at $t = 0$, followed by another linear change from $t = 0$ to $t_f = \tau$. From the symmetry of the Schrödinger equation, as in Secs. 5.3 and 5.4, we find $\mathbf{U}(0, -\tau) = \mathcal{U}$ and $\mathbf{U}(\tau, 0) = \sigma_3 \mathcal{U}^T \sigma_3$. The full propagator is $\mathbf{U}(\tau, -\tau) = \sigma_3 \mathcal{U}^T \sigma_3 \mathcal{U}$; explicitly,

$$\mathbf{U}(\tau, -\tau) = \begin{bmatrix} (\mathrm{Re}a - i\mathrm{Im}b)^2 - (\mathrm{Re}b - i\mathrm{Im}a)^2 & 2(\mathrm{Re}a\mathrm{Re}b + \mathrm{Im}a\mathrm{Im}b) \\ -2(\mathrm{Re}a\mathrm{Re}b + \mathrm{Im}a\mathrm{Im}b) & (\mathrm{Re}a + i\mathrm{Im}b)^2 - (\mathrm{Re}b + i\mathrm{Im}a)^2 \end{bmatrix}. \tag{5.26}$$

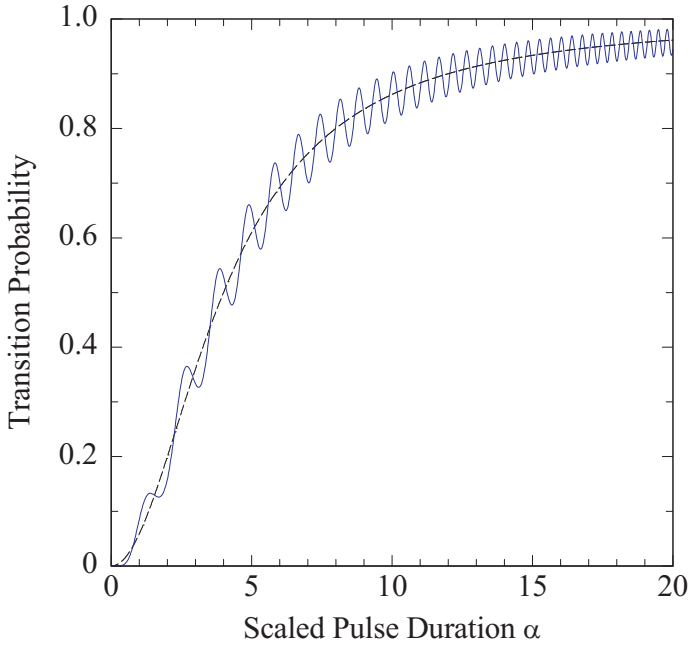

Figure 5.8: The transition probability for a *zigzag pulse* vs the dimensionless parameter α for $\delta = 2$. The solid curve is the exact probability (5.27) and the long-line dashed curve is asymptotics II (5.29).

Hence the exact transition probability reads

$$P = 4(\mathrm{Re}a\mathrm{Re}b + \mathrm{Im}a\mathrm{Im}b)^2. \tag{5.27}$$

Asymptotics I for P is obtained by using Eq. (A.2.7),

$$\begin{aligned} P \;\sim\; & \left\{ \sqrt{1-e^{-2\pi\delta^2}}\cos(\phi_1-\phi_2) \right. \\ & \left. +\frac{\delta}{\alpha}\left[(1-e^{-\pi\delta^2})\cos 2\phi_1 - (1+e^{-\pi\delta^2})\cos 2\phi_2\right] \right\}^2 \quad (\alpha \gg 1, \delta). \end{aligned} \tag{5.28}$$

Asymptotics II is obtained by using Eqs. (A.2.9); it reads

$$P \sim \frac{\alpha^2}{\alpha^2+4\delta^2} \quad (\alpha, \delta \gg 1). \tag{5.29}$$

The transition probability P is plotted in Fig. 5.8 as a function of α; it exhibits damped oscillations and tends to a value that depends on δ; for sufficiently large δ this value is close to unity. The asymptotics (5.29) describes very accurately the mean value of P.

Figure 5.9 shows P as a function of δ. The asymptotics (5.28) and (5.29) match very well the exact solution (5.27) once again. The Lorentzian decrease of P vs δ is a consequence of the discontinuity at time $t = 0$.

There is an interesting feature of this model, visible in Eq. (5.29): when $\alpha \gg \delta \gg 1$ we have $P \to 1$, which implies CPI. This CPI is caused by a δ-function-shaped nonadiabatic

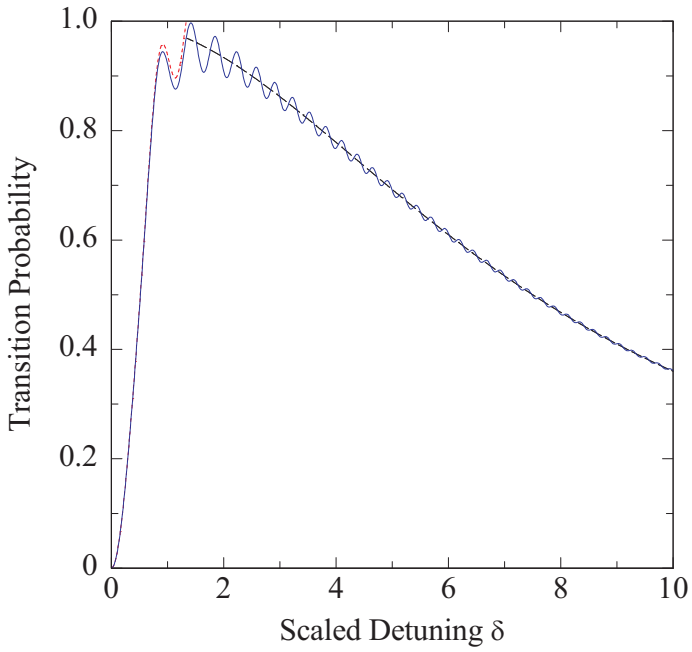

Figure 5.9: The transition probability for a *zigzag pulse* vs the dimensionless parameter δ for $\alpha = 15$. The solid curve shows the exact probability (5.27), the short-line dashed curve is asymptotics I (5.28) and the long-line dashed curve is asymptotics II (5.29).

coupling in the adiabatic basis as discussed elsewhere [44, 52]; it is encountered here too. A nearly complete inversion is seen in Fig. 5.9 for $\delta \approx 1$ to 3. For this CPI, both conditions $\delta \gg 1$ and $\alpha \gg \delta$ are essential; because α is only moderately large ($\alpha = 15$), these conditions are satisfied approximately only in a limited range of δ.

5.6 Adiabatic solution

We shall now derive the adiabatic solution for the general model (5.3) and the other four special models above. The adiabatic states $\varphi_+(t)$ and $\varphi_-(t)$ are defined as the eigenstates of the Hamiltonian (5.2), $\mathbf{H}(t)\varphi_\pm(t) = \hbar\epsilon_\pm(t)\varphi_\pm(t)$, with eigenvalues $\hbar\epsilon_\pm(t) = \pm\hbar\epsilon(t)$, where

$$\epsilon(t) = \tfrac{1}{2}\sqrt{\Omega^2(t) + \Delta^2(t)}. \tag{5.30}$$

The amplitudes of the adiabatic states $\mathbf{A}(t) = [A_+(t), A_-(t)]^T$ are connected with the original ones $\mathbf{C}(t)$ via the rotation matrix (5.5) as $\mathbf{C}(t) = \mathbf{R}(\theta(t))\mathbf{A}(t)$, where $\theta(t) = \frac{1}{2}\arctan[\Omega(t)/\Delta]$. The Schrödinger equation in the adiabatic basis reads

$$i\hbar\frac{d}{dt}\mathbf{A}(t) = \mathbf{H}_A(t)\mathbf{A}(t), \tag{5.31}$$

where

$$\mathbf{H}_A = \hbar\begin{bmatrix} \epsilon_- & -i\dot{\theta} \\ i\dot{\theta} & \epsilon_+ \end{bmatrix}. \tag{5.32}$$

If $|\dot{\theta}| \ll \epsilon$, then the evolution is adiabatic and the solution for the propagator in the adiabatic basis from time t_i to time t_f reads

$$\mathbf{U}_A(t_f, t_i) = \begin{bmatrix} e^{i\zeta} & 0 \\ 0 & e^{-i\zeta} \end{bmatrix}, \tag{5.33}$$

where

$$\zeta = \int_{t_i}^{t_f} \epsilon(t)dt = \left[\tfrac{1}{4}\alpha\sqrt{4\delta^2+\alpha^2} + \delta^2 \ln(\alpha + \sqrt{4\delta^2+\alpha^2})\right]_{\alpha_i}^{\alpha_f}. \tag{5.34}$$

The full propagator in the original basis for the model (5.3) reads

$$\mathbf{U}_{\text{adiab}}(t_f, t_i) = \mathbf{R}(\theta_f)\mathbf{U}_A(t_f, t_i)\mathbf{R}(-\theta_i), \tag{5.35}$$

with $\theta_{i,f} = \theta(t_{i,f})$. The adiabatic transition probability in the original basis is

$$P_{\text{adiab}} = \tfrac{1}{2} - \tfrac{1}{2}\frac{\Delta^2}{\epsilon(t_i)\epsilon(t_f)} - \tfrac{1}{2}\frac{\Omega(t_i)\Omega(t_f)}{\epsilon(t_i)\epsilon(t_f)}\cos 2\zeta. \tag{5.36}$$

Shark model ($t_i = 0$). The adiabatic transition probability of this model reads

$$P_{\text{adiab}} = \tfrac{1}{2} - \frac{\delta}{\sqrt{\alpha^2+4\delta^2}}, \tag{5.37}$$

which coincides with asymptotics II (5.16).

Double-shark model ($t_i = -t_f$). For this model we find

$$P_{\text{adiab}} = \frac{\alpha^2}{\alpha^2+4\delta^2}\cos^2\zeta, \tag{5.38}$$

which is equal to asymptotics II (5.21).

Tent model. For this model, the adiabatic solution reads

$$P_{\text{adiab}} = 0. \tag{5.39}$$

Zigzag model. In this model we have to account for the jump in $\Omega(t)$ at $t = 0$, see Fig. 5.1(d). This discontinuity causes a delta-function behaviour of the nonadiabatic coupling $\dot{\theta}(t)$ in the same point $t = 0$, which in turn causes a transition between the adiabatic states with an area equal to the area of the delta-function feature, which is $\theta_0 = \arctan(\alpha/2\delta)$. The propagator that describes this transition in the adiabatic basis is $\mathbf{R}(\theta_0)$. Hence the propagator $\mathbf{U}_A(t_f, t_i)$ in Eq. (5.35) is split by this transition and should be replaced by the sandwich $\mathbf{U}_A(t_f, 0)\mathbf{R}(\theta_0)\mathbf{U}_A(0, t_i)$. Hence the propagator in the original basis reads

$$\mathbf{U}_{\text{adiab}}(t_f, t_i) = \mathbf{R}(\theta_f)\mathbf{U}_A(t_f, 0)\mathbf{R}(\theta_0)\mathbf{U}_A(0, t_i)\mathbf{R}(-\theta_i). \tag{5.40}$$

with $\theta_f = \theta_i = 0$ now. After simple algebra the transition probability is obtained as

$$P_{\text{adiab}} = \frac{\alpha^2}{\alpha^2+4\delta^2}, \tag{5.41}$$

which is the same as asymptotics II (5.29).

It is evident from the above results that the adiabatic solution coincides with asymptotics II, which required $\alpha, \delta \gg 1$. A closer inspection of the adiabatic condition reveals that the adiabatic condition $|\dot{\theta}(t)| \ll \epsilon(t)$ translates into $2\delta \ll (\beta^2 t^2 + 4\delta^2)^{3/2}$. We notice that this condition is satisfied least well for $t = 0$; there the adiabatic condition reduces to

$$4\delta^2 \gg 1. \tag{5.42}$$

Hence, even only a moderately large δ ($\delta \gtrsim 1$) is sufficient to enforce adiabatic evolution.

The apparent discrepancy for the tent model, where the adiabatic solution produces a null probability, indicates that the respective asymptotics II (5.25) is of superadiabatic nature.

5.7 Conclusions

In this chapter, we have presented an analytically exactly soluble two-state model, in which the Rabi frequency is a linear function of time with a finite duration and the detuning is constant. This model is reminiscent of the famous Landau-Zener model where, however, the Rabi frequency is constant and the detuning is linear. Because the Hamiltonians, and the propagators, for these two models are related to each other by a basis rotation at an angle of $\pi/4$, we have used the known LZ solution to derive the propagator for the present model. The exact evolution matrix in the general case is expressed in terms of sums of products of parabolic cylinder functions $D_\nu(z)$.

We point out here that, without the basis rotation, the straightforward solution of the Schrödinger equation (5.1) leads to the Heun equation, and hence the propagator is expressed in terms of the Heun function; the latter is, however, much less studied than the Weber function and little is known, for instance, about its asymptotic expansions. In fact, the two approaches, with and without a basis rotation, allow one to derive interesting representations of the Heun functions as sums of products of Weber functions, unknown hitherto; this topic, however, lies outside the scope of this chapter and will be discussed elsewhere.

Several approximations in terms of simpler functions have been derived based on (i) the large-argument asymptotics of $D_\nu(z)$, and (ii) the large-argument-and-large-order asymptotics of $D_\nu(z)$. The former of these corresponds to a peak Rabi frequency much larger than the detuning and the inverse time duration $1/\tau$, whereas the latter requires that the peak Rabi frequency and the detuning are simultaneously much larger than $1/\tau$. These approximations have been applied to several physically distinct models. The *shark pulse* is an example of an asymmetric pulse. The antisymmetric *double-shark pulse* is an example of a pulse with zero

area, and also a pulse composed of two separated parts, similar to a Ramsey interferometer. The *tent model* is an example of a symmetric pulse, which experiences complete population return in the adiabatic limit. Finally, the *zigzag model* has a sign jump in the coupling at $t = 0$; it produces complete population inversion for sufficiently large Rabi frequency and detuning, despite its overall zero pulse area. All derived asymptotics fit very accurately the exact values in the relevant domains.

Chapter 6

Navigation between quantum states by quantum mirrors

Quantum state engineering in atoms and molecules traditionally uses three basic techniques for transfer of population, complete or partial, from one bound energy state to another, single or superposition state: resonant pulses of precise areas (e.g. π pulses in a two-state system or generalized π pulses for multiple states) [1], adiabatic passage using one or more level crossings [15], or stimulated Raman adiabatic passage (STIRAP) and its extensions [21]. All these techniques require the system to be initially in a single energy state; such a state can be easily prepared experimentally, e.g. by optical pumping. Some of these techniques are "tuned" to a specific initial condition: for example, STIRAP requires a counterintuitive pulse sequence to transfer population from state 1 to 3 in a 1-2-3 linkage, but it is largely irrelevant if the system starts in states 2 or 3 (with some exceptions for state 3) [21]. In other words, STIRAP is (very) useful in producing only one column (the first) of the unitary propagator. Similar conclusions apply, to a large extent, also to the other two techniques using pulse areas and level crossings.

These traditional techniques resolve only a small (although important) part of the general problem of quantum state engineering: given the initial and final states of an N-state system, find a physical set of operations that connect them. This problem requires the construction of the entire propagator, not just a single column or row.

In this chapter we introduce a technique for full quantum state engineering, which produces in a systematic manner a propagator that can connect any two preselected superposition states of an N-state quantum system, representing a *qunit* in quantum information [3, 4]. The two states can be pure as well as mixed, and the latter may have the same or different sets of dynamic invariants (constants of motion). The solution consists of two steps: first, find a propagator that connects the two states, and second, find a physical realization of this propagator.

The first part is the mathematical solution of this inverse problem in quantum mechanics, and the solution is different for three types of problems: (i) pure-to-pure states; (ii) mixed-to-mixed states with the same invariants; (iii) mixed-to-mixed states with different invariants. The case (iii), for instance, contains the important problem of engineering an arbitrary preselected mixed state and we pay special attention to it. In this latter respect our exact analytic results are alternative to the (approximate) numeric optimization procedure proposed by Karpati *et al* [53]; moreover, our approach allows one to engineer any preselected mixed state, whereas the method of Karpati *et al* [53] can only produce a class of mixed states.

The second part of the solution is the physical realization of the respective propagator. For this we use the recently introduced physical implementation of the quantum Householder reflection (QHR) [39, 54] and we show that QHR is a very powerful tool for quantum state engineering. Remarkably, in case (i) only a single QHR is needed to connect two pure states. In case (ii), a general U(N) propagator is necessary in the general case, which requires N QHRs. In case (iii), some sort of incoherent process is required in order to equalize the different dynamic invariants of the initial and final mixed states, and the remaining coherent U(N) part is realized by QHRs. We describe the use of two such incoherent processes: pure dephasing and spontaneous emission.

The Householder reflection [55] is a powerful and numerically very robust unitary transformation, which has many applications in classical data analysis, e.g., in solving systems of linear algebraic equations, finding eigenvalues of high-dimensional matrices, least-square optimization, QR decomposition, etc. [56]. In its quantum mechanical implementation [39, 54] it consists of a single interaction step involving N simultaneous pulsed fields of precise areas and detunings in an N-pod linkage pattern, wherein the N states of our system are coupled to each other via an ancillary excited state, as displayed in Fig. 6.1. We use two types of QHRs: standard and generalized; the latter involves an additional phase factor. The standard QHR can operate on or off resonance, whereas the generalized QHR requires specific detunings. Any unitary matrix can be decomposed into (and therefore, synthesized by) $N-1$ standard QHRs and a phase gate, or into N generalized QHRs, without a phase gate; hence only N physical operations are needed, which allows one to greatly reduce the number of physical steps, from $O(N^2)$ in existing U(2) realizations [57] to only $O(N)$ with QHRs.

This chapter is organized as follows. In Sec. 6.1 we review the standard and generalized QHR gates and their physical implementations. In Sec. 6.2 we show how two pure states can be connected by means of standard and generalized QHRs. In Sec. 6.3 we construct the propagator connecting two arbitrary mixed states with the same dynamic invariants. Engineering of an arbitrary preselected mixed qunit state is presented in Sec. 6.4. The conclusions are summarized

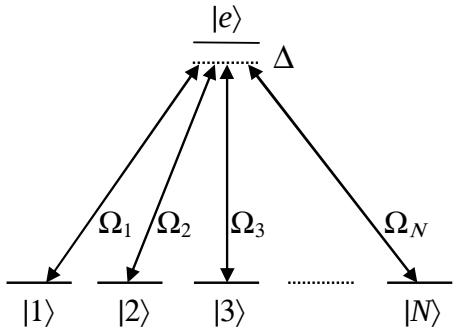

Figure 6.1: Physical realization of the quantum Householder reflection: N degenerate (in RWA sense) ground states, forming the *qunit*, coherently coupled via a common excited state by pulsed external fields of the same time dependence and the same detuning, but possibly different amplitudes and phases.

in Sec. 6.5.

6.1 Quantum Householder Reflection

6.1.1 Definition

The *standard* QHR is defined as

$$\mathbf{M}(v) = \mathbf{I} - 2\,|v\rangle\,\langle v|\,, \tag{6.1}$$

where $\mathbf{I}$ is the identity operator and $|v\rangle$ is an N-dimensional normalized complex column-vector. The QHR (6.1) is both hermitian and unitary, $\mathbf{M} = \mathbf{M}^\dagger = \mathbf{M}^{-1}$, which means that $\mathbf{M}$ is involutary, $\mathbf{M}^2 = \mathbf{I}$. In addition, $\det \mathbf{M} = -1$. For real $|v\rangle$ the Householder transformation (6.1) has a simple geometric interpretation: reflection with respect to an $(N-1)$-dimensional plane with a normal vector $|v\rangle$. In general, the vector $|v\rangle$ is complex and it is characterized by $2N-2$ real parameters (with the normalization condition and the unimportant global phase accounted for).

The *generalized* QHR is defined as

$$\mathbf{M}(v;\varphi) = \mathbf{I} + \left(e^{i\varphi} - 1\right)|v\rangle\,\langle v|\,, \tag{6.2}$$

where φ is an arbitrary phase. The standard QHR (6.1) is a special case of the generalized QHR (6.2) for $\varphi = \pi$: $\mathbf{M}(v;\pi) \equiv \mathbf{M}(v)$. The generalized QHR is unitary, $\mathbf{M}(v;\varphi)^{-1} = \mathbf{M}(v;\varphi)^\dagger = \mathbf{M}(v;-\varphi)$, and its determinant is $\det \mathbf{M} = e^{i\varphi}$.

6.1.2 Physical implementation

We have shown recently [39, 54] that the standard and generalized QHR operators can be realized physically in a coherently coupled N-pod system shown in Fig. 6.1. The N degenerate [in the rotating-wave approximation (RWA) sense [1]] ground states $|n\rangle$ $(n = 1, 2, \ldots, N)$, which represent the *qunit*, are coupled coherently by N external fields to an ancillary, excited state $|e\rangle \equiv |N+1\rangle$ [39]. The excited state $|e\rangle$ can generally be off resonance by a detuning $\Delta(t)$ [39], which must be the same for all fields. The Rabi frequencies $\Omega_1(t), \ldots, \Omega_N(t)$ of the couplings between the ground states and the excited state have the same pulse-shaped time dependence $f(t)$, but possibly different phases β_n and amplitudes χ_n,

$$\Omega_n(t) = \chi_n f(t) e^{i\beta_n} \quad (n = 1, 2, \ldots, N). \tag{6.3}$$

The qunit+ancilla RWA Hamiltonian reads

$$\mathbf{H}(t) = \frac{\hbar}{2} \begin{bmatrix} 0 & 0 & \cdots & 0 & \Omega_1(t) \\ 0 & 0 & \cdots & 0 & \Omega_2(t) \\ \vdots & \vdots & \ddots & \vdots & \vdots \\ 0 & 0 & \cdots & 0 & \Omega_N(t) \\ \Omega_1^*(t) & \Omega_2^*(t) & \cdots & \Omega_N^*(t) & 2\Delta(t) \end{bmatrix}, \tag{6.4}$$

The exact solution to the Schrödinger equation for the propagator $\mathbf{U}(t)$,

$$i\hbar \frac{d}{dt}\mathbf{U}(t) = \mathbf{H}(t)\mathbf{U}(t). \tag{6.5}$$

can be found in [39].

The *standard QHR* $\mathbf{M}(v)$ is realized on exact resonance ($\Delta = 0$), for any pulse shape $f(t)$, and for root-mean-square (rms) pulse area

$$A = 2(2k+1)\pi \quad (k = 0, 1, 2, \ldots), \tag{6.6}$$

where

$$A = \int_{-\infty}^{\infty} \Omega(t) dt, \tag{6.7}$$

with $\Omega(t) = \left[\sum_{n=1}^{N} |\Omega_n(t)|^2\right]^{1/2}$. Then the transition probabilities to the ancilla state vanish and the propagator within the qunit space is given exactly by the standard QHR $\mathbf{M}(v)$ (6.1). The components of the N-dimensional normalized complex vector $|v\rangle$ are the Rabi frequencies, with the accompanying phases [54],

$$|v\rangle = \frac{1}{\chi}\left[\chi_1 e^{i\beta_1}, \chi_2 e^{i\beta_2}, \ldots, \chi_N e^{i\beta_N}\right]^T, \tag{6.8}$$

where $\chi = \left(\sum_{n=1}^{N} \chi_n^2\right)^{1/2}$. Hence the qunit propagator represents a physical realization of the standard QHR in a single interaction step. Any QHR vector (6.8) can be produced on demand by appropriately selecting the peak couplings χ_n and the phases β_n of the external fields.

The *generalized QHR* $\mathbf{M}(v;\varphi)$ can be realized in the same N-pod system, but for specific detunings off resonance. Again the transition probabilities to the ancilla state must vanish; the corresponding rms pulse areas (6.7) in general depend on the pulse shape and differ from the resonance values (6.6). The propagator within the qunit space is the generalized QHR (6.2), wherein the phase φ depends on the interaction parameters. Although the parameters (i.e. the rms area and the detuning) of any needed generalized QHR can be found numerically for essentially any pulse shape, it is very convenient to use a hyperbolic-secant pulse shape, for which there is a simple exact analytic solution: the Rosen-Zener model [7],

$$f(t) = \operatorname{sech}(t/T), \tag{6.9a}$$

$$\Delta(t) = \Delta_0. \tag{6.9b}$$

For this pulse shape, the rms area (6.7) is $A = \pi\chi T$. A generalized QHR transformation $\mathbf{M}(v;\varphi)$ (6.2) is realized when the interactions satisfy again Eq. (6.8), and the pulse area and the detuning obey [39, 54]

$$A = 2\pi l \quad (l = 1, 2, \ldots), \tag{6.10a}$$

$$\varphi = 2\arg\prod_{k=0}^{l-1}\left[\Delta_0 T + i(2k+1)\right]. \tag{6.10b}$$

For any given φ, there are l values of Δ_0, which satisfy Eq. (6.10b) [39]. This is also the case for $\varphi = \pi$, i.e. for the standard QHR, for which one of the solutions is $\Delta_0 = 0$. Hence the standard QHR $\mathbf{M}(v)$ can be realized both on and off resonance, whereas the generalized QHR $\mathbf{M}(v;\varphi)$ can only be realized for nonzero Δ_0. The advantage of tuning off resonance is the lower transient population in the ancilla excited state, which would reduce the population losses if the lifetime of this state is short compared to the interaction duration.

This implementation is particularly suited for a qutrit ($N = 3$) formed of the magnetic sublevels of an atomic level with angular momentum $J = 1$; then the ancilla state should be a $J = 0$ state. The three pulsed fields can be delivered from the same laser by using beam splitters and polarizers, which would authomatically ensure that all of them have the same detuning and pulse shape. Moreover, with femtosecond pulses it would be possible to use pulse shapers [47], which can easily deliver pulses with the desired areas. Of course, the use of femtosecond pulses offers another advantage: decoherence is irrelevant on such time scales.

6.1.3 Householder decomposition of a U(N) propagator

The standard QHR $\mathbf{M}(v)$ and the generalized QHR $\mathbf{M}(v;\varphi)$ can be used for U(N) decomposition [54]. Any N-dimensional unitary matrix $\mathbf{U}$ ($\mathbf{U}^{-1}=\mathbf{U}^{\dagger}$) can be expressed as a product of $N-1$ standard QHRs $\mathbf{M}(v_n)$ ($n=1,2,\ldots N-1$) and a phase gate,

$$\Phi(\phi_1,\ldots,\phi_N)=\sum_{n=1}^{N}e^{i\phi_n}|n\rangle\langle n|=\mathrm{diag}\left\{e^{i\phi_1},\ldots,e^{i\phi_N}\right\}, \tag{6.11}$$

as

$$\mathbf{U}=\mathbf{M}(v_1)\,\mathbf{M}(v_2)\ldots\mathbf{M}(v_{N-1})\,\Phi(\phi_1,\phi_2,\ldots,\phi_N), \tag{6.12}$$

or as a product of N generalized QHRs,

$$\mathbf{U}=\mathbf{M}(v_1;\varphi_1)\,\mathbf{M}(v_2;\varphi_2)\ldots\mathbf{M}(v_N;\varphi_N). \tag{6.13}$$

6.2 Transition between pure states

The designed recipe for constructing a general U(N) transformation makes it possible to solve the important quantum mechanical problem of transfering an N-state quantum system from one arbitrary preselected initial superposition state to another such state, i.e. the inverse problem of quantum-state engineering. The cases of pure and mixed states require separate analysis.

6.2.1 Transition by standard QHR

General case

A pure qunit state is described by a state vector $|\Psi\rangle=\sum_{n=1}^{N}c_n|n\rangle$, where the vectors $|n\rangle$ represent the qunit basis states, and c_n is the complex-valued probability amplitude of state $|n\rangle$. Given the preselected initial state $|\Psi_i\rangle$ and the final state $|\Psi_f\rangle$ of the qunit, we wish to find a propagator $\mathbf{U}$, such that

$$|\Psi_f\rangle=\mathbf{U}|\Psi_i\rangle. \tag{6.14}$$

We shall show that one of the possible solutions of Eq. (6.14) reads

$$\mathbf{U}=\mathbf{M}(v_f)\mathbf{D}\mathbf{M}(v_i), \tag{6.15}$$

where $\mathbf{M}(v_i)$ and $\mathbf{M}(v_f)$ are standard QHRs. Here $\mathbf{D}$ is an N-dimensional unitary matrix, which, when acting upon a single qunit basis state $|n\rangle$, only shifts its phase,

$$\mathbf{D}|n\rangle=e^{i\phi_n}|n\rangle. \tag{6.16}$$

For example, $\mathbf{D}$ can be an arbitrary N-dimensional phase gate (6.11). Alternatively, $\mathbf{D}$ can be an arbitrary N-dimensional generalized QHR $\mathbf{M}(v;\varphi)$ with vector $|v\rangle$ orthogonal to the qunit state $|n\rangle$, $\langle v|n\rangle = 0$. Finally $\mathbf{D}$ can be the identity $\mathbf{D} = \mathbf{I}$.

In order to prove Eq. (6.15) we first define the vector

$$|v_{\alpha n}\rangle = \frac{|\Psi_\alpha\rangle - e^{i\varphi_{\alpha n}}|n\rangle}{\sqrt{2\left[1 - \mathrm{Re}\left(\langle\Psi_\alpha|n\rangle e^{i\varphi_{\alpha n}}\right)\right]}}, \tag{6.17}$$

where $|n\rangle$ is an arbitrarily chosen basis qunit state, $\varphi_{\alpha n} = \arg[\Psi_\alpha]_n$ and $\alpha = i, f$. The QHR $\mathbf{M}(v_{in})$ acting upon $|\Psi_i\rangle$ reflects it onto the single qunit state $|n\rangle$,

$$\mathbf{M}(v_{in})|\Psi_i\rangle = e^{i\varphi_{in}}|n\rangle. \tag{6.18}$$

The action of $\mathbf{D}$ upon $|n\rangle$ only shifts its phase, see Eq. (6.16). The action of $\mathbf{M}(v_{fn})$ upon $|n\rangle$ reflects this vector onto the final state,

$$\mathbf{M}(v_{fn})|n\rangle = e^{-i\varphi_{fn}}|\Psi_f\rangle. \tag{6.19}$$

Equations (6.18), (6.16) and (6.19) imply that

$$\mathbf{M}(v_{fn})\mathbf{D}\mathbf{M}(v_{in})|\Psi_i\rangle = e^{i\left(\varphi_{in}-\varphi_{fn}+\phi_n\right)}|\Psi_f\rangle, \tag{6.20}$$

which, up to an unimportant phase, proves Eq. (6.15).

The arbitrariness in the choice of the unitary matrix $\mathbf{D}$, and the intermediate basis state $|n\rangle$, means that the solution (6.15) for $\mathbf{U}$ is *not unique*. However, what is important is that it always exists. In fact the availability of multiple solutions offers some flexibility for a physical implementation. In particular we can always choose $\mathbf{D} = \mathbf{I}$; then the physical realization of the propagator $\mathbf{U}$ requires *only two standard QHRs*.

Special cases

In several important special cases *only a single standard QHR* is needed for pure-to-pure transition.

1. If the qunit is in a *single initial* basis state $|\Psi_i\rangle = |n\rangle$ then, as follows from Eq. (6.19), only one standard QHR $\mathbf{M}(v_{fn})$ is sufficient to transfer it into an arbitrary superposition state $|\Psi_f\rangle$, with $|v_{fn}\rangle$ given by Eq. (6.17).

2. Likewise, an arbitrary inital superposition state $|\Psi_i\rangle$ can be linked to any *single final* state $|\Psi_f\rangle = |n\rangle$ by only one standard QHR $\mathbf{M}(v_{in})$, with $|v_{in}\rangle$ given by Eq. (6.17).

3. If $|\Psi_i\rangle$ and $|\Psi_f\rangle$ are *orthogonal* ($\langle\Psi_f|\Psi_i\rangle = 0$), then again only a single standard QHR $\mathbf{M}(v)$, with $|v\rangle = \frac{1}{\sqrt{2}}\left(|\Psi_f\rangle - |\Psi_i\rangle\right)$, is sufficient to connect them.

4. If $|\Psi_i\rangle$ and $|\Psi_f\rangle$ are superpositional states with *real* coefficients, then again a single standard QHR $\mathbf{M}(v)$, with $|v\rangle = \left(|\Psi_f\rangle - |\Psi_i\rangle\right)/\sqrt{2\left(1 - \langle\Psi_f|\Psi_i\rangle\right)}$, is sufficient to link them.

6.2.2 Transition by generalized QHR

Generalized QHR is ideally suited for a pure-to-pure transition because, as it is easily seen, *only one generalized QHR* is sufficient to reflect state $|\Psi_i\rangle$ onto $|\Psi_f\rangle$,

$$\mathbf{U} = \mathbf{M}(v;\varphi), \tag{6.21}$$

where

$$|v\rangle = \frac{|\Psi_f\rangle - |\Psi_i\rangle}{\sqrt{2\left(1 - \mathrm{Re}\,\langle\Psi_f|\Psi_i\rangle\right)}}, \tag{6.22a}$$

$$\varphi = 2\arg\left(1 - \langle\Psi_f\,|\Psi_i\rangle\right) + \pi. \tag{6.22b}$$

In comparison with (6.15) the solution (6.21) is unique; there is no arbitrariness in the choice of the QHR vector $|v\rangle$ (up to an unimportant global phase) and the phase φ.

6.2.3 Examples

We consider a *qutrit* ($N = 3$), for which the QHR implementation is particularly suitable. As a first example, the transition from a single state to a superposition state,

$$|\Psi_i\rangle = |1\rangle \longrightarrow \frac{|1\rangle + |2\rangle + |3\rangle}{\sqrt{3}} = |\Psi_f\rangle\,, \tag{6.23}$$

is performed by a *single QHR* $\mathbf{M}(v)$, with

$$|v\rangle = \frac{1}{2}\sqrt{1 + \frac{1}{\sqrt{3}}}\left[\sqrt{3} - 1, -1, -1\right]^T. \tag{6.24}$$

Figure 6.2 shows the corresponding time evolutions of the populations and the state mismatch D. The latter is defined as the distance between the qutrit state vector $|\Psi(t)\rangle$ and the target state $|\Psi_f\rangle$,

$$D(t) = \frac{\sum_{mn}\left|\rho_{mn}(t) - \rho^f_{mn}\right|}{\sum_{mn}\left|\rho^i_{mn} - \rho^f_{mn}\right|}, \tag{6.25}$$

where ρ_{mn} are the elements of the qutrit density matrix ρ. This definition of D applies to pure and mixed states as well. The behavior of D allows us to verify that not only the populations but also the phases of the probability amplitudes of the target state $|\Psi_f\rangle$ are produced by the QHR. Indeed, as time progresses, D approaches zero, which implies that $|\Psi(t)\rangle$ aligns with $|\Psi_f\rangle$.

In another example, we transfer a two-state superposition to a three-state superposition,

$$\frac{|1\rangle + |3\rangle}{\sqrt{2}} \longrightarrow \frac{|1\rangle + e^{i\pi/3}\,|2\rangle + e^{i\pi/7}\,|3\rangle}{\sqrt{3}}, \tag{6.26}$$

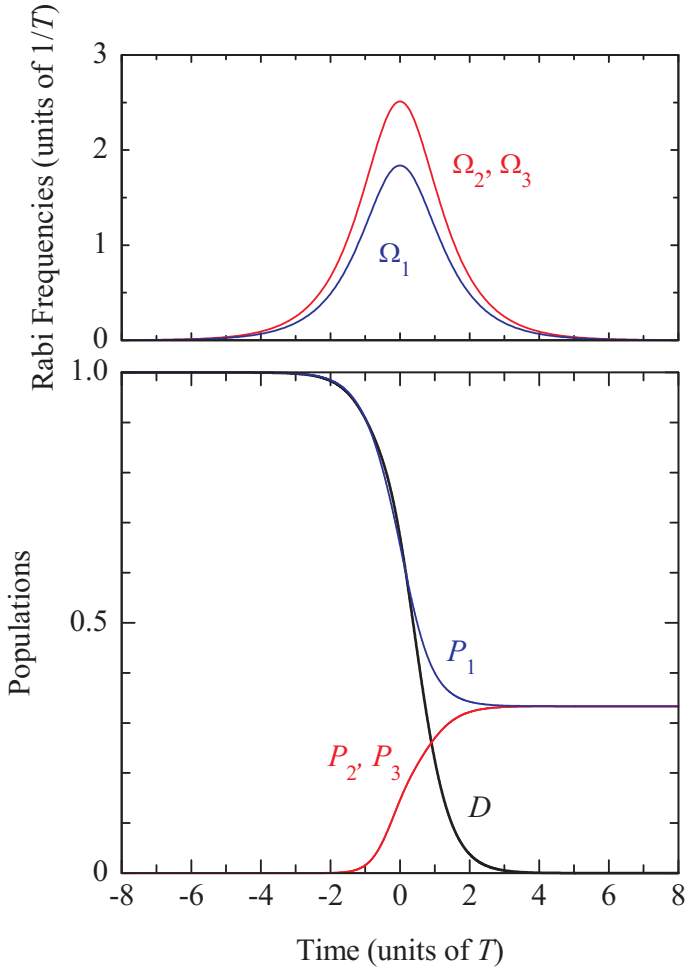

Figure 6.2: Time evolution of the pulsed fields (top) and the populations (bottom) for the transition (6.23) in a qutrit. We have assumed sech pulses and rms pulse area $A = 4\pi$ ($\chi T = 4$). The individual couplings χ_n ($n = 1, 2, 3$) are given by the components of the QHR vector (6.24), each multiplied by χ. The detuning is $\Delta_0 T = 1.732$ (which gives $\varphi = \pi$). The thick curve is the state mismatch (6.25).

by two standard QHRs, $\mathbf{U} = \mathbf{M}(v_f)\mathbf{M}(v_i)$, with

$$|v_i\rangle = [-0.383, 0, 0.924]^T, \tag{6.27a}$$

$$|v_f\rangle = \left[-0.460, 0.628e^{i\pi/3}, 0.628e^{i\pi/7}\right]^T, \tag{6.27b}$$

or by one generalized QHR, $\mathbf{U} = \mathbf{M}(v;\varphi)$, with

$$|v\rangle = \left[0.194e^{0.213\pi i}, 0.863e^{-0.454\pi i}, 0.467e^{-0.083\pi i}\right]^T, \tag{6.28}$$

and $\varphi = 0.574\pi$. Figure 6.3 shows the time evolution of the populations and the state mismatch (6.25) for a standard-QHR implementation, and Fig. 6.4 for generalized QHR. In both cases, the mismatch D vaniches, indicating the creation of the desired superposition (6.26). The

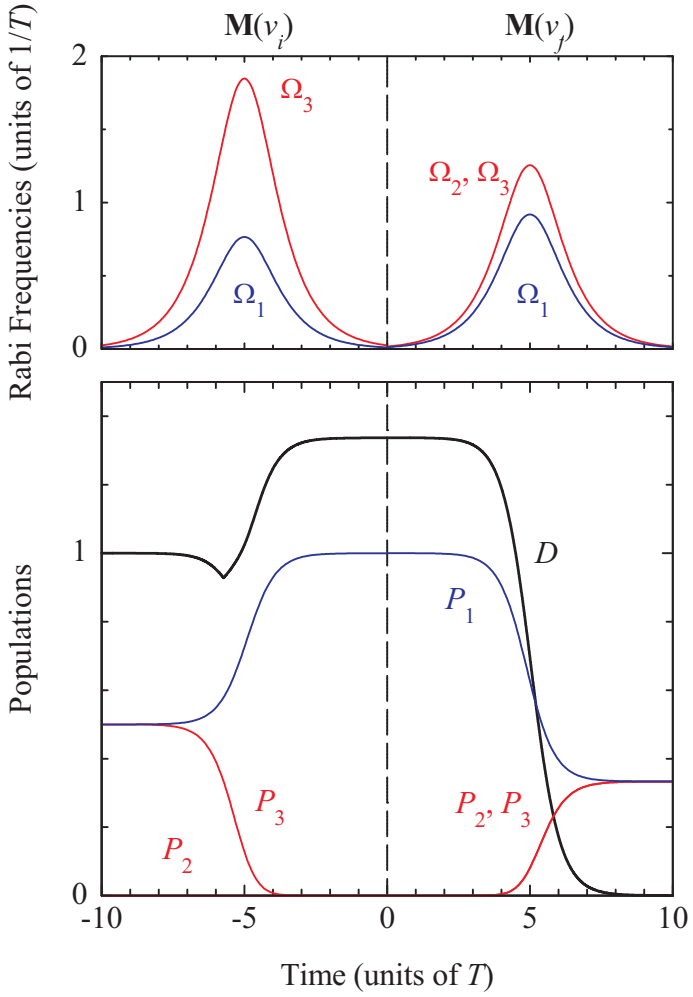

Figure 6.3: Time evolution of the pulsed fields (top) and the populations (bottom) for the transition (6.26) in a qutrit. We have assumed sech pulse shapes and rms pulse area $A = 2\pi$ ($\chi T = 2$). The individual couplings χ_n ($n = 1, 2, 3$) are given by the components of the standard QHRs (6.27), each multiplied by χ. The detuning is $\Delta T = 0$. The thick curve shows the state mismatch (6.25).

generalized-QHR implementation is clearly superior because it creates the target state in a single step.

In conclusion of this section, we have demonstrated that any two pure superposition qunit states can be connected by just a single generalized QHR, or by two standard QHRs. This suggests that QHR, and particularly the generalized version, is the most convenient and efficient tool for pure-to-pure state navigation in Hilbert space. We now turn our attention to the problem of connecting two arbitrary mixed states.

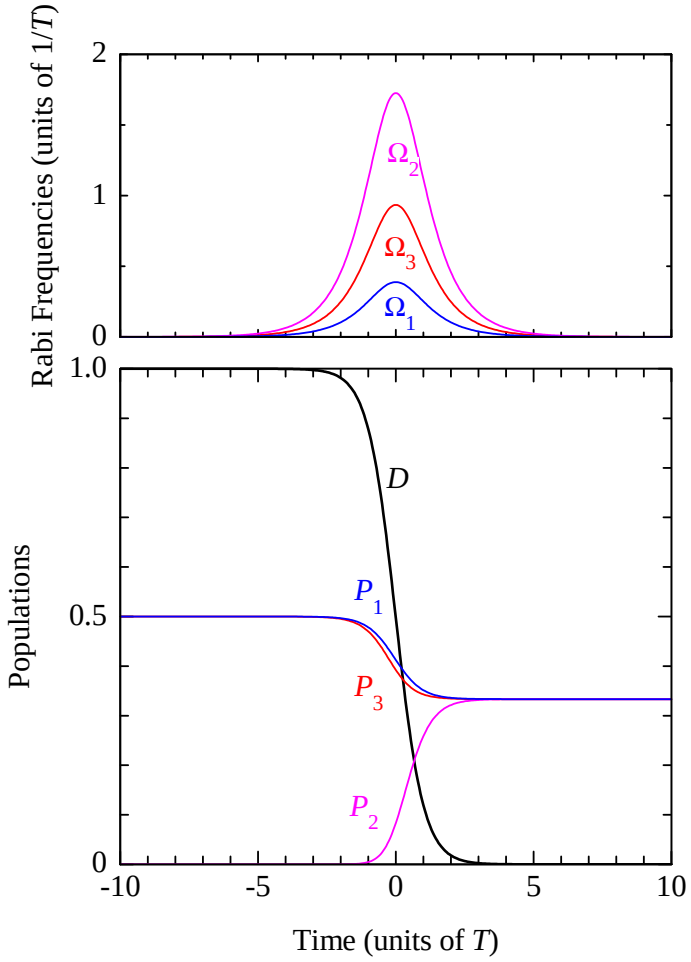

Figure 6.4: Time evolution of the pulsed fields (top) and the populations (bottom) for the transition (6.26) in a qutrit. We have assumed sech pulse shapes and rms pulse area $A = 2\pi$ ($\chi T = 2$). The individual couplings χ_n ($n = 1, 2, 3$) are given by the components of the generalized QHR (6.28), each multiplied by χ. The detuning is $\Delta T = 0.791$, which produces the desired phase $\varphi = 0.574\pi$. The thick curve shows the state mismatch (6.25).

6.3 Coherent navigation between mixed states

A mixed qunit state can be described by its density matrix ρ, whose spectral decomposition reads

$$\rho = \sum_{n=1}^{N} r_n \left|\psi_n\right\rangle \left\langle\psi_n\right| . \tag{6.29}$$

The eigenvalues r_n of ρ satisfy $\sum_{n=1}^{N} r_n = 1$, and $\left|\psi_n\right\rangle$ are the orthonormalized ($\left\langle\psi_k\right|\left.\psi_n\right\rangle = \delta_{kn}$) complex eigenvectors of ρ. The density matrix is hermitian; hence it can be parameterized by $N^2 - 1$ real parameters.

A hermitian Hamiltonian induces unitary evolution between an initial mixed state ρ_i and a

final state ρ_f,

$$\rho_f = \mathbf{U}\rho_i\mathbf{U}^\dagger. \tag{6.30}$$

A unitary evolution does not change the eigenvalues $\{r_n\}_{n=1}^N$, which are therefore dynamic invariants, which is easily seen from Eq. (6.30) (as an equivalent set of dynamic invariants one can take the set $\{\mathrm{Tr}\rho^n\}_{n=1}^N$). Therefore, a unitary propagator $\mathbf{U}$ can only connect mixed states with the same set of invariants $\{r_n\}_{n=1}^N$. In order to connect mixed states with different invariants we need an incoherent process; we shall return to this problem in the next section. Here we shall find the solution to the problem of linking two mixed states with the same invariants.

Because the eigenvalues $\{r_n\}_{n=1}^N$ of ρ_i and ρ_f are the same, we should have

$$\mathbf{R}_i^\dagger\rho_i\mathbf{R}_i = \mathbf{R}_f^\dagger\rho_f\mathbf{R}_f = \rho_0, \tag{6.31}$$

where the unitary matrices $\mathbf{R}_i$ and $\mathbf{R}_f$ diagonalize respectively ρ_i and ρ_f, so that $\rho_0 = \mathrm{diag}\{r_1, r_2, \ldots, r_N\}$. By replacing Eq. (6.31) into Eq. (6.30) we find

$$\rho_0 = \mathbf{D}\rho_0\mathbf{D}^\dagger, \tag{6.32a}$$

$$\mathbf{D} = \mathbf{R}_f^\dagger\mathbf{U}\mathbf{R}_i. \tag{6.32b}$$

Because $\mathbf{D}$ is a unitary matrix we find $\rho_0\mathbf{D} = \mathbf{D}\rho_0$. Since ρ_0 is diagonal, $\mathbf{D}$ must be diagonal too. There are no other restrictions on $\mathbf{D}$; hence $\mathbf{D}$ is an arbitrary diagonal matrix. It follows from Eq. (6.32b) that the solution for the unitary propagator in Eq. (6.30) is given by

$$\mathbf{U} = \mathbf{R}_f\mathbf{D}\mathbf{R}_i^\dagger. \tag{6.33}$$

The propagator (6.33) is not unique; it depends on the choice of the diagonal matrix $\mathbf{D}$. In particular, we can always choose $\mathbf{D} = \mathbf{I}$. Hence, the transfer between two mixed states requires a general U(N) propagator. The latter can be expressed as a product of $N-1$ standard QHRs $\mathbf{M}(v_n)$ ($n = 1, 2, \ldots, N-1$) and a phase gate $\mathbf{\Phi}(\phi_1, \phi_2, \ldots, \phi_N)$, Eq. (6.12), or by N generalized QHRs $\mathbf{M}(v_n; \varphi_n)$ ($n = 1, 2, \ldots, N$), Eq. (6.13) [54].

We take as an example a *qutrit*, with the arbitrarily chosen initial and final density matrices

$$\rho_i = \begin{bmatrix} 0.490 & 0.115e^{-0.789\pi i} & 0.158e^{0.107\pi i} \\ 0.115e^{0.789\pi i} & 0.336 & 0.018e^{-0.675\pi i} \\ 0.158e^{-0.107\pi i} & 0.018e^{0.675\pi i} & 0.175 \end{bmatrix}, \tag{6.34a}$$

$$\rho_f = \begin{bmatrix} 0.298 & 0.022e^{0.689\pi i} & 0.033e^{0.319\pi i} \\ 0.022e^{-0.689\pi i} & 0.180 & 0.177e^{0.909\pi i} \\ 0.033e^{-0.319\pi i} & 0.177e^{-0.909\pi i} & 0.523 \end{bmatrix}. \tag{6.34b}$$

These density matrices can be connected by the unitary propagator (6.33) with $\mathbf{D} = \mathbf{I}$: $\mathbf{U} = \mathbf{R}_f \mathbf{R}_i^\dagger$. The latter can be expressed as a product of two standard QHRs and one phase gate $\mathbf{U} = \mathbf{M}(v_1)\mathbf{M}(v_2)\mathbf{\Phi}$, with

$$|v_1\rangle = \left[0.612e^{0.532\pi i}, 0.091e^{0.211\pi i}, 0.785e^{0.690\pi i}\right]^T, \tag{6.35a}$$

$$|v_2\rangle = \left[0, 0.533e^{-0.181\pi i}, 0.846e^{0.859\pi i}\right]^T, \tag{6.35b}$$

$$\mathbf{\Phi} = \mathrm{diag}\{e^{-0.468\pi i}, e^{0.819\pi i}, e^{-0.350\pi i}\}, \tag{6.35c}$$

or by three generalized QHRs, $\mathbf{U} = \mathbf{M}(v_1;\varphi_1)\mathbf{M}(v_2;\varphi_2)\mathbf{M}(v_3;\varphi_3)$, with

$$|v_1\rangle = \left[0.721e^{0.659\pi i}, 0.080e^{-0.209\pi i}, 0.689e^{0.270\pi i}\right]^T, \tag{6.36a}$$

$$|v_2\rangle = \left[0, 0.813e^{0.469\pi i}, 0.582e^{-0.261\pi i}\right]^T, \tag{6.36b}$$

$$|v_3\rangle = [0, 0, 1]^T, \tag{6.36c}$$

$$\varphi_1 = -0.841\pi,\ \varphi_2 = 0.969\pi,\ \varphi_3 = -0.128\pi. \tag{6.36d}$$

Figure 6.5 shows the respective time evolution of the populations and the state mismatch (6.25) for the generalized-QHR realization (6.36). The first QHR $\mathbf{M}(v_3;\varphi_3)$ does not cause population changes because it is in fact a phase gate. As time progresses, the mismatch decreases and the target density matrix (6.34b) is approached.

6.4 Synthesis of arbitrary preselected mixed states

As it was shown in the previous sections, by applying one or more QHRs one can connect any two arbitrary pure states, or two arbitrary mixed states with the same dynamic invariants $\{r_n\}_{n=1}^N$. Mixed states with different invariants cannot be connected by coherent hermitian evolution because these invariants are constants of motion. Hence in order to connect mixed states with different invariants we need a mechanism with non-hermitian dynamics, which can alter the dynamic invariants.

In this section we shall describe two techniques for engineering an arbitrary mixed state, starting from a single pure state. This is the most interesting special case of the general problem of connecting two arbitrary mixed states, because the initial state can be prepared routinely by optical pumping. Moreover, the general mixed-to-mixed problem can be reduced to the single-to-mixed problem by optically pumping the initial mixed state into a single state.

The two techniques use a combination of coherent and incoherent evolutions. The coherent evolution uses QHRs, whereas the incoherent non-hermitian evolution is induced either by pure dephasing or spontaneous emission. We shall consider the two techniques separately.

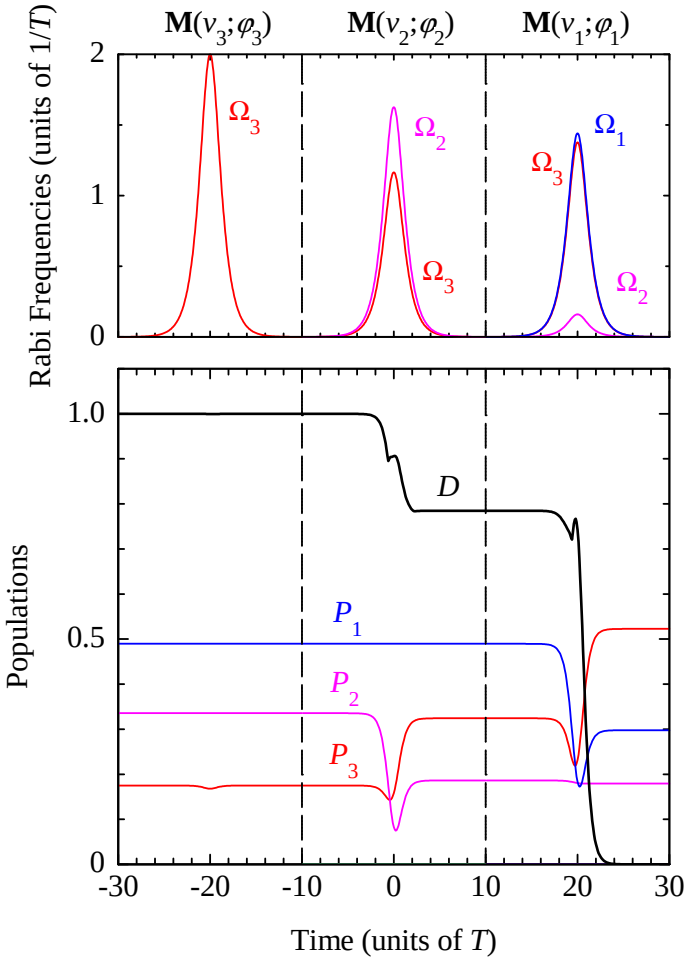

Figure 6.5: Time evolution of the pulsed fields (top), the populations and the state mismatch (bottom) for the transition between states (6.34a) and (6.34b) in a qutrit. We have assumed sech pulse shapes and rms pulse area $A = 2\pi$ ($\chi T = 2$). The individual couplings χ_n ($n = 1, 2, 3$) are given by the components of the generalized QHR (6.36), each multiplied by χ. The detunings are $\Delta_1 T = -0.255$, $\Delta_2 T = 0.049$, and $\Delta_3 T = -4.918$, which produce the QHR phases (6.36d).

6.4.1 Using dephasing

We assume that the qunit is initially in the single qunit state $\rho_i = |i\rangle\langle i|$, and we wish to transform the system to an arbitrary mixed state ρ_f. Let us denote the eigenvalues of ρ_f by r_n ($n = 1, 2, \ldots, N$). We proceed as follows.

- First, using the prescription from Sec. 6.2, we apply a single QHR to transfer state $|i\rangle$ to a pure superposition state, in which the populations are equal to the eigenvalues of ρ_f: $\rho_{nn} = r_n$ ($n = 1, 2, \ldots, N$). The phases of this superposition are irrelevant.

- In the second step we switch the dephasing on and let all coherences decay to zero. This can be done, for example, by using phase-fluctuating far-off-resonance laser fields. In the

end of this process, the density matrix will be diagonal, with the eigenvalues r_n of ρ_f on the diagonal, which implies that it will have the same dynamic invariants as ρ_f.

- The third step is to connect this intermediate state to the desired state ρ_f by a sequence of QHRs, as explained in the previous Sec. 6.3.

In summary, we need *three* steps: a single QHR, a dephasing process, and a sequence of N QHRs. Figure 6.6 shows the evolution of the populations and the state mismatch (6.25) during the engineering of the mixed state (6.34b) by the dephasing technique. The first step is the single QHR $\mathbf{M}(v)$, with QHR vector

$$|v\rangle = [-0.336, 0.816, 0.471]^T , \tag{6.37}$$

which transfers the single initial state $|1\rangle$ to the pure superposition state

$$\rho_1 = \begin{bmatrix} 0.6 & \sqrt{0.18} & \sqrt{0.06} \\ \sqrt{0.18} & 0.3 & \sqrt{0.03} \\ \sqrt{0.06} & \sqrt{0.03} & 0.1 \end{bmatrix} . \tag{6.38}$$

The second step is the pure dephasing process, which nullifies all coherences and leaves the density matrix in a diagonal form,

$$\rho_2 = \mathrm{diag}\,\{0.6, 0.3, 0.1\} . \tag{6.39}$$

The third step is a sequence of two generalized QHRs, which transfer ρ_2 into the desired final density matrix ρ_f, Eq. (6.34b). The QHR components read

$$|v_1\rangle = \left[0.689e^{0.454\pi i}, 0.280e^{0.436\pi i}, 0.668e^{-0.477\pi i}\right]^T , \tag{6.40a}$$

$$|v_2\rangle = \left[0, 0.793e^{0.740\pi i}, 0.609e^{0.025\pi i}\right]^T , \tag{6.40b}$$

$$\varphi_1 = 0.950\pi, \quad \varphi_2 = -0.760\pi. \tag{6.40c}$$

6.4.2 Using spontaneous emission

In the method, which uses spontaneous emission, we start again in a single qunit state $\rho_i = |i\rangle\langle i|$, and the target is the arbitrary mixed state ρ_f. The procedure now consists of only two steps: incoherent and coherent. It is particularly well suited for a qutrit, which we shall describe, although it is readily extended to more states. This method requires a closed qunit-ancilla transition; if the ancilla state can decay to other levels then the fidelity will be reduced accordingly.

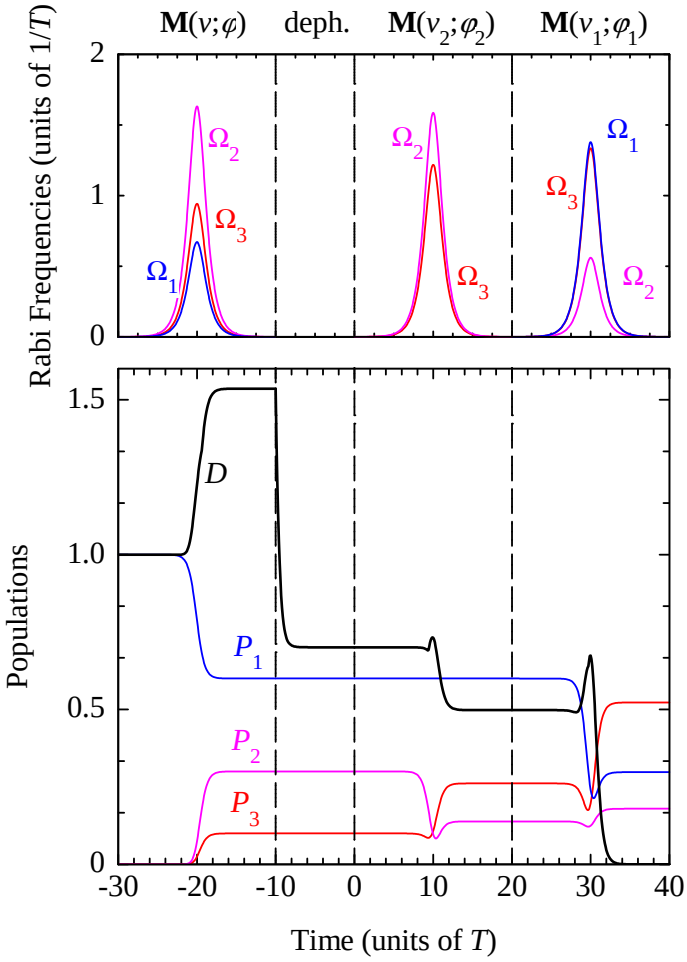

Figure 6.6: Time evolution of the pulsed fields (top), the populations and the state mismatch (6.25) (bottom) for mixed state engineering in a qutrit. The qutrit starts in state $|1\rangle$ and the target final state is given by Eq. (6.34b). We have assumed sech pulse shapes and rms pulse area $A = 2\pi$ ($\chi T = 2$). The individual couplings χ_n ($n = 1, 2, 3$) are given by the components of the generalized QHR (6.40), each multiplied by χ. The detunings are $\Delta_1 T = 0.072$ and $\Delta_2 T = -0.396$, which produce the desired QHR phases (6.40c). The dephasing rate is $\Gamma = 2/T$.

It is possible here to apply directly the incoherent step, which produces a density matrix with the desired final dynamic invariants, without the need to prepare first a coherent qunit superposition, as in the dephasing method above. The idea is to use laser-induced spontaneous emission from the ancilla excited state to prepare a completely incoherent superposition of the qunit states with populations ρ_{nn} equal to the eigenvalues r_n of ρ_f,

$$\rho = \sum_{n=1}^{3} r_n \left|n\right\rangle \left\langle n\right| . \tag{6.41}$$

For this we apply a sequence of appropriately chosen laser pulses from the qunit states to the excited state, which decays back to the qunit states and redistributes the population among them.

There are various scenarios possible, which can produce the desired incoherent qunit superposition. Here we describe a scenario which looks particularly simple and easy to implement for the qutrit formed of the magnetic sublevels $M = -1, 0, 1$ of a $J = 1$ level and an ancilla excited level with $J = 0$ (this implies also equal spontaneous decay branch ratios from the $J = 0$ level to the M sublevels of the qutrit). For definiteness, and without loss of generality, we assume that the eigenvalues of ρ_f are ordered as $r_1 \geqq r_2 \geqq r_3$. We need three pulses: a short pulse from state $|1\rangle$, a long pulse from state $|3\rangle$ and again a short pulse from state $|1\rangle$ (here short and long are related to the lifetime of the excited state).

The short pulse from the initially populated state $|1\rangle$, with excitation probability p_1, transfers population p_1 to the excited state, 1/3 of which decays back to each of the qutrit states. The ensuing density matrix reads

$$\rho_1 = \mathrm{diag}\left\{1 - \frac{2}{3}p_1, \frac{1}{3}p_1, \frac{1}{3}p_1\right\}. \tag{6.42}$$

We then apply a sufficiently long pulse from state $|3\rangle$, so that its population is completely depleted and distributed among states $|1\rangle$ and $|2\rangle$. The resulting density matrix is

$$\rho_2 = \mathrm{diag}\left\{1 - \frac{1}{2}p_1, \frac{1}{2}p_1, 0\right\}. \tag{6.43}$$

We now apply again a short pulse from state $|1\rangle$, with a different probability p_2, and then wait for spontaneous emission from the excited state. The result is

$$\begin{aligned}\rho_3 \;=\; & \mathrm{diag}\left\{\left(1 - \frac{1}{2}p_1\right)\left(1 - \frac{2}{3}p_2\right),\right. \\ & \left.\frac{1}{2}p_1 + \frac{1}{3}p_2\left(1 - \frac{1}{2}p_1\right), \frac{1}{3}p_2\left(1 - \frac{1}{2}p_1\right)\right\}.\end{aligned} \tag{6.44}$$

It is easy to show that in order to create the mixed state (6.41) we should have the probabilities

$$p_1 = 2\left(r_2 - r_3\right), \tag{6.45a}$$

$$p_2 = \frac{3r_3}{r_1 + 2r_3}. \tag{6.45b}$$

Because we assumed that $r_1 \geqq r_2 \geqq r_3$ the probabilities p_1 and p_2 belong to the interval $[0, 1]$ and are therefore well defined. Such probabilities can be produced by resonant pulses with appropriate pulse areas A_n. These pulses should be short compared to the lifetime of the excited state in order to avoid spontaneous emission during their action.

Once we have prepared the mixed qutrit state (6.41), which has the same invariants as ρ_f, we can apply QHRs to transfer this state into the desired final state ρ_f, as described in Sec. 6.3.

6.5 Conclusions

In this chapter we have proposed a technique, which allows to connect any two quantum superposition states, pure or mixed, of an N-state atom. This solution of the inverse problem in quantum mechanics contains two stages: (i) mathematical derivation of the propagator that links the desired initial and final density matrices, and (ii) physical realization of this propagator. In the most general case of arbitrary mixed states, the implementations combine coherent hermitian and incoherent non-hermitian interactions induced by pulsed laser fields. In general, the propagator is not unique, which reflects the multitude of paths between two qunit states; this also allows for some flexibility in the choice of most convenient path.

The physical realization uses an N-pod configuration of N lower states, forming the qunit, and an ancillary upper state. It is particularly convenient for a qutrit, where the $N = 3$ states are the magnetic sublevels of a $J = 1$ level and the ancilla state is a $J = 0$ level. Then only a single tunable laser is needed to provide the necessary polarized laser pulses.

The hermitian part uses a sequence of sets of short coherent laser pulses with appropriate pulse areas and detunings. For each set, the propagator of the N-pod represents a quantum Householder reflection (QHR). A sequence of *at most* N suitably chosen QHRs can synthesize any desired unitary propagator.

We have shown that two arbitrary preselected *pure* superposition states can be connected by a *single* QHR only, because the respective propagator has exactly the QHR symmetry. Two mixed states, with the same set of dynamic invariants, require a general U(N) transformation, which can be realized by at most N QHRs. This is a significant improvement over the existing setups involving $O(N^2)$ operations, which can be crucial in making quantum state engineering and operations with qunits experimentally feasible.

The most general case of two arbitrary mixed states with different dynamic invariants requires an incoherent step, which equalizes the invariants of the initial density matrix to those of the final density matrix. We have demonstrated how this can be done by using pure dephasing or spontaneous decay of the ancillary upper state. Once the invariants are equalized, the problem is reduced to the one of connecting two mixed states with the same invariants, which, as explained above, can be done by at most N QHRs. This method has been described for a qutrit, but it is easily generalized to an arbitrary qunit.

The present results can have important applications in the storage of quantum information. For example, a qubit can encode two continuous parameters: the population ratio of the two qubit states and the relative phase of their amplitudes. A qunit in a *pure* state can encode $2(N - 1)$ parameters ($N - 1$ populations and $N - 1$ relative phases), i.e. by using qunits

information can be encoded in significantly fewer particles than with qubits. Moreover, a *mixed* qunit state can encode as many as $N^2 - 1$ real parameters. This may be particularly interesting if the number of particles that can be used is restricted, e.g., due to decoherence [3, 4].

Chapter 7

Design of quantum Fourier transforms and quantum algorithms by using circulant Hamiltonians

Quantum information processing is built upon sequences of special unitary transformations. One of the most important of these is the quantum (discrete) Fourier transform (QFT), which is a key ingredient of many quantum algorithms [3, 58, 59], including Shor's factorization [60], the algorithms of Deutsch [61] and Simon [62], order finding, discrete logarithms, quantum phase estimation, etc. [3].

Traditionally, QFT on r qubits is implemented by a quantum circuit consisting of $O(r)$ Hadamard gates and $O(r^2)$ controlled-phase gates [63]. Experimental demonstrations include synthesis of 3-qubit QFT in nuclear magnetic resonance (NMR) systems [64], order finding with NMR [65], phase estimation with NMR [66], Shor's factorization in NMR [67], in ion traps [68], and using a "compiled version" of Shor's algorithm with photonic qubits [69, 70]. Further theoretical proposals for implementations of QFT include atoms in cavity QED [71], entangled multilevel atoms [72], trapped ions with Householder reflections [73], linear optics [74] with Cooley-Tukey's algorithm [75], waveguide arrays [76], etc.

The largest numbers factorized experimentally by Shor's algorithm hitherto are 15 [67, 68] and 21 [77]. The primary obstacle for demonstration of Shor's factorization for larger numbers is the large number of one- and two-qubit gates required. A "general-purpose" Shor's algorithm for an L-bit number demands L^3 gates and $5L+1$ qubits [78]; an implementation using a linear ion trap would require about $396L^3$ laser pulses [78]. "Special-purpose" algorithms that exploit special properties of the input number are much faster: the number 15 can be factored with 6 qubits and 38 pulses only [78].

Another practical difficulty of the QFT algorithm is the use of two-qubit control-phase gates, which, for large number of qubits, involve very small phases. To this end, an "approximate" QFT has been proposed [63, 79, 80], in which the phase shift gates requiring highest precision are omitted.

Griffiths and Niu proposed a "semiclassical" QFT, wherein the costly two-qubit gates are replaced by serial single-qubit rotations supplemented with classical measurements [81]. Such a semiclassical QFT has been demonstrated recently with three trapped ions [68].

In the present chapter, we propose to construct QFT by a novel approach which uses a special class of Hamiltonians, having a circulant symmetry. Such Hamiltonians have the advantage that their eigenvectors are the columns of the QFT (hence the latter diagonalizes the Hamiltonian), and they *do not depend* on the particular elements of the Hamiltonian, as far as the circulant symmetry is conserved. This important feature allows one to construct QFT in a *single interaction step*; it also makes this techniques robust against variations in the interaction parameters. The present work uses a similar approach as Unanyan *et al.* [82], who proposed to use circulant Hamiltonians in order to create coherent superpositions of states.

7.1 Background

Quantum Fourier transform. The N-dimensional QFT is defined with its action on an orthonormal basis $|0\rangle, |1\rangle, \ldots, |N-1\rangle$:

$$\mathbf{F}^N|n\rangle = \frac{1}{\sqrt{N}} \sum_{k=0}^{N-1} e^{2\pi ink/N}|k\rangle. \tag{7.1}$$

It transforms a single state into an equal superposition of states with specific phase factors. The inverse QFT is

$$(\mathbf{F}^N)^{-1}|n\rangle = \frac{1}{\sqrt{N}} \sum_{k=0}^{N-1} e^{-2\pi ink/N}|k\rangle. \tag{7.2}$$

In a matrix form QFT is a square matrix with elements

$$\mathbf{F}^N_{kn} = \frac{1}{\sqrt{N}} e^{2\pi ikn/N}. \tag{7.3}$$

Circulant matrix. An $N \times N$ matrix C of the form

$$C = \begin{bmatrix} c_0 & c_{N-1} & c_{N-2} & \cdots & c_1 \\ c_1 & c_0 & c_{N-1} & \cdots & c_2 \\ c_2 & c_1 & c_0 & \cdots & c_3 \\ \vdots & \vdots & \vdots & \ddots & \vdots \\ c_{N-1} & c_{N-2} & c_{N-3} & \cdots & c_0 \end{bmatrix} \tag{7.4}$$

is called a circulant matrix. It is a special case of a Toeplitz matrix [83] and it is completely defined by its first vector-column (or row). The other columns (rows) are just cyclic permutations of it. The circulant matrices have some very interesting properties. The most important one in the present context is that the eigenvectors of a circulant matrix of a given size are the vector-columns of the discrete Fourier transform (7.3) of the same size; hence they do not depend on the elements of the circulant matrix. The eigenvalues λ_n of the circulant matrix, though, are phased sums of the matrix elements:

$$\lambda_n = \sum_{k=0}^{N-1} c_k \exp\left(-i2\pi kn/N\right). \tag{7.5}$$

7.2 Design of the Hamiltonian

In order to synthesize QFT, we use a special time-dependent Hamiltonian of the form [82]

$$\mathbf{H}(t) = f(t)\mathbf{H}_0 + g(t)\mathbf{H}_1, \tag{7.6}$$

where $f(t)$ and $g(t)$ are (generally pulse-shaped) real-valued functions, such that $f(t)$ *precedes* $g(t)$ in time, i.e.

$$0 \overset{-\infty\leftarrow t}{\longleftarrow} \frac{g(t)}{f(t)} \overset{t\to\infty}{\longrightarrow} \infty. \tag{7.7}$$

For instance, we can take

$$f(t) = [1 - \tanh(t/T)]/2, \tag{7.8a}$$

$$g(t) = [1 + \tanh(t/T)]/2. \tag{7.8b}$$

Therefore, the Hamiltonian (7.6) has the asymptotics

$$\mathbf{H}_0 \overset{-\infty\leftarrow t}{\longleftarrow} \mathbf{H}(t) \overset{t\to\infty}{\longrightarrow} \mathbf{H}_1. \tag{7.9}$$

We demand $\mathbf{H}_0$ to be a diagonal matrix in which the energies of all states (the diagonal elements) are non-degenerate

$$\mathbf{H}_0 = \mathrm{diag}(E_1, E_2, \ldots, E_N). \tag{7.10}$$

For $\mathbf{H}_1$ we choose a circulant matrix, with the condition that the eigenvalues should be well separated from each other. Because the Hamiltonian has to be Hermitian, $\mathbf{H}_1$ is not a most general circulant matrix, but a Hermitian circulant matrix.

Because the Hamiltonian (7.6) at $t \to \infty$ has a circulant symmetry, its eigenvectors are the vector-columns of QFT. However, each eigenvector $|n\rangle$ may have an adiabatic phase factor $e^{i\alpha_n}$, acquired in the end of the evolution, which may be different for each $|n\rangle$. This means that

for such a Hamiltonian (7.6), adiabatic evolution will perform the QFT (7.1) (possibly after renumbering of the basis states), but with some additional phases α_n,

$$\mathbf{F}^N|n\rangle = \frac{1}{\sqrt{N}} e^{i\alpha_n} \sum_{k=0}^{N-1} e^{2\pi i n k/N} |k\rangle. \tag{7.11}$$

The phases α_n are just integrals over the quasienergies, as follows from the adiabatic theorem [84]. The inverse Fourier transform would be

$$(\mathbf{F}^N)^{-1}|n\rangle = \frac{1}{\sqrt{N}} \sum_{k=0}^{N-1} e^{-i\alpha_k} e^{-2\pi i n k/N} |k\rangle, \tag{7.12}$$

and it can be accomplished by adiabatic evolution with the Hamiltonian

$$\mathbf{H}(t) = g(t)\mathbf{H}_0 + f(t)\mathbf{H}_1. \tag{7.13}$$

For example, for $N = 4$ we can have

$$\mathbf{H}_0 = \mathrm{diag}(-E, -E/3, E/3, E) \tag{7.14a}$$

$$\mathbf{H}_1 = \begin{bmatrix} 0 & V & 0 & V^* \\ V^* & 0 & V & 0 \\ 0 & V^* & 0 & V \\ V & 0 & V^* & 0 \end{bmatrix}. \tag{7.14b}$$

For laser-driven atomic and molecular transitions, the interaction V is given by the Rabi frequency Ω: $V = \frac{1}{2}\hbar\Omega$. Insofar as the eigenvalues of the circulant matrix are given by Eq. (7.5), one has to choose the interaction energy V in such a way that the eigenenergies have well separated values. Another requirement for adiabatic evolution is that the functions $f(t)$ and $g(t)$ change sufficiently slowly, so that the nonadiabatic coupling $\langle \dot{\chi}_m(t) \mid \chi_n(t) \rangle$ between each pair of adiabatic states $|\chi_m(t)\rangle$ and $|\chi_n(t)\rangle$ remains negligibly small compared to the separation of the eigenenergies $\varepsilon_m(t)$ and $\varepsilon_n(t)$,

$$|\varepsilon_m(t) - \varepsilon_n(t)| \gg |\langle \dot{\chi}_m(t) \mid \chi_n(t) \rangle| \sim \frac{1}{T}, \tag{7.15}$$

where T is the interaction duration.

In the numeric examples we use a hyperbolic-secant mask for the functions $f(t)$ and $g(t)$:

$$f(t) = \mathrm{sech}\,(t/\tau)[1 - \tanh(t/T)], \tag{7.16a}$$

$$g(t) = \mathrm{sech}\,(t/\tau)[1 + \tanh(t/T)]. \tag{7.16b}$$

These factors are chosen for implementation feasibility; they do not change the (all-important) asymptotic behaviour of the eigenstates $|\chi_n(t)\rangle$. Figure 7.1 shows the evolution of the eigenvalues of the Hamiltonian (7.6) for $V = E(1 + i/3)$. For this choice of V the eigenenergies are non-degenerate (except at infinite times, which is irrelevant because there is no interaction) and the adiabatic evolution is enabled.

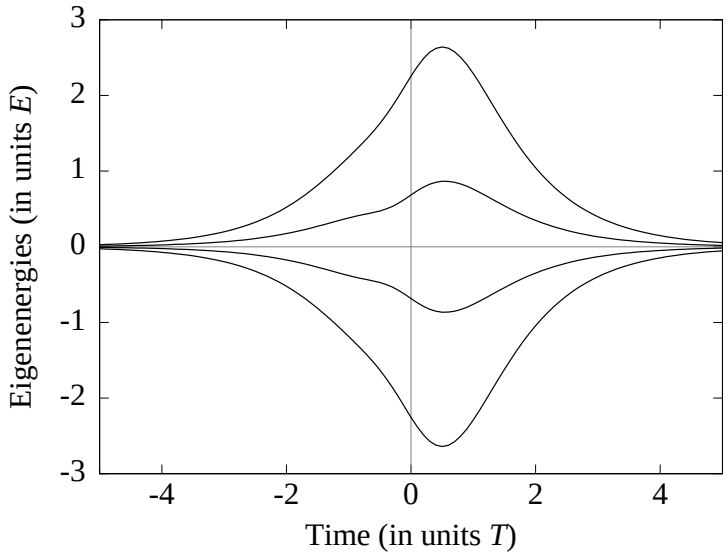

Figure 7.1: Eigenvalues of the Hamiltonian (7.6) as a function of time for $\mathbf{H}_0$ and $\mathbf{H}_1$ given by Eqs. (7.14a) and (7.14b), with $V = E(1+i/3)$, whereas $g(t)$ and $f(t)$ are given by Eqs. (7.16a) and (7.16b).

7.3 Quantum phase estimation

We shall show now that the QFT propagator (7.11), which results from the Hamiltonian (7.6), can be used to realize quantum algorithms, despite the presence of the adiabatic phase factors $e^{i\alpha_n}$. We consider the quantum phase estimation algorithm [3], which is the key for many other algorithms, such as Shor's factorization. We briefly summarize here the essence of this algorithm.

Let us consider a unitary operator $\mathbf{U}$, which has an eigenvector $|u\rangle$ and a corresponding eigenvalue $\exp(2\pi i\phi)$, where $\phi \in [0,1)$. We assume that we are able to prepare state $|u\rangle$ and to perform the controlled-$\mathbf{U}^{2^j}$ operation, for non-negative integer j. The goal of the algorithm is to estimate ϕ. To this end, the algorithm uses two registers. The first register contains r qubits initially in state $|0\rangle$ and the second one starts in state $|u\rangle$, containing as many qubits as needed to store $|u\rangle$.

The procedure starts with the application of a Hadamard transform [3] to the first register, followed by the application of controlled-$\mathbf{U}$ operations on the second register, with $\mathbf{U}$ raised to successive powers of two. The final state of the first register is

$$2^{-r/2}(|0\rangle + e^{2\pi i 2^{r-1}\phi}|1\rangle)_1(|0\rangle + e^{2\pi i 2^{r-2}\phi}|1\rangle)_2 \cdots (|0\rangle + e^{2\pi i 2^{0}\phi}|1\rangle)_r = 2^{-r/2}\sum_{k=0}^{2^r-1} e^{2\pi i k\phi}|k\rangle, \quad (7.17)$$

and the second register stays in state $|u\rangle$. Now let us suppose that ϕ can be expressed using a

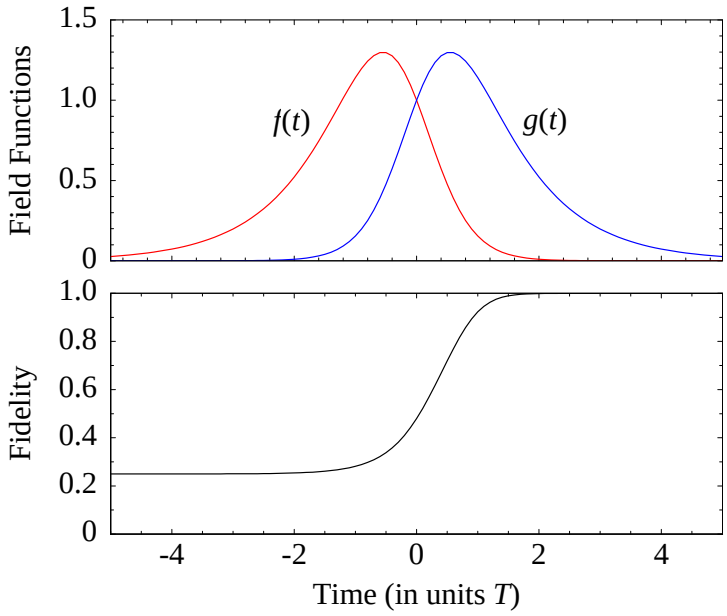

Figure 7.2: Upper frame: Field functions $f(t)$ and $g(t)$, Eqs. (7.16a) and (7.16b). Lower frame: Fidelity of phase estimation during the inverse Fourier transform. The parameters are: $\phi = 0.75$, $\tau = T$, $V = E(1 + i/3)$, $E = 10/T$.

r-bit expansion

$$\phi = 0.\phi_1\phi_2 \dots \phi_r = \frac{\phi_1}{2} + \frac{\phi_2}{4} + \cdots + \frac{\phi_r}{2^r}, \tag{7.18}$$

where $0.\phi_1\phi_2 \dots \phi_r$ represents a binary fraction. Then state (7.17) can be written as

$$2^{-r/2}(|0\rangle + e^{2\pi i 0.\phi_r}|1\rangle)_1(|0\rangle + e^{2\pi i 0.\phi_{r-1}\phi_r}|1\rangle)_2 \cdots (|0\rangle + e^{2\pi i 0.\phi_1\phi_2\cdots\phi_r}|1\rangle)_r. \tag{7.19}$$

Finally, we apply the inverse QFT in order to obtain the product state $|\phi_1 \cdots \phi_r\rangle$. In our case we apply the phased inverse QFT (7.11) and find

$$e^{-i\alpha(\phi)}|\phi_1 \cdots \phi_r\rangle, \tag{7.20}$$

where $\alpha(\phi)$ is an adiabatic phase that depends on ϕ. Since this global phase α has no physical meaning, a measurement in the computational basis would give us exactly ϕ. We note that if ϕ cannot be written as a r bit expansion (7.18), this procedure can still produce a good approximation to ϕ with high probability [3].

In Fig. 7.2 we plot the probability of state (7.20) during the inverse Fourier transformation (7.12). This probability is evaluated by solving numerically the Schrödinger equation for the Hamiltonian (7.13) and is used as a measure of the fidelity. The figure shows that when the phase ϕ has an exact expansion as a binary fraction, the final probability tends to unity.

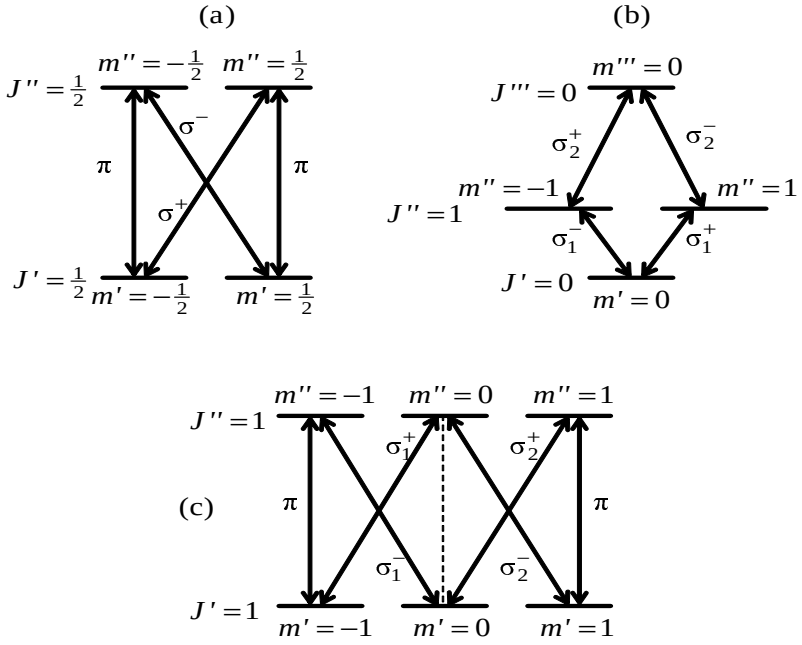

Figure 7.3: Systems, which can be used in order to realize a circulant Hamiltonian: (a) $J' = \frac{1}{2} \leftrightarrow J'' = \frac{1}{2}$ system, (b) $J' = 0 \leftrightarrow J'' = 1 \leftrightarrow J''' = 0$ system, and (c) $J' = 1 \leftrightarrow J'' = 1$ system, where the $m' = 0 \leftrightarrow m'' = 0$ transition is dipole forbidden.

7.4 Implementations

In this section we discuss a few simple systems, which can be used for implementing the Hamiltonian (7.6).

$J' = \frac{1}{2} \leftrightarrow J'' = \frac{1}{2}$ system. As a first example we consider the system formed of the magnetic sublevels in a $J' = \frac{1}{2} \leftrightarrow J'' = \frac{1}{2}$ transition shown in Fig. 7.3(a), where J is the total angular momentum of each level. We apply two linearly polarized fields (the two polarization directions being perpendicular), the second one seen as a superposition of two circularly polarized fields (σ_+ and σ_-). By ordering the magnetic sublevels in the sequence $|m' = -\frac{1}{2}\rangle$, $|m'' = \frac{1}{2}\rangle$, $|m' = \frac{1}{2}\rangle$, $|m'' = -\frac{1}{2}\rangle$, and by suitably tuning the strengths and the relative phase of the two independent fields, we can adjust the interaction elements of the Hamiltonian and produce the desired circulant form (7.14b). We note that because of the different signs of some of the Clebsch-Gordan coefficients, one should redefine one of the probability amplitudes by changing its sign.

As we want to implement the full Hamiltonian (7.6), we also need to realize its first part $\mathbf{H}_0$. It is especially important to remove the degeneracies between the magnetic sublevels. This can be accomplished by using a static magnetic field, which induces m-dependent Zeeman shifts, and a far-off resonant laser pulse, which will cause Stark shifts. Let the energy splitting due

to Zeeman shift be $E_{\rm Z}$ (the same for both ground and excited levels). The Stark shifts are generally different for the two levels: $E_{\rm g,S}$ and $E_{\rm e,S}$, where 'g' and 'e' stand, respectively, for ground and excited. Hence, in order to realize the Hamiltonian (7.14a), we need to solve the following algebraic system

$$\begin{aligned} -\tfrac{1}{2}E_{\rm Z} + E_{g,{\rm S}} &= -E, && (7.21a)\\ \tfrac{1}{2}E_{\rm Z} + E_{g,{\rm S}} &= -E/3, && (7.21b)\\ -\tfrac{1}{2}E_{\rm Z} + E_{e,{\rm S}} &= E/3, && (7.21c)\\ \tfrac{1}{2}E_{\rm Z} + E_{e,{\rm S}} &= E, && (7.21d) \end{aligned}$$

which gives $E_{\rm Z} = E_{\rm e,S} = -E_{\rm g,S} = \frac{2}{3}E$. Moreover, because the energies of $\mathbf{H}_0$ need not be exactly evenly separated, our method is robust against fluctuations in the field parameters. Making a reference to Eq. (7.6) and Fig. 7.2, we conclude that the Stark and Zeeman fields, with the time dependence $f(t)$, have to be applied before the polarized laser fields, with time dependence $g(t)$.

$J' = 0 \leftrightarrow J'' = 1 \leftrightarrow J''' = 0$ system. Another system with $N = 4$ is the diamond system depicted in Fig. 7.3(b). Here again two linearly polarized laser fields are needed, but now they have parallel polarization directions. One advantage of this system is that only magnetic fields are sufficient to realize the first part of the Hamiltonian. The disadvantage is that the two independent fields generally come from two different lasers, because of the different frequencies of the transitions.

$J' = 1 \leftrightarrow J'' = 1$ system. The $J' = 1 \leftrightarrow J'' = 1$ system, depicted in Fig. 7.3(c), contains six coupled m sublevels. In this system the circulant symmetry occurs because $m' = 0 \leftrightarrow m'' = 0$ is a dipole forbidden transition. By ordering the magnetic sublevels in the sequence $|m' = -1\rangle$, $|m'' = 0\rangle$, $|m' = 1\rangle$, $|m'' = 1\rangle$, $|m' = 0\rangle$, $|m'' = -1\rangle$ we obtain a Hamiltonian of the type

$$\mathbf{H}_1 = \frac{\hbar}{2}\begin{bmatrix} 0 & -\Omega_1 & 0 & 0 & 0 & -\Omega_2 \\ -\Omega_1^* & 0 & \Omega_1^* & 0 & 0 & 0 \\ 0 & \Omega_1 & 0 & \Omega_2 & 0 & 0 \\ 0 & 0 & \Omega_2^* & 0 & -\Omega_1^* & 0 \\ 0 & 0 & 0 & -\Omega_1 & 0 & \Omega_1 \\ -\Omega_2^* & 0 & 0 & 0 & \Omega_1^* & 0 \end{bmatrix}, \qquad (7.22)$$

where Ω_1 and Ω_2 are the Rabi frequencies between, respectively, states with different m and states with the same m. Each Clebsch-Gordan coefficient is incorporated in the respective Rabi

frequency. The Rabi frequencies are complex (needed to avoid eigenvalue degeneracies), with a phase difference between the left and right circularly polarized components. After a phase transformation of the amplitudes, $c_n \to e^{i\beta_n} c_n$, with suitably chosen phase factors β_n, we can make the Hamiltonian take the form of a circulant matrix. The selection of the phases β_n amounts to solving a simple linear algebraic system.

The first part of the Hamiltonian $\mathbf{H}_0$ can be realized with auxiliary magnetic and electric fields, as for the $J' = \frac{1}{2} \leftrightarrow J'' = \frac{1}{2}$ system.

7.5 Conclusions

The intrinsic symmetry of circulant matrices allows one to design Hamiltonians that can produce a discrete Fourier transform on a set of quantum states in a natural manner and in a single step, without the need to apply a large number of consecutive quantum gates. The designed Hamiltonian has different asymptotics: it is a nondegenerate diagonal matrix in the beginning and a circulant matrix in the end (or vice versa); the time dependence that connects the two should be sufficiently slow in order to enable adiabatic evolution. The resulting unitary transformation, which this Hamiltonian produces, differs from the standard QFT by additional (adiabatic) phase factors in the matrix columns; we show, however, that one can still construct the quantum phase estimation algorithm, which is an essential subroutine in many quantum algorithms. We have presented examples of simple atomic systems, the Hamiltonians of which can be tailored to obtain circulant symmetry. The construction of large-scale systems with circulant symmetry requires the design of a *closed-loop* linkage pattern; for instance, a chain of nearest-neighbor interactions supplemented with a (direct or effective) interaction between the two ends of the chain.

Chapter 8

Contributions: summary

The present thesis studied different aspects of the light-matter interaction and considered specific applications. Below, the contribution of the author are presented.

Chapter 2 analyzes the properties of the detection signal in a two-state system, depending on the fashion in which it is collected. It is shown that the post-pulse populations of the ground and excited states, and the ionization signal collected during the excitation, possess different symmetry properties with respect to the frequency chirp rate and the static frequency detuning.

In Chapter 3 the accuracy of the adiabatic-elimination approximation is analyzed for calculating the acquired phases, caused by far-off-resonant pulsed laser fields. In this chapter the conditions for the applicability of this approximation are derived and it is shown that the adiabatic approximation is a far more accurate method for evaluating the phase shifts.

In Chapter 4 an analytically exactly soluble two-state model is presented, in which a hyperbolic-secant-shaped pulsed interaction has a phase jump of ϕ at the time of its maximum. The jump phase ϕ can be used as a control parameter for the two-state transition probability.

In Chapter 5 is presented a class of exact analytic solutions of the time-dependent Schrödinger equation for a two-state quantum system coherently driven by a nonresonant external field. The coupling is a linear function of time with a finite duration and the detuning is constant.

Chapter 6 introduces a technique which allows one to connect *any* two arbitrary (pure or mixed) superposition states of an N-state quantum system. The proposed solution to this inverse quantum mechanical problem is analytical, exact and very compact. The technique uses standard and generalized quantum Householder reflections (QHR), which require external pulses of precise areas and frequencies.

In Chapter 7 is proposed a technique for design of quantum Fourier transforms, and ensuing quantum algorithms, in a single interaction step by engineered Hamiltonians of circulant

symmetry.

Appendix A

Basic and Auxiliary Results

A.1 Relevant properties of the Gauss hypergeometric function and the Euler Γ-function

The Gauss hypergeometric function $F(\lambda,\mu;\nu;z)$ satisfies the Gauss hypergeometric equation [40],

$$z(1-z)w'' + [\nu - (\lambda+\mu+1)z]\,w' - \lambda\mu w = 0. \tag{A.1.1}$$

The Gauss function has the following properties [40]

$$\frac{d}{dz}F(\lambda,\mu;\nu;z) = \frac{\lambda\mu}{\nu}F(\lambda+1,\mu+1;\nu+1;z), \tag{A.1.2a}$$

$$\frac{d}{dz}\left[z^{\nu-1}F(\lambda,\mu;\nu;z)\right] = (\nu-1)z^{\nu-2}F(\lambda,\mu;\nu-n;z), \tag{A.1.2b}$$

$$F(\lambda,\mu;\nu;z) = (1-z)^{\nu-\lambda-\mu}\,F(\nu-\lambda,\nu-\mu;\nu;z), \tag{A.1.2c}$$

$$F(\lambda,\mu;\nu;0) = 1, \tag{A.1.2d}$$

$$F(\lambda,\mu;\nu;1) = \frac{\Gamma(\nu)\Gamma(\nu-\lambda-\mu)}{\Gamma(\nu-\lambda)\Gamma(\nu-\mu)}, \tag{A.1.2e}$$

$$F(\lambda,\mu;\frac{\lambda+\mu+1}{2};\tfrac{1}{2}) = \frac{\sqrt{\pi}\Gamma(\frac{\lambda+\mu+1}{2})}{\Gamma(\frac{\lambda+1}{2})\Gamma(\frac{\mu+1}{2})} \tag{A.1.2f}$$

$$F(\lambda,-\lambda;\nu;\tfrac{1}{2}) = \pi^{1/2}2^{-\nu}\Gamma(\nu)\left[\frac{1}{\Gamma\left(\frac{\lambda+\nu}{2}\right)\Gamma\left(\frac{\nu-\lambda+1}{2}\right)} + \frac{1}{\Gamma\left(\frac{\lambda+\nu+1}{2}\right)\Gamma\left(\frac{\nu-\lambda}{2}\right)}\right], \tag{A.1.2g}$$

$$F(1+\lambda,1-\lambda;1+\nu;\tfrac{1}{2}) = \frac{\nu}{\lambda}\pi^{1/2}2^{1-\nu}\Gamma(\nu)\left[\frac{1}{\Gamma\left(\frac{\lambda+\nu}{2}\right)\Gamma\left(\frac{\nu-\lambda+1}{2}\right)} - \frac{1}{\Gamma\left(\frac{\lambda+\nu+1}{2}\right)\Gamma\left(\frac{\nu-\lambda}{2}\right)}\right]. \tag{A.1.2h}$$

The Γ-function obeys the reflection formula [40]

$$\Gamma(z)\Gamma(1-z) = \frac{\pi}{\sin\pi z}, \tag{A.1.3}$$

and has the asymptotics expansions [40]

$$\ln\Gamma(z) \sim \tfrac{1}{2}\ln 2\pi + \left(z-\tfrac{1}{2}\right)\ln z - z + \frac{1}{12z} + O(|z|^{-3}), \tag{A.1.4a}$$

$$\frac{\Gamma(z+a)}{\Gamma(z+b)} \sim z^{a-b}\left[1 + \frac{(a+b-1)\,(a-b)}{2z} + O(|z|^{-2})\right]. \tag{A.1.4b}$$

A.2 Relevant properties of the parabolic cylinder function

The parabolic cylinder (Weber) function $D_\nu(z)$ [40] is a solution of the Weber equation

$$\frac{d^2}{dz^2}D_\nu(z) + \left(\nu + \tfrac{1}{2} - \tfrac{1}{4}z^2\right)D_\nu(z) = 0. \tag{A.2.5}$$

The power series expansion is relevant for small $|z|$ and has the form [85]

$$D_\nu(z) = 2^{\nu/2}\pi^{1/2}e^{z^2/4}\sum_{n=0}^{\infty}\frac{\left(-z\sqrt{2}\right)^n}{n!\Gamma\left[\frac{1}{2}(1-n-\nu)\right]}. \tag{A.2.6}$$

The large-argument asymptotic expansions are relevant when $|z| \gg 1, |\nu|$. The basic one is [40]

$$D_\nu(z) \sim z^\nu e^{-\frac{1}{4}z^2}\left[\sum_{n=0}^{N}\frac{(-\frac{1}{2}\nu)_n(\frac{1}{2}-\frac{1}{2}\nu)_n}{n!(-\frac{1}{2}z^2)_n} + \mathcal{O}\left(\left|z^2\right|^{-N-1}\right)\right], \tag{A.2.7}$$
$$(|z|\to\infty,\ |\arg z| < 3\pi/4,\ \nu \text{ fixed})$$

where $(a)_n = \Gamma(a+n)/\Gamma(a)$. The asymptotics for other values of $\arg z$ is found by using the connection formula [40]

$$D_\nu(z) = e^{i\pi\nu}D_\nu(-z) + \frac{\sqrt{2\pi}}{\Gamma(-\nu)}e^{i(\nu+1)\pi/2}D_{-1-\nu}(-iz). \tag{A.2.8}$$

The existence of different asymptotic expansions for different values of $\arg z$ is a manifestation of the Stokes phenomenon [86, 87].

The large-argument-and-large-order asymptotic expansions are relevant when both $|z|$ and $|\nu|$ are simultaneously much larger than unity [50]. These expansions are generally more complicated than the weak-coupling asymptotics (A.2.7). For the particular functions involved in the present models the asymptotic expansions can be derived from the general results of Olver [50];

their leading terms are [49]

$$D_{i\delta^2}(\alpha e^{-i\pi/4}) \sim \cos\theta\; e^{\pi\delta^2/4+i\eta}, \tag{A.2.9a}$$

$$D_{-i\delta^2}(\alpha e^{i\pi/4}) \sim \cos\theta\; e^{\pi\delta^2/4-i\eta}, \tag{A.2.9b}$$

$$D_{-1-i\delta^2}(\alpha e^{i\pi/4}) \sim \frac{\sin\theta}{\delta}\; e^{\pi\delta^2/4-i\eta-i\pi/4}, \tag{A.2.9c}$$

$$D_{-1+i\delta^2}(\alpha e^{-i\pi/4}) \sim \frac{\sin\theta}{\delta}\; e^{\pi\delta^2/4+i\eta+i\pi/4}, \tag{A.2.9d}$$

$$D_{i\delta^2}(\alpha e^{3i\pi/4}) \sim \cos\theta\; e^{-3\pi\delta^2/4+i\eta} + \frac{\delta\sqrt{2\pi}\;\sin\theta}{\Gamma\left(1-i\delta^2\right)}\; e^{-\pi\delta^2/4-i\eta-i\pi/4}, \tag{A.2.9e}$$

$$D_{-1+i\delta^2}(\alpha e^{3i\pi/4}) \sim \frac{\sin\theta}{\delta}\; e^{-3\pi\delta^2/4+i\eta-3i\pi/4} + \frac{\sqrt{2\pi}\;\cos\theta}{\Gamma\left(1-i\delta^2\right)}\; e^{-\pi\delta^2/4-i\eta}, \tag{A.2.9f}$$

where α and δ are assumed positive and large ($\alpha \to \infty, \delta \to \infty,\ \alpha/\delta$ is arbitrary), $\theta = \frac{1}{2}\arctan(2\delta/\alpha)$, and

$$\eta = \tfrac{1}{2}\alpha\sqrt{\alpha^2+4\delta^2} - \tfrac{1}{2}\delta^2 + \delta^2 \ln\left[\tfrac{1}{2}\left(\alpha + \sqrt{\alpha^2+4\delta^2}\right)\right], \tag{A.2.10}$$

The first four expansions, for phases of the arguments equal to $\pi/4$, are derived [49] directly from Olver's results [50]. The last two asymptotics, for phases of the argument equal to $3\pi/4$, are obtained from Eqs. (A.2.9a)-(A.2.9d) by using the connection formula (A.2.8).

A.3 Invariances of the survival probabilities

We show here, that the survival probabilities $P_{1\to1}$ and $P_{2\to2}$ in a lossy two-state system do not depend on the sign change of the odd part $\Delta_{\rm o}(t)$ and the even part $\Delta_{\rm e}(t)$ of the detuning, provided the Rabi frequency $\Omega(t)$ and the loss rate $\Gamma(t)$ are even functions of time. We write the Hamiltonian in the interaction representation,

$$\mathbf{H}(t) = \frac{\hbar}{2}\begin{bmatrix} 0 & \Omega(t)e^{-iD(t)} \\ \Omega(t)e^{iD(t)} & 0 \end{bmatrix}, \tag{A.3.11}$$

with $D(t) = \int_0^t \left[\Delta(t') - \frac{1}{2}i\Gamma(t')\right] dt'$. The formal solution for the evolution operator is expressed using the Dyson series

$$\mathbf{U}(\infty,-\infty) = 1 + \sum_{n=1}^{\infty} \mathbf{U}_n(\infty,-\infty), \tag{A.3.12}$$

where

$$\begin{aligned}\mathbf{U}_n(\infty,-\infty) \;=\; & \left(\frac{-i}{\hbar}\right)^n \int_{-\infty}^{\infty} \delta t_1 \int_{-\infty}^{t_1} \delta t_2 \cdots \int_{-\infty}^{t_{n-1}} \delta t_n \\ & \times \mathbf{H}(t_1)\mathbf{H}(t_2)\cdots\mathbf{H}(t_n)\end{aligned} \tag{A.3.13}$$

and $t_1 > t_2 > \cdots > t_n$. It is straightforward to show that the even powers of the Hamiltonian in the sum in Eq. (A.3.12) generate diagonal matrices, while the odd powers are anti-diagonal matrices. We consider the diagonal elements first. Let us examine the simplest diagonal term in the Dyson series, which for $n = 2$ reads

$$\mathbf{U}_2(\infty, -\infty) = -\tfrac{1}{4} \int_{-\infty}^{\infty} dt_1 \int_{-\infty}^{t_1} dt_2 \begin{bmatrix} \Omega_1\Omega_2 e^{-i(D_1 - D_2)} & 0 \\ 0 & \Omega_1\Omega_2 e^{i(D_1 - D_2)} \end{bmatrix}. \tag{A.3.14}$$

The subscripts in Ω_k and D_k indicate the instant of time t_k. The higher powers of the Hamiltonian in the Dyson series have a similar simple form.

By using simple transformations of variables, it can be shown that $\mathbf{U}_2(\infty, -\infty)$ is invariant under the transformation $\Delta_\mathrm{o} \leftrightarrow -\Delta_\mathrm{o}$, while the change $\Delta_\mathrm{e} \leftrightarrow -\Delta_\mathrm{e}$ leads only to complex conjugation. These results are also valid for the higher even-order terms of the Dyson series, which means that the considered transformations do not change the absolute values of the diagonal elements of the evolution matrix. This, in turn, proves the invariance of the survival probabilities.

These arguments obviously do not hold for the odd terms in the sum, which means that in the presence of losses $\Gamma > 0$ the transition probabilities $P_{1\to 2}$ and $P_{2\to 1}$ are *not* invariant with respect to the sign flips $\Delta_\mathrm{o} \leftrightarrow -\Delta_\mathrm{o}$ and $\Delta_\mathrm{e} \leftrightarrow -\Delta_\mathrm{e}$.

A.4 Solution of the Carroll-Hioe model for complex parameters

In order to solve the Carroll-Hioe model (1.19), we begin with a phase transformation of the probability amplitudes,

$$c_1(t) \to c_1(t), \quad c_2(t) \to c_2(t) \exp\left[-i \int_0^t \Delta(\tau) d\tau\right], \tag{A.4.15}$$

which brings the Schrödinger equation into the interaction representation

$$i\frac{d}{dt}c_1(t) = \tfrac{1}{2}\Omega(t) e^{-iD(t)} c_2(t), \tag{A.4.16a}$$

$$i\frac{d}{dt}c_2(t) = \tfrac{1}{2}\Omega(t) e^{iD(t)} c_1(t), \tag{A.4.16b}$$

where $D = \int_0^t \Delta(\tau) d\tau$, i.e.,

$$D = (S_0 - i\Gamma_0) T \arctan\left[\sinh\left(t/T\right)\right] + BT \ln\left[\cosh\left(t/T\right)\right]. \tag{A.4.17}$$

We now change the independent variable from t to z [14],

$$z = \frac{\sinh\left(t/T\right) - i}{\sinh\left(t/T\right) + i}, \tag{A.4.18}$$

and denote $C_n(z) = c_n(t(z))$ $(n = 1, 2)$. As t changes from $-\infty$ to ∞, the variable z changes from 1 to $e^{2\pi i}$. By following the derivation of Carroll and Hioe [14], we obtain the following solution for $C_1(z)$ in terms of the Gauss hypergeometric function $F(a, b; c; z)$ [48],

$$\begin{aligned} C_1(z) &= z^{-r-(\sigma-i\gamma+i\beta)/4} \\ &\times \Big[Az^{2r} F\left(-i\beta/2 + r + q, -i\beta/2 + r - q; 1 + 2r; z\right) \\ &+ BF\left(-i\beta/2 - r + q, -i\beta/2 - r - q; 1 - 2r; z\right) \Big], \end{aligned} \tag{A.4.19}$$

where

$$r = \tfrac{1}{4}\sqrt{\alpha^2 + (\sigma + i\beta - i\gamma)^2}, \tag{A.4.20a}$$

$$q = \tfrac{1}{4}\sqrt{\alpha^2 + (\sigma - i\beta - i\gamma)^2}, \tag{A.4.20b}$$

and

$$\alpha = \Omega_0 T, \quad \sigma = S_0 T, \quad \gamma = \Gamma_0 T, \quad \beta = BT. \tag{A.4.21}$$

The integration constants A and B can be determined from the initial conditions $c_1(-\infty) = 1$, $c_2(-\infty) = 0$:

$$A = \frac{\Gamma(-i\beta)\Gamma(-2r)}{\Gamma(-r + q - i\beta/2)\Gamma(-r - q - i\beta/2)}, \tag{A.4.22a}$$

$$B = \frac{\Gamma(-i\beta)\Gamma(2r)}{\Gamma(r + q - i\beta/2)\Gamma(r - q - i\beta/2)}. \tag{A.4.22b}$$

Then the solution for $C_1(z)$ reads

$$\begin{aligned} C_1(z) &= z^{-(\sigma-i\gamma+i\beta)/4} \\ &\times \Bigg[z^{-r} \frac{\Gamma(-i\beta)\Gamma(2r)}{\Gamma(-i\beta/2 + r + q)\Gamma(-i\beta/2 + r - q)} \\ &\times F\left(-i\beta/2 - r + q, -i\beta/2 - r - q; 1 - 2r; z\right) \\ &+ z^{r} \frac{\Gamma(-i\beta)\Gamma(-2r)}{\Gamma(-i\beta/2 - r + q)\Gamma(-i\beta/2 - r - q)} \\ &\times F\left(-i\beta/2 + r + q, -i\beta/2 + r - q; 1 + 2r; z\right) \Bigg] \end{aligned} \tag{A.4.23}$$

In a similar manner we derive the solution for the probability amplitude $C_2(z)$, by using

Eq. (A.4.16a),

$$\begin{aligned} C_2(z) = &-\frac{\alpha}{4} 2^{i\beta} z^{(\sigma - i\gamma + i\beta)/4 - r} e^{\pi(\beta - i\sigma + \gamma)/2} \\ &\times \Bigg[\frac{\Gamma(1 - i\beta)\Gamma(2r)}{\Gamma(1 - i\beta/2 + r + q)\Gamma(1 - i\beta/2 + r - q)} \\ &\times F\left(i\beta/2 - r + q, i\beta/2 - r - q; 1 - 2r; z\right) \\ &+ z^{2r} \frac{\Gamma(1 - i\beta)\Gamma(-2r)}{\Gamma(1 - i\beta/2 - r + q)\Gamma(1 - i\beta/2 - r - q)} \\ &\times F\left(i\beta/2 + r + q, i\beta/2 + r - q; 1 + 2r; z\right) \Bigg]. \end{aligned} \tag{A.4.24}$$

From Eqs. (A.4.23) and (A.4.24), and recalling the transformation (A.4.15), one can derive the propagator elements U_{11} and U_{21} in the original basis by using the Gauss summation formula

$$F(a, b; c; 1) = \frac{\Gamma(c - a + b)\Gamma(c)}{\Gamma(c - a)\Gamma(c - b)}. \tag{A.4.25}$$

The result is

$$U_{11}(\infty) = e^{-\pi(i\sigma + \gamma)/2} \frac{e^{\pi\beta/2} \cos 2\pi q - e^{-\pi\beta/2} \cos 2\pi r}{\sinh \pi\beta}, \tag{A.4.26a}$$

$$\begin{aligned} U_{21}(\infty) = &-i \frac{\pi\alpha}{2} 2^{i\beta} (\cosh t_f)^{-i\beta} e^{-\pi(\gamma + i\sigma)/2} \Gamma(1 - i\beta)^2 \\ &\times \left[\Gamma\left(1 - i\beta/2 + r + q\right) \Gamma\left(1 - i\beta/2 + r - q\right)\right. \\ &\left. \times \Gamma\left(1 - i\beta/2 - r + q\right) \Gamma\left(1 - i\beta/2 - r - q\right)\right]^{-1}. \end{aligned} \tag{A.4.26b}$$

In a similar fashion, we can derive the solution for the model (1.19) for the initial conditions $c_1(-\infty) = 0$, $c_2(-\infty) = 1$, which will give us the propagator elements U_{12} and U_{22}. We use that Eqs. (A.4.16) are of the same form as for initial conditions $c_1(-\infty) = 1$, $c_2(-\infty) = 0$, but for $\Delta \to -\Delta$, i.e. $\beta \to -\beta$, $\sigma \to -\sigma$, $\gamma \to -\gamma$, $r \to r$, $q \to q$. By using Eqs. (A.4.15) and (A.4.17) we obtain

$$\begin{aligned} U_{12}(\infty) = &-i \frac{\pi\alpha}{2} 2^{-i\beta} (\cosh t_f)^{i\beta} e^{-\pi(\gamma + i\sigma)/2} \Gamma(1 + i\beta)^2 \\ &\times \left[\Gamma\left(1 + i\beta/2 + r + q\right) \Gamma\left(1 + i\beta/2 + r - q\right)\right. \\ &\left. \times \Gamma\left(1 + i\beta/2 - r + q\right) \Gamma\left(1 + i\beta/2 - r - q\right)\right]^{-1}, \end{aligned} \tag{A.4.27a}$$

$$U_{22}(\infty) = e^{-\pi(i\sigma + \gamma)/2} \frac{e^{\pi\beta/2} \cos 2\pi r - e^{-\pi\beta/2} \cos 2\pi q}{\sinh \pi\beta}. \tag{A.4.27b}$$

The transition probabilities $P_{m \to n} = |U_{nm}(e^{2\pi i})|^2$ are given explicitly by Eqs. (2.16) and (2.17).

Appendix B

Publications and Conferences

B.1 Publications of the author used for the dissertation

1. P. A. Ivanov, B. T. Torosov and N. V. Vitanov,
   Navigation between quantum states by quantum mirrors,
   Phys. Rev. A **75**, 012323 (2007).

2. B. T. Torosov and N. V. Vitanov,
   Coherent control of a quantum transition by a phase jump,
   Phys. Rev. A **76**, 053404 (2007).

3. B. T. Torosov and N. V. Vitanov,
   Exactly soluble two-state quantum models with linear couplings,
   J. Phys. A: Math. Theor. **41**, 155309 (2008).

4. B. T. Torosov and N. V. Vitanov,
   Phase shifts in nonresonant coherent excitation,
   Phys. Rev. A **79**, 042108 (2009).

5. B. T. Torosov and N. V. Vitanov,
   Design of quantum Fourier transforms and quantum algorithms by using circulant Hamiltonians,
   Phys. Rev. A **80**, 022329 (2009).

6. B. T. Torosov, G. S. Vasilev and N. V. Vitanov,
   Symmetries and asymmetries in coherent atomic excitation by chirped laser pulses,
   Opt. Commun. **283**, 1338 (2010).

B.2 Participated international conferences, schools and workshops

1. 6-11 May 2007, 9th European Cconference on Atoms, Molecules and Photons (ECAMP IX), Crete, Greece (poster contribution).

2. 13-17 June 2007, 3rd Annual Workshop on Control of Quantum Dynamics of Atoms, Molecules and Ensembles by Light (CAMEL III), Sozopol, Bulgaria (oral contribution)

3. 27-31 August 2007, First European Young Scientists Conference on Quantum Information, Vienna, Austria (poster contribution).

4. 3-7 September 2007, 1st EMALI mini school, Kaiserslautern, Germany.

5. 27-29 March 2008, LII Annual Conference of the Finnish Physical Society, Turku, Finland (oral contribution).

6. 24-28 June 2008, 4th Annual Workshop on Control of Quantum Dynamics of Atoms, Molecules and Ensembles by Light (CAMEL IV), Nessebar, Bulgaria (oral contribution)

7. 2-5 July 2008, 40th EGAS Conference, Graz, Austria (poster contribution).

8. 27 July - 1 August 2008, 21st International Conference on Atomic Physics (ICAP XXI), Storrs, USA (poster contribution).

9. 3-17 May 2009, QUROPE09 International School"Quantum Information and Many-Body Systems", Cortona, Italy.

10. 23-27 May 2009, 16th Central European Workshop on Qunatum Optics (CEWQO 2009), Turku, Finland (poster contribution).

11. 23-28 June 2009, 5th Annual Workshop on Control of Quantum Dynamics of Atoms, Molecules and Ensembles by Light (CAMEL V), Nessebar, Bulgaria (oral contribution)

12. 2-7 August 2009, Gordon Research Conference on Quantum Control Of Light and Matter, South Hadley, USA (poster contribution).

13. 7-15 September 2009, 3rd EMALI Mini School and EMALI Annual Meeting, Pisa, Italy.

14. 21-25 September 2009, QIPC 2009 International Conference on Quantum Information Processing and Communications, Rome, Italy (poster contribution).

Bibliography

[1] B. W. Shore, *The Theory of Coherent Atomic Excitation* (Wiley, New York, 1990).

[2] A. Abraham, *The Principles of Nuclear Magnetism* (Clarendon, Oxford, 1961); C. P. Slichter, *Principles of Magnetic Resonance* (Springer, Berlin, 1990).

[3] Nielsen MA and Chuang IL 1990 *Quantum Computation and Quantum Information* (Cambridge University Press).

[4] D. Bouwmeester, A. Ekert and A. Zeilinger, *The Physics of Quantum Information: Quantum Cryptography, Quantum Teleportation, Quantum Computation* (Springer-Verlag, Berlin, 2001).

[5] I. I. Rabi, Phys. Rev. **51**, 652 (1937).

[6] L. D. Landau, Physik Z. Sowjetunion **2**, 46 (1932); C. Zener, Proc. R. Soc. Lond. Ser. A **137**, 696 (1932).

[7] N. Rosen and C. Zener, Phys. Rev. **40**, 502 (1932).

[8] L. Allen and J. H. Eberly, *Optical Resonance and Two-Level Atoms* (Dover, New York, 1987).

[9] F. T. Hioe, Phys. Rev. A **30**, 2100 (1984).

[10] A. Bambini and P. R. Berman, Phys. Rev. A **23**, 2496 (1981).

[11] Y. N. Demkov and M. Kunike, Vestn. Leningr. Univ. Fiz. Khim. **16**, 39 (1969); F. T. Hioe and C. E. Carroll, Phys. Rev. A **32**, 1541 (1985); J. Zakrzewski, Phys. Rev. A **32**, 3748 (1985).

[12] Y. N. Demkov, Sov. Phys.-JETP **18**, 138 (1964).

[13] E. E. Nikitin, Opt. Spectrosc. **13**, 431 (1962); E. E. Nikitin, Adv. Quantum Chem. **5**, 135 (1970).

[14] C. E. Carroll and F. T. Hioe, J. Phys. A: Math. Gen. **19**, 3579 (1986).

[15] N. V. Vitanov, T. Halfmann, B. W. Shore and K. Bergmann, Ann. Rev. Phys. Chem. **52**, 763 (2001).

[16] A. Präkelt, M. Wollenhaupt, C. Sarpe-Tudoran, and T. Baumert, Phys. Rev. A **70**, 063407 (2004); M. Krug, T. Bayer, M. Wollenhaupt, C. Sarpe-Tudoran, T. Baumert, S. S. Ivanov, and N. V. Vitanov, New J. Phys. **11**, 105051 (2009).

[17] M. Wollenhaupt, V. Engel and T. Baumert, Annu. Rev. Phys. Chem. **56**, 25 (2005).

[18] J. S. Melinger, A. Hariharan, Suketu R. Gandhi, W. S. Warren, J. Chem. Phys. **95**, 2210 (1991); B. Broers, H. B. van Linden van den Heuvell, and L. D. Noordam, Phys. Rev. Lett. **69**, 2062 (1992); C. Trallero-Herrero, D. Cardoza, T. C. Weinacht, and J. L. Cohen, Phys. Rev. A **71**, 013423 (2005); S. D. Clow, C. Trallero-Herrero, T. Bergeman, and T. Weinacht, Phys. Rev. Lett. **100**, 233603 (2008); C. Trallero-Herrero, J. L. Cohen, T. Weinacht, Phys. Rev. Lett. **96**, 063603 (2006).

[19] M. Wollenhaupt *et al.*, in *Springer Handbook of Lasers and Optics*, Ch. 12 (Springer, 2007); M. Wollenhaupt, A. Prakelt, C. Sarpe-Tudoran, D. Liese, T. Bayer and T. Baumert, Phys. Rev. A **73**, 063409 (2006); T. Bayer, M. Wollenhaupt, C. Sarpe-Tudoran, T. Baumert, Phys. Rev. Lett. **102**, 023004 (2009).

[20] D. A. Varshalovich, A. N. Moskalev and V. K. Khersonskii, *Quantum Theory of Angular Momentum* (World Scientific, Singapore, 1988).

[21] U. Gaubatz, P. Rudecki, S. Schiemann, K. Bergmann, J. Chem. Phys. **92**, 5363 (1990); S. Schiemann, A. Kuhn, S. Steuerwald, K. Bergmann, Phys. Rev. Lett. **71**, 3637 (1993); N. V. Vitanov, M. Fleischhauer, B. W. Shore, and K. Bergmann, Adv. At. Mol. Opt. Phys. **46**, 55 (2001).

[22] E. C. G. Stückelberg, Helv. Phys. Acta **5**, 369 (1932).

[23] N. V. Vitanov and S. Stenholm, Phys. Rev. A **55**, 2982 (1997).

[24] L. K. Grover, Phys. Rev. Lett. **79**, 325 (1997).

[25] T. Calarco, D. Jaksch, J. I. Cirac and P. Zoller, J. Opt. B **4**, 430 (2002).

[26] A. Ekert, M. Ericsson, P. Hayden, H. Inamori, J. A. Jones, D. K. L. Oi and V. Vedral, J. Mod. Opt. **47**, 2501 (2000).

[27] X. Lacour, S. Guérin, N. V. Vitanov, L. P. Yatsenko, and H. R. Jauslin, Opt. Commun. **264**, 362 (2006); H. Goto and K. Ichimura, Phys. Rev. A **70**, 012305 (2004).

[28] J.-C. Diels and W. Rudolph, *Ultrashort Laser Pulse Phenomena: Fundamentals, Techniques, and Applications on a Femtosecond Time Scale* (Academic, San Diego, 1996);

[29] G.L. Long, Phys. Rev. A **64**, 022307 (2001).

[30] E. Brion, L. H. Pedersen and K. Mølmer, J. Phys. A: Math. Theor. **40**, 1033 (2007).

[31] G. S. Vasilev and N. V. Vitanov, Phys. Rev. A **70**, 053407 (2004).

[32] A. M. Dykhne, Sov. Phys. JETP **11**, 411 (1960); Sov. Phys. JETP **14**, 941 (1962); J. P. Davis and P. Pechukas, J. Chem. Phys. **64**, 3129 (1976).

[33] N. V. Vitanov, B. W. Shore, L. Yatsenko, K. Böhmer, T. Halfmann, T. Rickes and K. Bergmann, Opt. Commun. **199**, 117 (2001); T. Halfmann, T. Rickes, N. V. Vitanov and K. Bergmann, Opt. Commun. **220**, 353 (2003).

[34] C. Guerlin, J. Bernu, S. Deléglise, C. Sayrin, S. Gleyzes, S. Kuhr, M. Brune, J.-M. Raimond, and S. Haroche, Nature **448**, 889 (2007).

[35] B. W. Shore, Acta Physica Slovaka **58**, 243 (2008).

[36] E. Majorana, Nuovo Cimento **9**, 43 (1932).

[37] F. Bloch and I. I. Rabi, Rev. Mod. Phys. **17**, 237 (1945).

[38] J. R. Morris and B. W. Shore, Phys. Rev. A **27**, 906 (1983).

[39] E.S. Kyoseva and N.V. Vitanov, Phys. Rev. A **73**, 023420 (2006).

[40] A. Erdélyi, W. Magnus, F. Oberhettinger, F. G. Tricomi, *Higher Transcendental Functions* (McGraw-Hill, New York, 1953).

[41] N. V. Vitanov and K.-A. Suominen, Phys. Rev. A **56**, R4377 (1997).

[42] N. V. Vitanov, J. Phys. B **31**, 709 (1998).

[43] P. A. Ivanov, N. V. Vitanov and M. B. Plenio, Phys. Rev. A **78**, 012323 (2008); I. E. Linington, P. A. Ivanov and N. V. Vitanov, Phys. Rev. A **79**, 012322 (2009).

[44] N. V. Vitanov, New J. Phys **9**, 58 (2007).

[45] R. S. Judson and H. Rabitz, Phys. Rev. Lett. **68**, 1500 (1992).

[46] N. V. Vitanov and P. L. Knight, Opt. Commun. **121**, 31 (1995).

[47] T. Brixner, T. Pfeifer, G. Gerber, M. Wollenhaupt and T. Baumert, in *Femtosecond Laser Spectroscopy* edited by P. Hannaford (Springer, New York, 2005), Chap 9.

[48] M. Abramowitz and I. A. Stegun, *Handbook of Mathematical Functions* (Dover, New York, 1964).

[49] N. V. Vitanov and B. M. Garraway, Phys. Rev. A **53**, 4288 (1996).

[50] F. W. J. Olver, J. Res. Nat. Bur. Stand. B **63**, 131 (1959).

[51] N. V. Vitanov, J. Phys. B **27**, 1351 (1994); N. V. Vitanov and P. L. Knight, J. Phys. B **28**, 1905 (1995).

[52] G. S. Vasilev and N. V. Vitanov, Phys. Rev. A **73**, 023416 (2006).

[53] A. Karpati, Z. Kis, and P. Adam, Phys. Rev. Lett. **93**, 193003 (2004).

[54] P.A. Ivanov, E.S. Kyoseva and N.V. Vitanov, Phys. Rev A **74**, 022323 (2006).

[55] A. S. Householder, J. ACM **5**, 339 (1958).

[56] J. H. Wilkinson, Comput. J. **3**, 23 (1960); Numer. Math. **4**, 354 (1962); J. M. Ortega, Numer. Math. **5**, 211 (1963); D. J. Mueller, Numer. Math. **8**, 72 (1966).

[57] M. Reck, A. Zeilinger, H. J. Bernstein, and P. Bertani, Phys. Rev. Lett. **73**, 58 (1994). A. Muthukrishnan and C. R. Stroud Jr., Phys. Rev. A **62**, 052309 (2000); G. K. Brennen, D. P. O'Leary and S. S. Bullock, Phys. Rev. A **71**, 052318 (2005); S. S. Bullock, D. P. O'Leary and G. K. Brennen, Phys. Rev. Lett. **94**, 230502 (2005); A. B. Klimov, R. Guzmán, J. C. Retamal, and C. Saavedra, Phys. Rev. A **67**, 062313 (2003).

[58] R. Jozsa, Proc. R. Soc. Lond. A **454**, 323 (1998).

[59] C. M. Bowden, G. Chen, Z. Diao, A. Klappenecker, J. Math. Anal. Appl. **274**, 69 (2002).

[60] P. W. Shor, in Proceedings of the 35th Annual Symposium on the Foundations of Computer Science, edited by S. Goldwasser (IEEE Computer Society, Los Alamitos, CA, 1994), p. 124; SIAM J. Sci. Statist. Comput. **26**, 1484 (1997); arXiv:quant-ph/9508027v2.

[61] D. Deutsch, Proc. R. Soc. Lond. A **400**, 97 (1985); D. Deutsch and R. Jozsa, Proc. R. Soc. Lond. A **439**, 553 (1992).

[62] D. R. Simon, in Proceedings of the 35th Annual Symposium on the Foundations of Computer Science, edited by S. Goldwasser (IEEE Computer Society, Los Alamitos, CA, 1994), p. 116; SIAM J. Comput. **26**, 1474 (1997).

[63] D. Coppersmith, arXiv:quant-ph/0201067v1 (1994 IBM Internal Report).

[64] Y. S. Weinstein, M. A. Pravia, E. M. Fortunato, S. Lloyd, and D. G. Cory, Phys. Rev. Lett. 86, 1889 (2001).

[65] L. M. K. Vandersypen, M. Steffen, G. Breyta, C. S. Yannoni, R. Cleve, and I. L. Chuang, Phys. Rev. Lett. **85**, 5452 (2000)

[66] J.-S. Lee, J. Kim, Y. Cheong, and S. Lee, Phys. Rev. A. **66**, 042316 (2002).

[67] L. M. K. Vandersypen, M. Steffen, G. Breyta, C.S. Yannoni, M. H. Sherwood, and I. L. Chuang, Nature **414**, 883 (2001).

[68] J. Chiaverini, J. Britton, D. Leibfried, E. Knill, M.D. Barrett, R. B. Blakestad, W. M. Itano, J. D. Jost, C. Langer, R. Ozeri, T. Schaetz, D. J. Wineland, Science **308**, 997 (2005).

[69] B. P. Lanyon, T. J. Weinhold, N. K. Langford, M. Barbieri, D. F. V. James, A. Gilchrist, and A. G. White, Phys. Rev. Lett. **99**, 250505 (2007).

[70] C.-Y. Lu, D. E. Browne, T. Yang, J.-W. Pan, Phys. Rev. Lett. **99**, 250504 (2007).

[71] M.O. Scully and M. S. Zubairy, Phys. Rev. A **65**, 052324 (2002).

[72] A. Muthukrishnan and C. R. Stroud Jr, J. Mod. Opt. **49**, 2115 (2002).

[73] P. A. Ivanov and N. V. Vitanov, Phys. Rev. A **77**, 012335 (2008).

[74] R. Barak and Y. Ben-Aryeh, J. Opt. Soc. Am. B **231**, 24 (2007).

[75] J. W. Cooley and J. W. Tukey, Math. Comput. **19**, 297 (1965).

[76] R. Akis, D. K. Ferry, Appl. Phys. Lett. **79** 2823 (2001).

[77] X. Peng, Z. Liao, N. Xu, G. Qin, X. Zhou, D. Suter, and J. Du, Phys. Rev. Lett. **101**, 220405 (2008).

[78] D. Beckman, A. N. Chari, S. Devabhaktuni, and J. Preskill, Phys. Rev. A **54**, 1034 (1996).

[79] A. Barenco, A. Ekert, K.-A. Suominen, and P. Törmä, Phys. Rev. A **54**, 139 (1996).

[80] D. Cheung, Proc. of the Winter International Symposium of Information and Communication Technologies (WISICT 2004), pp. 192-197; arXiv:quant-ph/0403071v1.

[81] R. B. Griffiths and C.-S. Niu, Phys. Rev. Lett. **76**, 3228 (1996).

[82] R. G. Unanyan, B. W. Shore, M. Fleischhauer, and N. V. Vitanov, Phys. Rev. A **75**, 022305 (2007).

[83] F. R. Gantmacher, *Matrix Theory* (Springer, Berlin, 1986).

[84] A. Messiah, *Quantum Mechanics* (North-Holland, New York, 1962).

[85] K. M. Abadir, J. Phys. A **26**, 4059 (1993).

[86] R. B. Dingle, *Asymptotic Expansions: Their Derivation and Interpretation* (Academic Press, London, 1973).

[87] F. W. J. Olver, *Asymptotics and Special Functions* (Academic Press, London, 1974)